Universidade de Aveiro Departamento de Física
2010

Lúcio Figueiredo de Rezende

Dinâmica em múltiplas escalas na Margem Continental Leste Brasileira.

Multi-scale dynamics on the Eastern Brazilian Margin.

Universidade de Aveiro Departamento de Física
2010

Lúcio Figueiredo de Rezende

Dinâmica em múltiplas escalas na Margem Continental Leste Brasileira.

Trabalho apresentado à Universidade de Aveiro como requisito necessário à obtenção do grau de Doutor em Física, realizada sob a orientação do Doutor Paulo Manuel Cruz Alves da Silva, Professor Auxiliar do Departamento de Física da Universidade de Aveiro e, do Doutor Mauro Cirano, Professor Adjunto do Instituto de Física da UFBA (Brasil).

Apoio financeiro do *Programa Alβan* no âmbito do II ciclo do programa de bolsas de alto nível para a América Latina (Processo E04D028784BR) e, da *Universidade Estadual de Santa Cruz*, Estado da Bahia, Brasil.

o júri

presidente

Doutor Joaquim José Borges Gouveia
Professor Catedrático do Departamento de Economia, Gestão e Engenharia Industrial
Universidade de Aveiro

Doutora Isabel Ambar
Professora Catedrática
Faculdade de Ciências da Universidade de Lisboa

Doutor Álvaro Júdice Ribeiro Peliz
Investigador Auxiliar do Instituto Oceanográfico
Faculdade de Ciências da Universidade de Lisboa

Doutor Jesús Manuel Pereira Dubert
Professor Auxiliar do Departamento de Física
Universidade de Aveiro

Doutor Mauro Cirano
Professor Adjunto do Instituto de Física
Universidade Federal da Bahia.
Orientador - Brasil

Doutor Paulo Manuel Cruz Alves da Silva
Professor Auxiliar do Departamento de Física
Universidade de Aveiro
Orientador - Portugal

Acknowledgements

I am indebted to my supervisors, ***Dr. Paulo Silva*** and ***Dr. Mauro Cirano***, for their support and guidance during the course of this project. It has been an honor to work with both.

I wish to thank ***Dr. Álvaro Peliz***, for the assistance with the model implementation as well as for the many science insights along the task. I am also extremely grateful to ***Dr. Martinho Almeida*** for his assistance with the tidal forcing implementation and for being always available to help. Many thanks also to the colleagues at the *Ocean and Atmosphere Science Laboratory*, for making my permanence in Portugal an easier task and for the Colleagues at UFBA, for making my permanence in Salvador memorable.

I wish to thank the ***Alβan programme*** for the financial support along two consecutive years at the *Universidade de Aveiro* and, ***Universidade Estadual de Santa Cruz*** for having supported my research activities for so many years.

Finally, I would like to express my appreciation to each and everyone, that having crossed my life during these years, have brought me join and confidence, making this a memorable time. Specially I would like to thank my dear ***Patrícia***, for being so patient and adorably careful with me.

To all saints, inhabiting at *Bahia de Todos os Santos* people's heart, I dedicate this work.

palavras-chave

Oceanografia da Margem Continental Leste Brasileira, Modelação Numérica, Dinâmica Estuarina, Correntes de Maré.

resumo

Este trabalho combina esforços de simulação numérica e de análise de dados para investigar a dinâmica em diversos compartimentos (oceano aberto, plataforma continental e zona costeira-estuarina) e, em multiplas escalas, na Margem Continental Leste Brasileira (MCLB). A circulação de largo e mesoescala espacial e a propagação da maré barotrópica são investigadas através de uma configuração aninhada do modelo numérico ROMS. O estudo da dinâmica regional da Baía de Camamu (CMB) baseia-se na análise de dados locais. A MCLB, localizada a SW do Atlântico Sul entre $8°$S e $20°$S, possui plataforma estreita, batimetria complexa, e baixa produtividade primária. A sua dinâmica é influenciada pela divergência da Corrente Sul Equatorial (CSE). As simulações refletem as conexões sazonais e espaciais entre a Corrente do Brasil e a Contra Corrente Norte do Brasil , em conexão com a dinâmica da CSE. As simulações revelam atividades vorticais nas proximidades da costa e interações com a dinâmica costeira, cujos padrões são descritos. A validação do modelo em mesoescala é baseada em cálculos de energia cinética turbulenta e em dados históricos de transporte. A CMB, localizada a $13°40'$S, abriga uma comunidade piscatória tradicional e extenso de manguezal. Situa-se porém sobre uma bacia sedimentar com grande reservas de óleo e gás, estando em tensão permanente de impacto ambiental. Neste trabalho sumarizamos as condições físicas regionais e investigamos sua dinâmica interna, focando sua variabilidade em amostragens realizadas sob condições de seca (Setembro de 2004) e de chuva (Julho de 2005). Finalmente, o modelo numérico ROMS é forçado com o sinal de maré, empregando-se uma configuração simples (com coeficientes de atrito de fundo constantes e condições hidrográficas homogéneas), com o intuito de avaliar sua resposta e investigar a natureza da propagação da maré barotrópica na MCLB, convergindo na CMB. A análise da resposta do modelo à maré basea-se em séries históricas do nível do mar para a MCLB e dados recentes da CMB.

keywords Eastern Brazilian Margin Oceanography, Numerical Modeling, Estuarine Dynamics, Tidal Currents.

abstract This work combines numerical and data analysis efforts to investigate the multi-scale dynamics on the ocean, shelf and estuarine compartments of the Eastern Brazilian Margin (EBM). The large and mesoscale circulation and the barotropic tidal propagation are investigated with a nested configuration of the Regional Ocean Modeling System - ROMS. Regional Baía de Camamu (CMB) dynamics is investigated based on the analysis of an original field data covering dry and rainy conditions. The EBM is an oligotrophic and bathymetrically complex zone, on the NW South Atlantic ($8^{\circ}S$ to $20^{\circ}S$), whose dynamics is influenced by the divergence of the South Equatorial Current (SEC). The oceanic circulation reflects the seasonal and spatial relations between the southward Brazil Current and the northward North Brazil Undercurrent (NBUC), in connection to the SEC dynamics. While on the top layer (0-100 m) the circulation presents a pronounced spatial variability, on subsurface waters (100-500 m) the NBUC connects the EBM continuously. A first order description of eddies activities and its interaction with the near-shelf dynamics were considered. Eddy kinetic energy (EKE) calculated from AVISO sea level anomaly and transport estimates provides a validation of the mesoscale model results. CMB is a shallow bay system that sustains artisanal fisheries and extensive mangrove, but lies over a sedimentary basin with large oil and gas reserves, being under environmental pressure. We summarize the regional CMB physical setting and investigate the inner dynamics, its variability and major driving factors along Sept. (2004) and July (2005) field survey. Finally, tidal signals are added to the numerical model system with the objective of evaluating the model response, by using a simple configuration (that applies constant bottom stress and homogeneous hydrographic conditions), and to investigate the nature of the barotropic tidal propagation along different spatial scales over the EBM and towards CMB. The model tidal response is evaluated with historical short period tidal gauge data for the EBM and recent CMB pressure sensor data.

Contents

List of Figures

List of Tables

Chapter 1

Introdution

The present thesis is a compilation of three independent and original science works related to the oceanography of the Eastern Brazilian Margin. The Eastern Brazilian Margin is a low productive and bathymetrically complex zone of the Western South Atlantic whose dynamics is influenced by the large scale South Equatorial Current divergence. The main goal of this work is to combine numerical and data analysis efforts to investigate the multi-scale dynamics on the ocean, shelf and estuarine compartments, exploring the connections between scales, whenever possible.

Each work is presented on a self-contained chapter, containing its own introduction, objectives and concluding remarks. The presenting order was established in terms of spatial scales, from the large to the regional scale. A topic regarding the modelling of barotropic tidal currents is presented at the end, since it integrates the different spatial scales involved. In order to keep this dissertation as close as possible to the scientific article format but still attaining to the classical academic dissertation form, this document presents a common abstract, a general introduction and a closing *final remarks and future work perspectives* chapter. A common bibliography with reference to the citing pages is also included. Since the Eastern Brazilian Margin is a lesser investigated zone of the Western South Atlantic, cross-referencing among the chapters was unavoidable.

1.1 Geographical outline: Bahia and the Eastern Brazilian Margin

In this work a multi-level grid and framework was adopted to investigate the ocean, shelf and estuarine processes of the Eastern Brazilian Margin. The investigated zone, geographically limited from $8°S$ to $20°S$ is politically bordered by the Brazilian states of *Pernambuco* (partially), *Alagoas*, *Sergipe*, *Bahia* and *Espirito Santo* (partially). The *Bahia* state however, whose coastline extends from 11°27′S to 18°20′S, along 1183 km, covers most of the domain, being the geographical focus of this study. Figure 1.1 presents the geographical framework considered. Inner diagram in grid L0, depicts the estate of *Bahia*, within Brazil and South America.

Salvador is the political capital of the state of *Bahia* and its major city. There are about 2,998,056 inhabitants in the city of *Salvador* and 3,475,000 on the metropolitan zone, making it the third most populous metropolitan zone in Brazil. The population density was 4,093 inhabitants per square kilometer [IBGE, 2008a]. *Salvador* was founded in 1549 being the first colonial capital of Brazil (until 1763) and was an active slave port on the trade connection between Brazil and West Africa for over three centuries [Alencastro, 2000; Verger, 2002]. Nowadays, most of the population is mixed descended from slaves and Iberian settlers (53.8%) or negroes (28.5%) [IBGE, 2008b]. The Black African were mainly Bantu speakers ($> 2/3$) from Angola and Congo and, secondarily Yoruba speakers from Nigeria, Ghana, Togo and Benin [Vianna Filho, 2008].

The former slave market has since developed petrochemical industries and oil refineries and still holds a major export port, lying at the heart of the *Recôncavo Baiano*, a rich agricultural and industrial region on the Northern portion of coastal *Salvador*, surrounding *Baía de Todos os Santos*. Tourism and marine activities is increasing in importance in *Bahia* economy, a major Brazilian destination for international leisure tourism. The local terrain is diverse, from flat to rolling to hills and low mountains.

1.2 Marine system characterization and stresses

The Eastern Brazilian Margin has a mesotidal regime, presents a generally narrow continental shelf and receives moderate to low river discharges along over 30 fluvial courses, the largest of which being the *São Francisco* (10°30′S) and the *Jequitinhonha* (15°52′S) rivers [Knoppers et al., 1999]. A transition from siliciclastic dominant sediments on the coastline to pure carbonates towards the middle and outer shelves, characterizes the continental shelf of tropical Brazil [Leão, 2002].

The Eastern Brazilian Margin is considered a Class III, low productivity ($< 150 gC/m^2/yr$) ecosystem based on the $SeaWiFS$ global primary productivity [U. S. Department of Commerce, 2004]. Fishing is practiced on a small scale being mostly artisanal, catches tends to be low. Herring, snapper, mackerel, and albacore are some of the commercial species harvested. Snapper, triggerfish, swimcrabs and Atlantic seabobs are dominant in the landings of Abrolhos Bank and tunas species are caught offshore around seamounts and banks [Ekau and Knoppers, 2003]. Nevertheless the Eastern Brazilian Margin encompasses some important coastal and estuarine systems, such as *Baía de Todos os Santos*, *Baía de Camamu* and the *Abrolhos Bank*, where the productivity is certainly higher, although data is scant.

Baía de Todos os Santos is the second largest embayment along the Brazilian coast presenting a area of $1223 km^2$ and an average depth of 9.8 m [Lessa et al., 2001; Cirano and Lessa, 2007], being located adjacent to *Salvador*. The inner bay circulation is mostly tidally driven and does not vary significantly throughout the year [Cirano et al., 2007]. The bay watershed is impacted by the pressure of *Salvador* intensive industrial, commercial and fishing activity [Leão, 2002]. *Baía de Camamu* is a shallow system which occupies a flooding area of approximately 384 km^2 being an important fishing, mining and touristic site located at the central *Bahia* estate (14°S; 39°W). Contrasting with *Baía de Todos os Santos*, on *Baía de Camamu* the watershed is surrounded by small cities and extensive mangrove vegetation [Oliveira, 2000]. *Baía de Camamu* also

presents numerous small islands and several small-scale fisheries communities whose population is engaged on artisanal fishing [Souza and Petrere-Jr, 2008] and subsistence agriculture practices. Prior to this work there were no study regarding the seasonality of *Baía de Camamu* dynamics.

Finally, on the Southern *Bahia* coastal zone, from 16°S to 20°S, the topography is marked by two major banks, the Royal Charlotte bank and the *Abrolhos* bank. Between those, an extended and irregular shelf projects towards the sea (The shelf width, with a mean extension around 35-45 km, widens to 110 km near Royal Charlotte and to 190 km at Abrolhos Bank). Within the *Abrolhos* Bank, from 10 to 65 km from the coast, a reef complex that occupies an area of approximately 6,000 km2 holds the southernmost and most extensive coral reef environment in the South Atlantic Ocean, with 16 species of stony coral recorded [Leão, 2002]. This is a spot of great biological importance, colonized by many archaic, endemic coral species, resultant from the isolation of a late tertiary community. [Leão, 2002]. On its Southern flanks, subsurface nutrient enrichment due to upwelling of nutrient-rich South Atlantic Central Water has been reported [Summerhayes et al., 1976; Ekau, 1999; Gaeta et al., 1999]. The physical nature of this upwelling is not yet fully understood being attributed to instabilities of the Brazil Current over the irregular topography [Ekau, 1999; Gaeta et al., 1999] while Pereira et al. [2005] points out the effect of internal tides and steep topography, enhancing the upwelling in the zone.

There is evidence of pressure over the coral reefs, and coral bleaching has been reported in northern *Bahia* and in *Abrolhos* reefs but the levels of mortality still remain low [Ekau and Knoppers, 2003]. The coast is very vulnerable to tanker movement and oil spills occurred in 1974 (*Esso Garden State*), 1975 (*Yarik Ibn Ziyad*), 1978 (*Brazilian Marina*), 1985 (*Marina*) and 1986 (*Brotas*) among the major occurrences. In each case the spill involved more than 10,000 barrels of oil [Ekau and Knoppers, 2003]. Floating paraffin compounds, from the 2001 (*Pietro Bárbaro*) spill and drift bottles released on a marine educational action were used to chart the shelf circulation at the time [Rezende,

2001].

Furthermore, in the past few years there has been increasing attention on giant oil reserves struck along the Brazilian margin. Recently, eighteen areas on the Eastern Brazilian shelf were offered for concession on international auctions, including six shallow areas, a few kilometers from *Baía de Camamu*. Commercial gas exploration on the nearby shelf have started on 2007 [ANP, 2009]. The local residents fears of episodic or systematic contamination of *Baía de Camamu* by such activities. Simulations performed by Amorim [2005] predict that accidental oil spill from such fields, in the worst scenario, could reach the bay within one day.

Despite extending over a zone with great social, economic and environmental relevance, the Eastern Brazilian Margin dynamics and connectivity is virtually unknown. The large scale and mesoscale dynamic in the Eastern Brazilian Margin is deeply influenced by the South Equatorial Current Divergence and its seasonal variability. The South Equatorial Current is a broad, westward flowing current that connects the tropical and the subtropical Atlantic Ocean through the South Atlantic subtropical gyre. As its southern branch approaches the Eastern Brazilian Margin, carrying subtropical Benguela Current water towards the shelf, it bifurcates into the Northward flowing North Brazil Current system and the Southward flowing Brazil Current system [Stramma et al., 1990; Stramma and Schott, 1999]. According to Rodrigues et al. [2007], the bifurcation latitude varies poleward with depth, from $10°S$ to $14°S$ near the surface to $27°S$ at the 1000 m depth. After they are formed, these major current system (Brazil and North Brazil) dominates the upper ocean circulation along the Brazilian Margin. The Eastern Brazilian margin is located on the divergence zone, being subject to numerous variabilities on the large and mesoscale dynamics. Nowadays, a wide uncertainty regarding this region dynamics remains and very few published science are available to guide.

1.3 Objectives of this work.

In this work a multi-level grid and framework was adopted to investigate the large, mesoscale and regional marine processes on the Eastern Brazilian Margin. In *Chapter 2* our main goal is to establish a view of the seasonal mesoscale circulation on the Eastern Brazilian Margin, retaining on the solution the connections and forcing from the large-scale (ie: the South Equatorial Current divergence and variabilities) and emphasizing the temporal and spatial connectivity along the Margin. This is obtained with the implementation of a nested configuration into the community based Regional Ocean Modeling System - ROMS. [Haidvogel et al., 2000; Shchepetkin and McWilliams, 2005]. Following, we make an attempt to establish a first order description of the mesoscale activities revealed on the model simulation. Some possible interactions between the meanders, the shelf and the near-coastal processes are speculated as those may have sound environmental relevance on the oligotrophic Eastern Brazilian Margin. The geographical framework comprises grids L0 and L1 in Figure 1.1.

Regional *Baía de Camamu* processes are investigated based on the analysis of an relatively extensive field data set (*Chapter 3*). Part of this data had previous been treated by Amorim [2005] and on numerous unpublished and unrestricted technical reports at *Universidade Federal da Bahia*, among other cited sources. We now present a novel interpretation of this data, adding original data into our analysis and looking on the seasonal dynamical patterns, covering dry (September, 2004) and rainy (July, 2005) conditions. This chapter intends to summarize the regional *Baía de Camamu* physical setting and investigate the inner dynamics, the seasonal variability and the major driving factors, being a science contribution regarding the multidisciplinary discussion on *Baía de Camamu* maritime planning and preservation. The geographical framework is presented in Figure 1.1, bottom right.

In *Chapter 4*, tidal signals are added to the Eastern Brazilian Margin numerical model system discussed on *Chapter 2*. The model, now receives two separated one-way

off-line nested domains with spatial resolution of $\sim 3km$ and $\sim 1km$, comprising the coastal and estuarine systems in the zone between the cities of *Salvador* and *Ilhéus* and higher resolution focus on *Baía de Camamu*. The primary objective is to evaluate the model system response by using a simple model configuration (that applies constant bottom stress and homogeneous hydrographic conditions) and to investigate the nature of the barotropic tidal propagation along different spatial scales, towards the shallower domains on the shelf, near shore and inner *Baía de Camamu*. Secondly, is discussed the paths to follow in order to set a coastal modelling system that allows estuarine connections and some science hypotheses are discussed based on the tidal simulation results. The geographical framework comprises grids L2 and a local grid (L3), similar to the Baía de Camamu framework, presented in Figure 1.1.

Along this thesis, the connections between scales are focused in various aspects, such as in the large and meso scale interplay discussed on *Chapter 2*, or at the tidal propagation, englobing various spatial scales, discussed on *Chapter 4*. Finally, the closing *Chapter5* discusses ideas for future studies, remarking what was achieved on each topic.

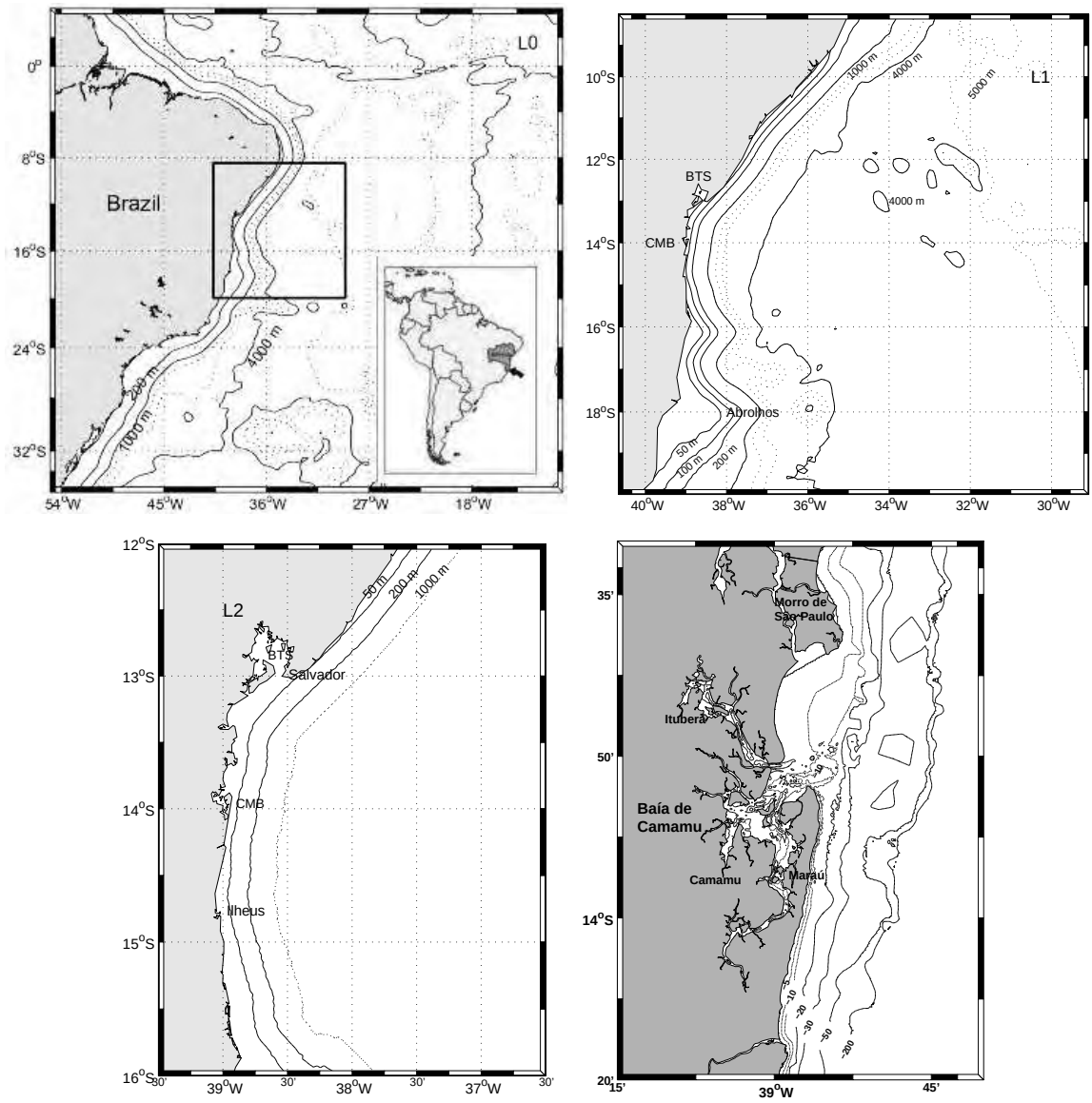

Figure 1.1: Outline of the Eastern Brazilian Margin, depicting the large, mesoscale and regional grids bathymetry and *Baía de Camamu* framework. The Large scale grid (L0) covers the western South Atlantic, spanning from equatorial latitudes to $35°S$; The mesoscale grid (L1), covers the Eastern Brazilian Margin. The regional grid (L2) allows investigation of costal systems and features such as *Baía de Todos os Santos*(BTS) and *Baía de Camamu*(CMB), while the finest-resolution framework is centered on *Baía de Camamu* and its connection with the coastal ocean. The work domain is centered, in multi-scale domains, on the coastal zone of the state of *Bahia*(inner diagram in L0), whose coastline extends from 11°27′S to 18°20′S. Indicated are the cities of *Salvador, Ilheús*, the municipalities surrounding CMB: *Camamu*, *Maraú*, *Ituberá*, *Morro de São Paulo* and the *Abrolhos* bank for geographical reference.

1.4 Science results and divulgation.

The author declares that the intellectual content of this thesis, its physical interpretation and conclusions is the product of his personal work and effort under the close supervision, support and guidance from *Dr. Paulo Silva* (Universidade de Aveiro) and *Dr. Mauro Cirano* (Universidade Federal da Bahia). The assistance from others in the project's conception, modeling setting, data handling and figure presentation has been acknowledged and deeply appreciated.

The following papers are being prepared primarily based on the thesis presented here. The final article however may differ slightly from the thesis content as it is subject to conciseness, to direct contributions from the associated authors or from anonymous referees, among other possible intervenience. The author of this thesis is committed to have these papers published and assumes the major responsibility in the process (dates reflects the expected publishing year):

Rezende, L., Silva P., Cirano M., Peliz A. and Dubert J., 2010: Mean circulation, seasonal cycle and eddy interactions in the Eastern Brazilian Margin, a nested ROMS model. *(submitted)*

Rezende, L., Amorim F., Cirano M., Silva P. and Hatje, V., 2010: The oceanography of *Baía de Camamu* ($14°S$), Brazil: Physical setting, hydrodynamics and the influence of an extreme flow event. *(in preparation)*

Rezende, L., Cirano M., Silva, P. and Almeida, M. M, 2011: Tidal currents in the Eastern Brazilian Margin and on inner *Baía de Camamu*. *(in preparation)*

The following abstracts and talks were based upon work results from this thesis:

Rezende, L. F., Silva P., Peliz A., Dubert J., and Cirano M., 2006. *A Nested model for the Eastern Brazilian Shelf: Cross - shelf eddy interactions and validation on altimeter data.* In: European Geosiences Union - General Assembly, Vienna, Austria, April 02-07, 2006. (Open section on ocean sciences, coastal and shelf Oceanography).

Rezende, L. F., Silva P., Peliz A., Dubert J. and Cirano M., 2006. *Mesoscale variability on the Eastern Brazilian Shelf through a Roms nested model.* In: 2006 Roms/Toms Workshop, 2006, Alcalá de Henares. The 2006 Roms/Toms workshop proceedings.

Rezende, L. F., Silva P., and Cirano M., 2006. *Dinâmica da Plataforma Continental Leste Brasileira através da Modelagem Numérica: Da origem da Corrente do Brasil ás Feições dinâmicas do Banco de Abrolhos.* In: III Seminário de investigadores e estudantes brasileiros em Portugal (SIEBRAP 2006). Resumos do III SIEBRAP, Editora da Universidade de Aveiro, 2006.

Rezende, L. F., Silva P., and Cirano M., 2007. *The circulation in the Eastern Brazilian Margin through a nested ROMS model.* In: I Wokshop Produtividade, Sustentabilidade e Utilização do ecossistema do *Banco de Abrolhos*, São Paulo. October, 2007.

Rezende, L. F. *Conectividade Física (e Biológica ?) na Plataforma Continental Leste Brasileira, do Banco de Abrolhos á Baía de Todos os Santos.* In: X SIMBIO (Simpósio de Biologia do Sul da Bahia), Mesa redonda sobre corredores ecológicos. Universidade Estadual de Santa Cruz, ilhéus, November, 2008.

Chapter 2

Mean circulation, seasonal cycle and eddy interactions in the Eastern Brazilian Margin, a nested ROMS model

2.1 Introduction

The Eastern Brazilian Margin (EBM) of the northwestern South Atlantic ($8°S$ to $20°S$, Figure 2.1) presents typical conditions of a tropical passive margin dominated by western boundary currents. Apart from a complex geometry around the Abrolhos Banks, on its southern limit, the EBM presents a dominantly open and narrow continental shelf, receives low river discharges and is almost entirely covered by biogenic carbonate sediments [Knoppers et al., 1999]. According to the $SeaWiFS$ global primary productivity [U. S. Department of Commerce, 2004], this margin is considered a Class III, low productivity ecosystem ($< 150 gC/m^2/yr$).

On the EBM, the circulation is remarkably influenced by the South Equatorial Current (SEC) bifurcation. The SEC is a broad, westward flowing current that connects the tropical and the subtropical Atlantic Ocean through the South Atlantic subtropical

gyre. As the southern branch of the SEC approaches the EBM, carrying subtropical Benguela Current water towards the shelf, it bifurcates into the northward flowing North Brazil Undercurrent (NBUC) and the southward flowing Brazil Current (BC) [Stramma et al., 1990; Stramma and Schott, 1999]. According to Rodrigues et al. [2007], this bifurcation latitude varies poleward with depth, from $10°S$ to $14°S$ near the surface to $27°S$ at the 1000 m depth.

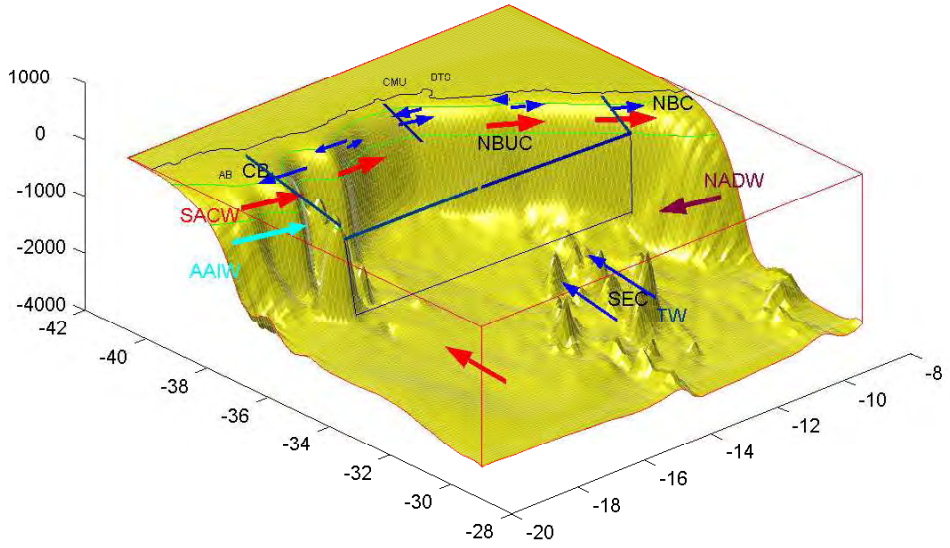

Figure 2.1: Schematic diagram of the main EBM flow patterns. The acronyms indicate the estimated position for the South Equatorial Current (SEC), the Brazil Current (BC), the North Brazil Undercurrent (NBUC) and the North Brazil Current (NBC). The colored vectors refer to the water masses distribution, indicating the layers associated to the Tropical Water (TW), the South Atlantic Central Water (SACW), the Antarctic Intermediate Water (AAIW) and the North Atlantic Deep Water (NADW). The *Abrolhos Bank* (AB), *Baía de Todos os Santos* (BTS), *Baía de Camamu* (CMU) and the reference transects used on section 2.4 are also indicated.

The NBUC is the component of the North Brazil Current System that, occupying the top 1000 m of the water column, flows along the northeast coast of Brazil, until the *Cabo de São Roque* ($\sim 5°S$). From this point, as it flows northwestward towards the Equator, the NBUC receives an additional inflow from the SEC, becoming an intensified surface current known as the North Brazil Current (NBC) [Schott et al., 1998].

While the NBC is an intense western boundary current and the dominant surface circulation feature in the western tropical Atlantic Ocean [Silveira et al., 1994], the BC is a weak and shallow western boundary flow [e.g., Evans et al., 1983]. It carries warm water along the Brazilian coast, from its origin to about $38°S$, when it leaves the coast, forming the Brazil-Malvinas Confluence [Gordon, 1989]. At tropical latitudes, the BC is a shallow flow characterized only by the oligotrophic, warm and salty Tropical Water (TW, $T > 20°C$ and $S > 36$) [Emilsson, 1961]. As the BC reaches subtropical latitudes it becomes deeper and gradually incorporates the nutrient-richer, colder and fresher South Atlantic Central Water (SACW, $6°C < T < 20°C$ and $34.6 < S < 36$) [Miranda, 1985]. Reid [1989] defines this SACW southward flow to be found at latitudes south of 20°C.

Until now, the most functional description of the oceanographic processes on the EBM are probably the works of Stramma et al. [1990] and Rodrigues et al. [2007]. The first authors, based on a historical hydrographic data set, described the geostrophic circulation for the region, while Rodrigues et al. [2007] investigated the seasonal variability of the SEC bifurcation. According to Rodrigues et al. [2007], on the upper thermocline, the bifurcation variability is associated to changes in the local wind stress curl due to the annual north-south excursion of the marine ITCZ complex. On the top 200 m, the bifurcation latitude reaches its southernmost position in July ($\sim 17°S$) and its northernmost position in November($\sim 13°S$). As the SEC bifurcation moves south (north), the NBUC transport increases (decreases) and the BC transport decreases (increases).

From a mesoscale perspective, the variability of the divergence, the seasonal relation between the BC and the NBC and the interaction between the oceanic processes with the near-shelf environments are still open issues on the EBM dynamics. The first practical difficulty that one faces when planning a regional modeling study on this region is perhaps the establishment of a reliable annual cycle to be used at the boundary conditions. The straightforward solution would be the interpolation of local data on

the frontiers but unfortunately, the available data are still scarce and irregularly sampled on time and space, as summarizes Stramma et al. [1990], using most of the data ever surveyed on the region. Therefore, possible ways to cope with this problem, according to Penven et al. [2006] are: i) to have the boundary conditions provided from an independent basin-scale or a global model, which according to those authors may generate doubtful consistency with the local simulation or ii) to develop a nested grid capability, where a hierarchy of embedded, structured-grid models are able to interact between each other. In this work we adopted the second procedure and here the regional boundary condition is provided by the courser grid run, whose boundary conditions themselves come from a global model, with compatible resolution and processes.

The EBM encompasses many important coastal systems, such as *Baía de Todos os Santos* (BTS), *Baía de Camamu* (CMU) and the *Abrolhos Bank*(Figure 2.1). The BTS, the second largest coastal embayment along the Brazilian coast with $1086 km^2$ [Lessa et al., 2001], is located adjacent to the city of *Salvador*, a metropolitan area with over 3 million inhabitants, being impacted by the pressure of an intensive industrial, commercial and fishing activity [Leão, 2002]. The CMU, located just 100 km south of *Salvador*, is an important fishing, mining and tourist site, surrounded by an extensive mangrove vegetation. Finally, the *Abrolhos Bank* is a site of great biological importance, holding a reef complex that occupies an area of approximately 6,000 km^2, representing the southernmost and most extensive coral reef environmental in the South Atlantic [Leão, 2002]. Despite the fact that the EBM extends over a zone with such social and environmental relevance, its marine connectivity is virtually unknown.

Our major aim in this work is to establish a model view of the seasonal circulation on the EBM, retaining on the solution, the connections from the large-scale circulation. To accomplish this task, we structured this chapter in the following sections. The nesting capability integrated into the Regional Ocean Modeling System [Penven et al., 2006] along with the modeling design is presented in section 2. The results are presented into four different sections. The initial part being devoted to the validation

of the model itself. The second and third parts of the results discusses the main aspects of seasonal and spatial circulation patterns on the EBM, respectively while in the forth and final part of the results, some of the possible interactions between the meanders, the shelf and the near-coastal processes are explored, as an attempt to establish a first order description of the mesoscale activities revealed by the regional simulation. Finally, the last section of this manuscript presents a summary of the major results presented, emphasizing the physical aspects of the EBM temporal and spatial connectivity.

2.2 The modeling design and the two nested grids

The numerical model used in this study is a primitive, nested, three dimensional, stretched terrains - sigma following curvilinear coordinate, Regional Ocean Modeling System (ROMS) [Haidvogel et al., 2000; Shchepetkin and McWilliams, 2005]. ROMS applies the Boussinesq approximation and hydrostatic balance, solving the momentum equations in a Earth-centered rotating environment.

In this work a two level, one way nesting capability has been integrated into ROMS to obtain mesoscale solutions, while preserving the large-scale circulation. The nesting downscaling was performed through the Adaptive Refinement in Fortran (AGRIF) procedure, through the ROMS-AGRIF, at ROMS Processing tools [Penven, 2003]. This 1-way embedding procedure has been successfully applied in various dynamical systems, such as the Peru Current System [Penven et al., 2005], the Californian Upwelling System [Penven et al., 2006] and the Western Iberian Shelf [Teles-Machado et al., 2007], among others.

A regional grid of 1/12°, here named the Mesoscale Grid (MG), spanning approximately from 8°S to 20°S and from 29°W to 40°W was nested on the larger scale grid (1/4°), referred as the Large Grid (LG), encompassing a larger domain of the Western South Atlantic Ocean, from 5°N to 35°S and from 10°W to 55°W (Figure 2.2). Since the

near-shore currents have a spatial scale of o(1-30) km, while the offshore dynamics has a spatial scale o(30-100) km, the MG ($\sim$ 9 km grid cell resolution) is then capable of solving the mesoscale dynamics connecting the near-shore, the shelf and the ocean basin, while the LG ($\sim$ 27 km grid cell resolution) is intended to solve the large scale dynamics.

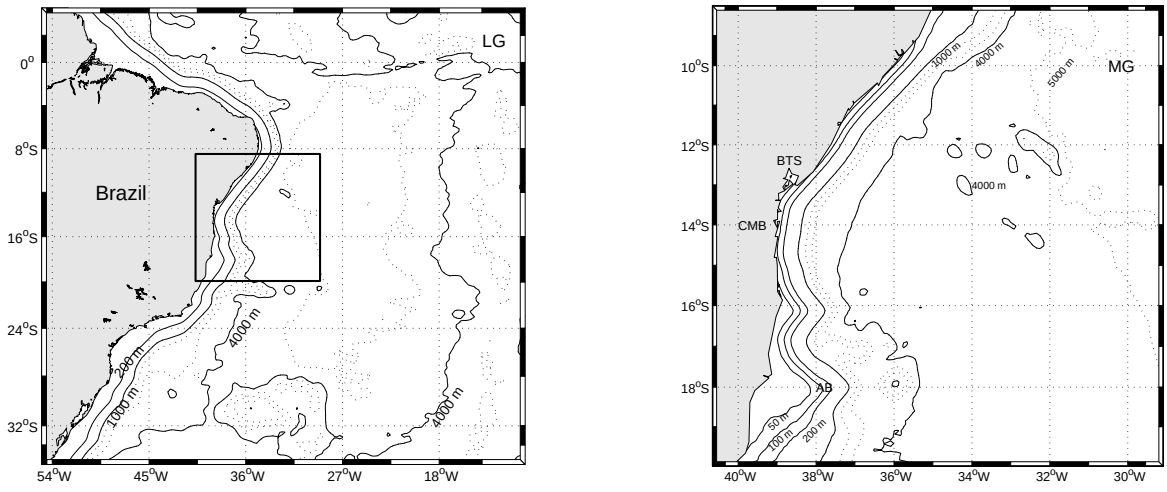

(a) (b)

Figure 2.2: ROMS nested grid system and bathymetry used: (a) Large Grid (LG) and (b) Mesoscale Grid (MG). Solid lines represent the 50 (MG only), 100 (MG only), 200, 1000 and 4000 m isobaths. The 2000, 3000 and 5000 m isobaths are represented as dotted lines

The model was initialized with Levitus climatology and forced by climatological monthly winds, heat and fresh water fluxes from the COADS - Comprehensive Ocean-Atmosphere Data Set [Da Silva et al., 1994], running for a 15 years period. The strategy adopted was to run the LG grid alone for the first ten years and then to have the one-way nesting procedure implemented for the following 5 years run. The LG uses radiational, active, implicit, open boundary conditions, where the solution at the boundary is nudged towards dated monthly mean outputs (1990 to 2004) of the Simple Ocean Data Assimilation (SODA) reanalysis [Carton et al., 2000b,a]. The lateral boundary conditions for the MG were provided by the LG grid. Explicit lateral viscosity is null in the entire domain except at the sponge layers (the closest 6 grid lines from the boundary), where it increases smoothly to a value of 1000 $m^2\ s^{-1}$ for LG and 330 $m^2\ s^{-1}$ for MG. A nonlocal, K-profile planetary (KPP) boundary layer scheme [Large et al., 1994]

parameterizes the sub-grid-scale vertical mixing processes.

The bottom topography was interpolated from ETOPO2 - 2' gridded global relief data [U. S. Department of Commerce, 2001] for both grids and, where necessary, it was smoothed to fit the bathymetric gradient to a maximum slope factor ($r = \Delta h/(h_1 + h_2) \cong 0.2$), in order to prevent pressure gradient errors associated to the sigma coordinate system [Haidvogel et al., 2000]. Tables 2.1 summarize the model configuration for LG and MG grids.

Table 2.1: Model configuration parameters

Parameter	**LG**	**MG**	
L	179	138	Pts. in longitude direction
M	169	141	Pts. in latitude direction
ΔS	$1/4^\circ$	$1/12^\circ$	Horizontal resolution
Δt	1800 s	600 s	Baroclinic time step
Δt_f	40 s	13.3	Barotropic time step
Common Parameters			
N	30		Number of s-levels
Θ_s	6.0		Sigma coord. stretch. factor
D	10.0 m		Minimum model depth
R	$3.0 \times 10^{-4} m.s^{-1}$		Linear bottom drag coeff.

2.3 The model validation approach

The basis of validation is to assess a model response by comparing its output to physically measured data, such as currents, hydrography or mesoscale variability. Mesoscale variability is a major characteristic of ocean dynamics and may be estimated with global coverage altimetric data [Brachet et al., 2004]. A validation of the LG model results with altimetric derived mesoscale variability is presented on sections 2.3.1 and 2.3.2. This procedure assumes a special interest, regarding the paucity of *in situ* data available [Backeberg, 2006]. Further on, a comparison of modeled transport with selected transport values from the literature is presented on section 2.3.3.

2.3.1 Eddy kinetic energy

The ocean mesoscale variability was estimated based on the eddy kinetic energy (EKE), calculated from TOPEX/Poseidon, ERS-1/2 and Jason combined data for sea level anomaly (SLA), obtained from the archiving, validation, and interpretation of satellites oceanographic - AVISO [Ducet et al., 2000]. Since mesoscale structures present typical time-space scales of 10 to 100 days and 50 to 500 km, the merging of multi altimeter data on the AVISO data set allows for a realistic sea level and geostrophic velocity calculation, resulting on a good quality mesoscale observation [Ducet et al., 2000]. The altimeter SLA data used covers a 5 years period, from January 2000 to December 2004 and presents a 1/3° spatial resolution.

The analyzed model data also covers a 5 years period of sea surface height (MSSH), and each output represents an average over a 10 days period. The model eddy kinetic energy was estimated from the model sea level anomalies (MSLA), using a similar procedure to the altimeter data pre-processing. The MSLA was computed from MSLA = MSSH -$\overline{MSSH}$, where the bar represents a mean over the five years period. Only the larger scale grid simulation, that has a similar spatial resolution to altimetric data, was

used in this analysis.

Both altimetric (SLA) and the model (MSLA) were used to compute the surface zonal (Ug') and meridional (Vg') velocity anomalies, using the geostrophic approximation :

$$Ug' = [-\frac{g}{f}(\frac{\partial \eta}{\partial y})] \tag{2.1}$$

$$Vg' = [\frac{g}{f}(\frac{\partial \eta}{\partial x})] \tag{2.2}$$

Where, g is the gravity acceleration, f, the Coriolis parameter, $\partial\eta/\partial x$ and $\partial\eta/\partial y$ are the meridional and zonal gradients of SLA and MSLA. The variance of the velocity anomaly field corresponds to the eddy kinetics energy (EKE):

$$EKE = [\frac{1}{2}\{(Ug')^2 + (Vg')^2\}] \tag{2.3}$$

Figure 2.3 (left panels) present the mean EKE distribution for altimetry (top) and ROMS (bottom) along the LG domain, while Figure 2.3 (right panels) presents a zoom of the same distribution on the EBM region. Maximum values of EKE are found on the energetic, equatorial zonal circulation. Minimum values are found on the oceanic region located between $8°S$ to $24°S$. In the EBM, an EKE intensification occurs on the outer shelf vicinity, reflecting the high variability of the western boundary dynamics associated to the northward flow of the NBC system and the southward BC flow. South of this region, the LG domain shows the BC flow, marked by relative high EKE variability along the southern coast of Brazil. Secondary EKE peaks, with values > 300 cm^2s^{-2} are seen around $\sim 35°S$, marking the confluence of the BC with the northward flow of the Malvinas Current system [Saraceno et al., 2004].

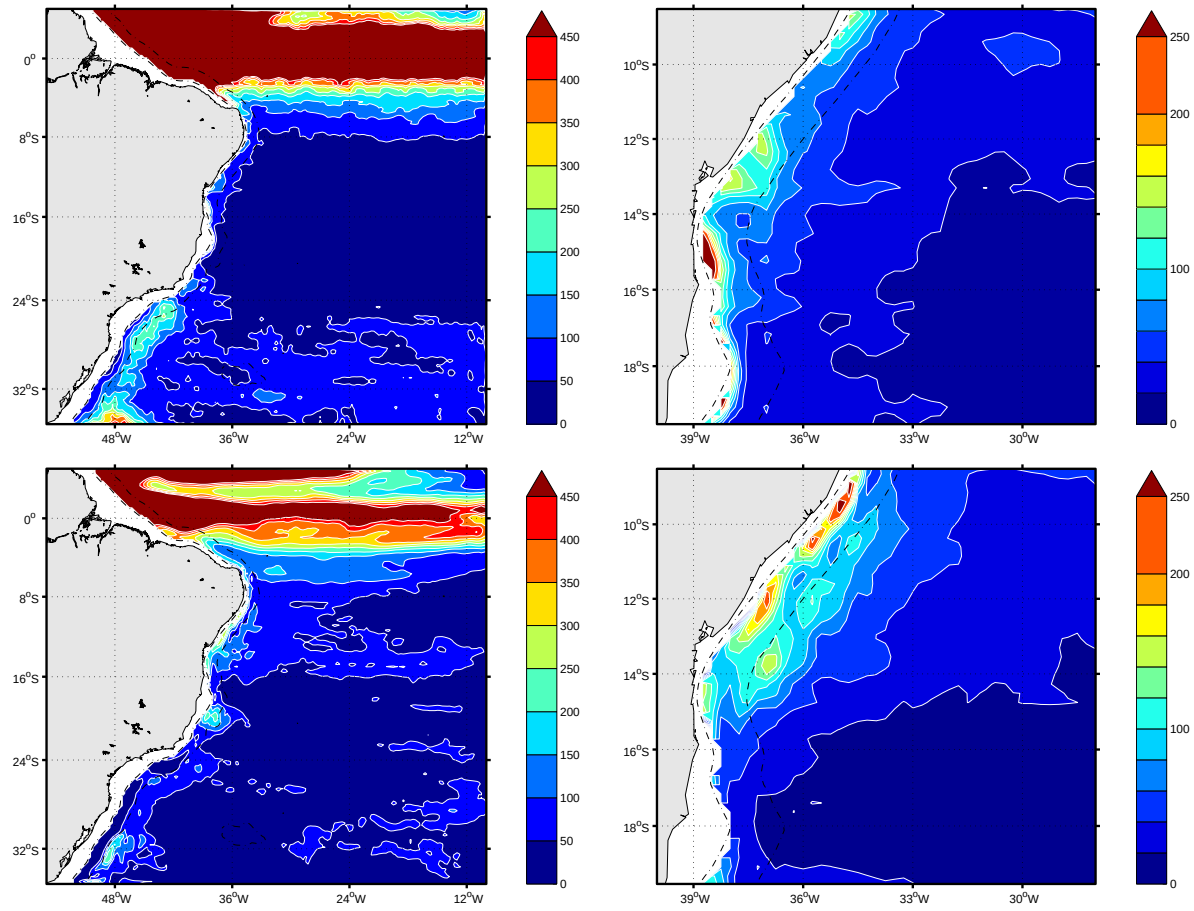

Figure 2.3: Mean EKE ($cm^2\ s^{-2}$) in the western South Atlantic (left) and detailed representation in the Eastern Brazilian Margin (right). The top panels represent the Altimeter and the lower panels represent ROMS. Dashed lines represent the 200 and 2000 m isobaths. Color scale is broken for values $> 450 cm^2.s^{-2}$ (left) and $> 200 cm^2.s^{-2}$ (right).

In order to have a zonal view of the EKE results, we have also computed the mean zonal EKE (Figure 2.4). This zonal estimate was obtained by time and space averaging the EKE results, from the 200 m isobath to 30°W, on one degree steps (7(±0.5)°S to 35(±0.5)°S), focusing on the western basin signal. The lower latitude EKE signal was omitted, as geostrophy breaks down near the Equator.

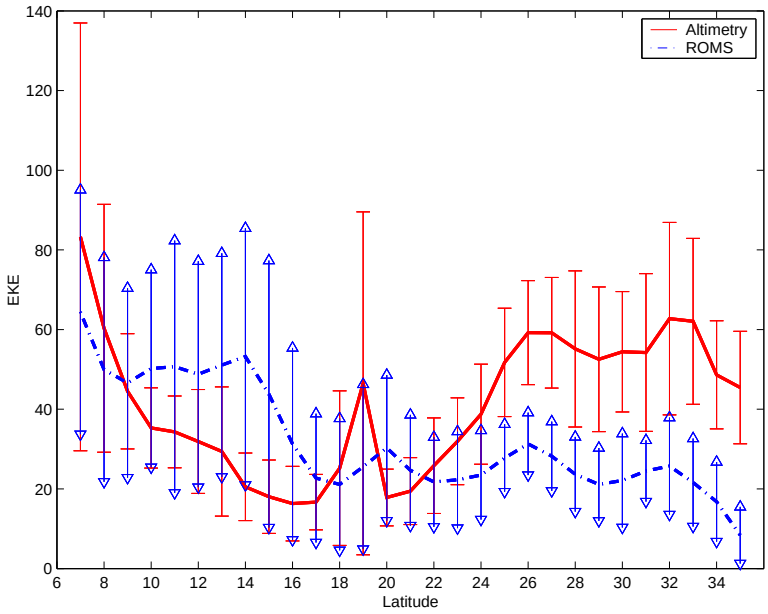

Figure 2.4: Mean zonal EKE distribution ($cm^2\ s^{-2}$) from altimeter and ROMS. Error bars represents the standard deviation from the mean.

Overall, ROMS captures the spatial EKE distribution with reasonable confidence, but tends to underestimate the ocean variability towards the northern (e.g., the energetic equatorial circulation zone) and the southern grid extensions (e.g., the Brazil-Malvinas confluence zone). An extended LG domain could possibly reduce this effect but also increase the computational time. Along the EBM, ROMS captures the larger energy associated to the western boundary currents, but shows larger variability and higher mean EKE, which could be partially ascribed to the remaining differences on the spacial resolution between ROMS and the altimetry.

The evaluation of the EKE was also used to obtain an optimal model configuration. Prior experiments were established with alternative boundary and forcing data sets. The results (not shown) revealed less intensity and larger discrepancy on the model EKE, specially on the EBM region, justifying our option for the SODA boundary conditions and COADS wind forcing and fluxes, whose comparative results showed better convergence.

2.3.2 Sea surface height anomalies

The austral summer and winter mean distribution for sea surface height anomalies (SSHA) is presented on Figure 2.5 for the altimetry (left) and ROMS (right) along the Western South Atlantic. A similar procedure was used by Penven et al. [2005] to validate ROMS along the Pacific coast of Peru.

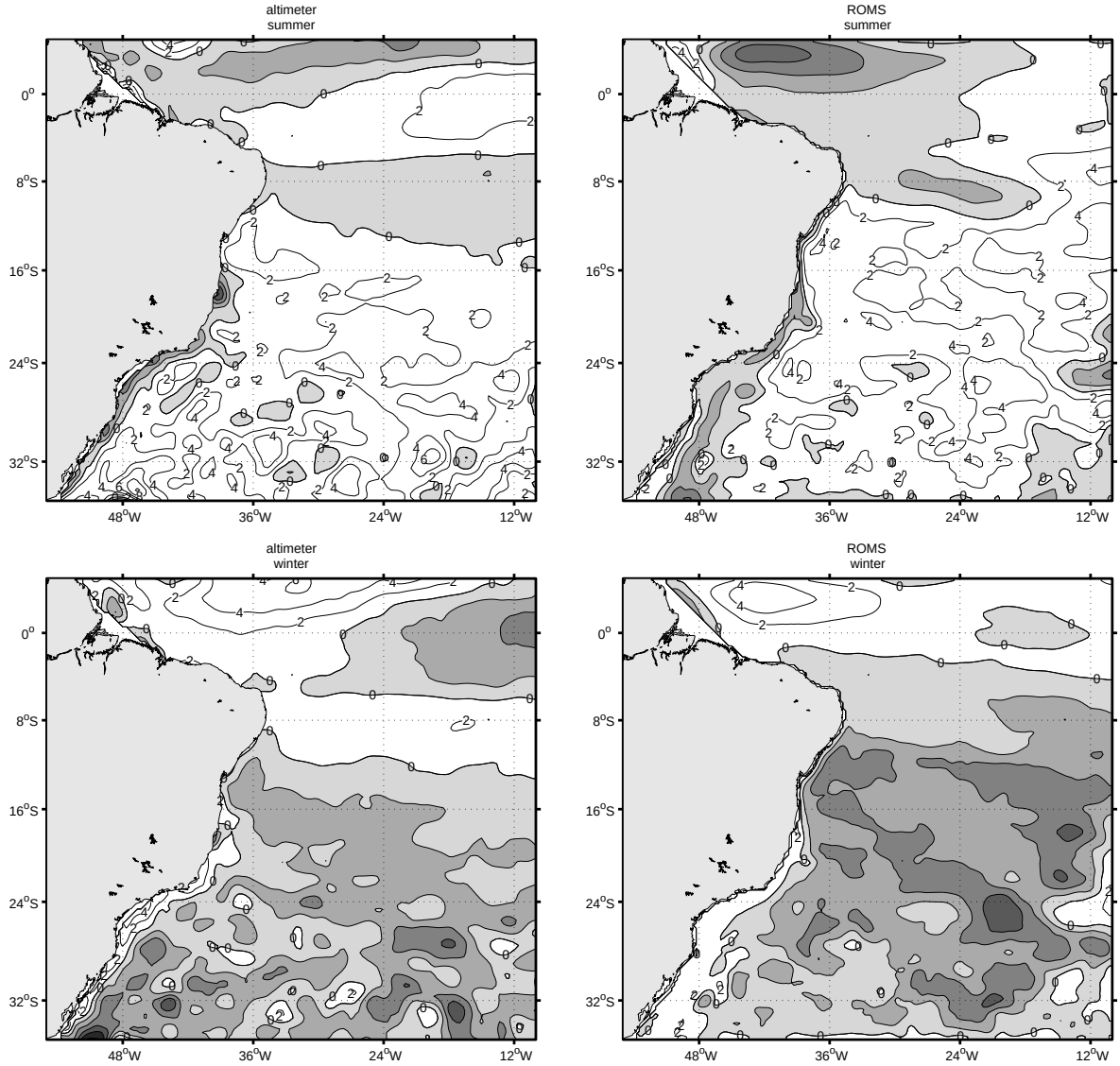

Figure 2.5: Summer and winter mean sea surface height anomalies for altimeter (left) and ROMS (right). Shading represents negative anomalies. The contour interval is 2 cm.

Higher anomalies are noticeable above the Equator and bordering the outer shelf, south of $10°S$. For the later case, the elongated outer shelf feature is coincident with the BC region and is associated with the intensification of the coastal upwelling events during summer, enhancing the negative anomalies. During winter, the prevalent south-east winds regime increase the Ekman transport towards the coast, intensifying the positive anomalies. Major differences between the EKE maps of altimetry and the model are found in the region comprised from $2°N$ to $4°S$, east of $24°W$ during winter. Altimetry suggests that EKE is much reduced in that region but such behavior is not seen in ROMS. This may be related to the failure of ROMS to reproduce some features of the equatorial circulation due to imposition of artificial boundaries on its vicinity. At latitudes higher than $24°S$, the anomalies show a very irregular pattern, with an increase of variability values at the Brazil-Malvinas confluence zone. Despite certain discrepancies, ROMS is able to capture the SSHA seasonality and presents a reasonably good spatial agreement with the altimeter data, particulary along the EBM.

2.3.3 The large scale flow pattern and transport validation

From ROMS LG model results, the general circulation patterns on the Western South Atlantic evolves from a zonal regime, typical for the equatorial dynamics, to a more irregular oceanic regime, towards higher latitudes (Figure 2.6). Along the EBM, the SEC feeds the western boundary current system, imposing variability and determining the flow patterns.

On the surface (0-100 m) layer (Figure 2.6a), the model captures the position and magnitude of a northward surface flow, associated to the NBC system (north of 12^oS) and a southward flow, associated with the BC system, south of 12^oS. Close to the SEC bifurcation, both current systems carry the oligotrophic and warm TW, brought by the SEC. At the sub-surface (100-500 m) layer (Figure 2.6b), the SEC bifurcation, which at this layer transports SACW, is captured by the model between 16^oS to 20^oS. Along the EBM, the northward NBUC flow appears as the most prominent dynamical feature.

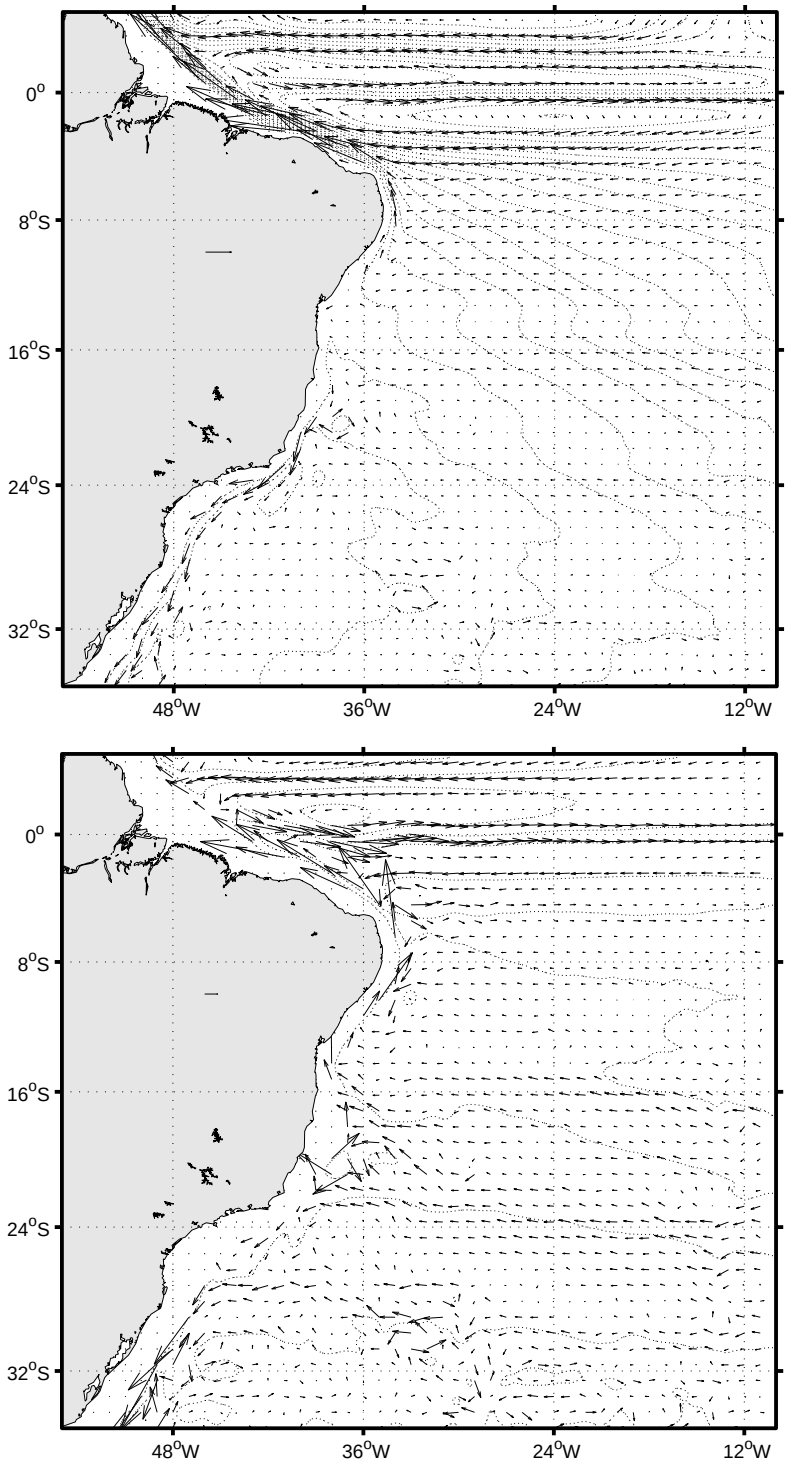

Figure 2.6: Annual mean flow (vectors) and stream function (isolines) in the western South Atlantic integrated for the layer: (a) 0-100 m and (b) 100-500 m, LG model results. The vector scale is 0.4 m s^{-1} for (a) and 0.2 m s^{-1} for (b).

According to these patterns, most of the top (0-500 m) EBM is characterized by an opposing flow, where the southward surface flow, associated to the BC, is opposed to a northward flow, underneath, associated to the NBUC. The BC appears as a relatively weaker flow that runs along the Brazilian coast and gets stronger beyond 24°S. At latitudes north of 10^oS the NBUC merges with the surface flow and the NBC system emerges, appearing as an intensified northwestward flow, moving beyond the Equator.

In order to compare our modeled results with observation, we summarized some typical EBM transport values from literature on Table 2.2. Most of the existing values are based on geostrophic estimates from historical and highly spaced hydrographic data, presenting a qualitative view of the flow but possibly biasing narrow flows, such as the intense NBUC flow, whose core is confined to a width of less than 100 km along most of the EBM (Figure 2.7). Nevertheless, geostrophic estimates are still a reference for model validation in spite of a few direct measurements made in the upper EBM (Table 2.2).

Schott et al. [2005], based on current meter array series, found a mean transport of 15.3 Sv for the upper NBUC at 11°S. The same authors, but based on five LADCP ship transects also found a mean transport of 13.5 Sv at the ($\sigma_\theta < 26.8$) layer section, west of 31.5°S (Table 2.2). These values are compatible with our model result of 14.2 Sv for the northward annual transport for the layer 0-400 m at 11°S (not shown) and higher than the geostrophic estimate of 4.7 Sv at 10°S and the 5.7 Sv geostrophic estimate for the $9° - 13°$S transect, presented by Stramma et al. [1990].

For the remaining EBM, no direct measurements have yet been published. Stramma et al. [1990] estimated a southward transport of 2.1 Sv, for February, at 15°S (Table 2.2). Our 0-100m model value, at 14°S, reveals an annual net value of 0.5 Sv, with a seasonal intensification trend towards summer. On this surface layer, where most of the BC transport occurs, and specifically for February, we found a comparable net transport of ~ 2.0 Sv (not shown).

Table 2.2: Observed meridional transport (Sv) along the Eastern Brazilian Margin. When the transport is based on geostrophic calculation, the reference level is indicated. Negative values indicate a southward transport. $1Sv = 10^6 m^3 s^{-1}$

Latitude/ Transect Long.	**Depth Ref.**	**Data Period**	**Transp. [Sv]**	**Flow System / layer**	**Reference**
$10°5'$ / $30°1'$ W	390-500m	Feb.(1975)	4.7	Transect	1
11°S	Moored Current Meter	Mar.(2000) to Mar.(2004)	15.3	Upper NBUC /$\sim (0-400m)$	2
			10.4	Lower NBUC /$\sim (400-1200m)$	
11°S	ADCP/ LADCP	Mar.(2000) to Ago.(2004)	1.6	NBUC / $\sigma_\theta < 24.5$	2
			12.9	NBUC / $24.5 \leq \sigma_\theta < 26.8$	
			10.9	NBUC / $26.8 \leq \sigma_\theta < 32.15$	
9°-13°S / 30°W	390-510m	Sep.(1926)	5.7	Transect	1
15°S / 29°59′W	470-530m	Feb.(1975)	-2.1	Transect	1
19°S	130 $cl\ ton^{-1}$ ($\sim 520m$)	Sep.(1967)	-6.5	BC	3
19°S / 30°05′W	560-670	Sep.(1967)	-0.8 (-3.7)	Transect (BC)	1
19°S	500m	Apr.(1982)	-5.3	BC	4
19°25′S	470-640m	Jun.(1970)	-5.7	BC	1
19°30′S	480-560m	Mar.(1957)	-1.0	BC	
20°03′S	590-630m	Jan.(1975)	-1.9	BC	

References: 1. Stramma et al. [1990]; 2. Schott et al. [2005];
3. Miranda and Castro [1982]; 4. Evans et al. [1983];

At 18°S, both model and geostrophic estimates reflect the dominance of the BC on the surface flow. Miranda and Castro [1982] estimated the BC transport to be of 6.5 Sv, with most of it occurring on the first 200 m. Stramma et al. [1990], using a similar data set (a closer sampled transect from September 1967) with a slightly different reference level, found a southward net transport of 0.8 Sv, for the section west of 30°S, and a BC estimate of 3.7 Sv, suggesting an intensive opposing flow along the section. Other estimates (Table 2.2) show the BC transport varying from 1.0 to 5.3 Sv . Our model presents an annual mean of 2.8 Sv for the surface layer (not shown).

Below the SACW layer, there are two major water masses, the Antarctic Intermediate Water (AAIW) and the North Atlantic Deep Water (NADW). Both layer presents a well defined circulation in our model. North of 25°S, and apart from some recirculation, the AAIW layer flows towards the Equator. Stramma and England [1999] center the SEC bifurcation at the AAIW layer south of 25° S. The model flow at the NADW layer reveals a continuous southward flow and again, a significant recirculation at the EBM, probably a reflection of the complex margin bathymetry. Although, we do not further discuss the results for the AAIW and NADW layers, the general flow pattern reported in the literature [e.g., Stramma and England, 1999; Silveira et al., 2000; Cirano et al., 2007; Rodrigues et al., 2007] seen to be captured by the model.

Moreover, considering the nesting capability, the LG and MG solutions exhibited a similar vertical structure. For comparison, the mean zonal section at 14°S for January is represented in Figure 2.7 for both grids. On the top 1500 m, they simulate a well defined western boundary flux, with the BC being represented by a southward surface flow extending to about 150 m on the shelf/slope region. Below this surface flow, the most prominent feature is the northward flowing SACW and AAIW, which extends from 200 m to about 1500 m. It is interesting to notice that, at depths deeper than 1500 m, the MG solution shows a less intense and more realistic southward NADW flow (velocities around 0.1 m s^{-1}), not underneath the AAIW flow, but with some displacement to the east. Although both solutions resemble a similar structure, the MG presents a more

detailed and accurate vertical flow distribution than the LG results, reflecting the more realistic bathymetric outline and the efficiency of the nesting procedure.

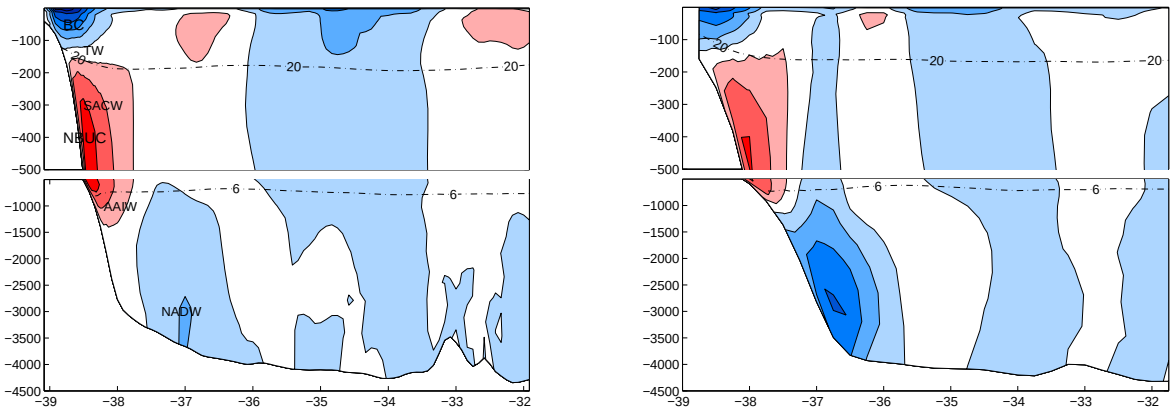

(a) (b)

Figure 2.7: Vertical section at 14°S of the modeled mean meridional velocity from (a) MG and (b) LG, in January. Red (blue) shades represent positive northward (negative southward) flow. The isotherms of 20°C and 6°C indicate the interfaces between TW/SACW and SACW/AAIW, respectively. The contour interval is 0.1 m s^{-1} and the acronyms are indicated in Figure 2.1.

2.4 The seasonal cycle

In order to investigate the seasonality of the circulation on the EBM, we analyzed monthly mean results for MG, calculated over a five years period and based on ten days average outputs. Focusing on the western boundary dynamics, zonal sections were established at the center of the region (14°S) and symmetrically on the northern (10°S) and southern (18°S) extensions of the domain. A meridional section was also established along 34°W meridian, in order to evaluate the SEC transport into the system. The reference sections are illustrated in Figure 2.1. The zonal section position combined with the EBM bathymetric outline may be visualized in Figure 2.8.

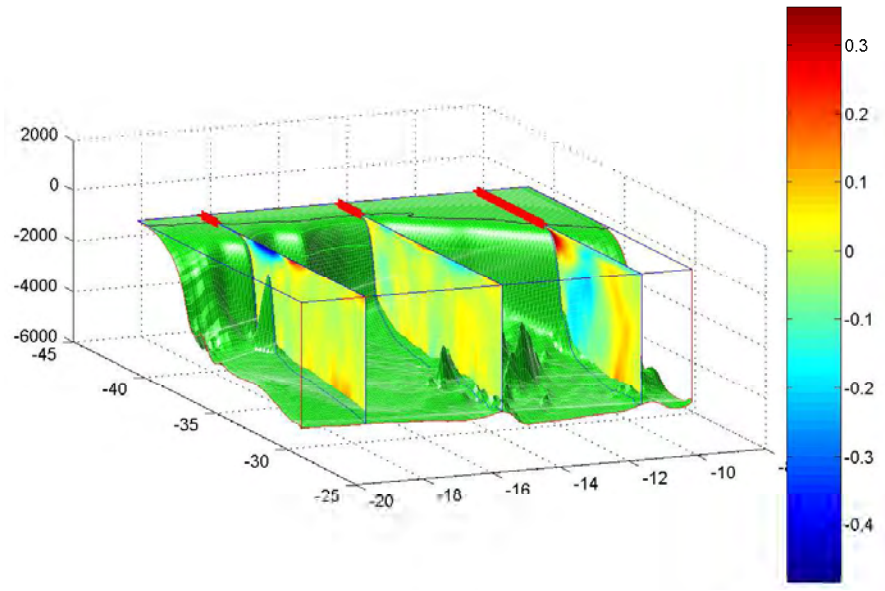

Figure 2.8: Diagram outlining the position of the zonal sections on the EBM. The vertical structure is an representation of a 10 days average of the meridional velocity (m s^{-1}), with illustrative purposes only.

The spatial and temporal variability on the EBM meridional flow through these 3 sections is synthesized in Figure 2.9, which shows the vertical structure for January, April, July and October at these sections. The isotherms of 20°C and 6°C indicate the interfaces between TW/SACW and SACW/AAIW, respectively.

Figure 2.9 shows that the EBM is subject to a marked spatial character and an intense seasonal variability. For instance, the south flowing BC appears as a seasonal flow (January and October) confined to the top few meters at 10°S and as a deeper and permanent flow at 18°S. This flow is stronger towards the austral summer. On the other hand, the north flowing NBUC appears as a permanent feature along the entire domain, getting stronger and merging with the surface flow at the northern section. The NBUC transport peaks towards the middle of the year. Quantitative transport estimates provides the basis for a EBM dynamics characterization, which is described next.

Considering that our main interest is the shelf-slope region, the meridional volume transport was calculated on each section, from the coast to the eastern limit of the main flow, which lies approximately at the 4000 m isobath. Therefore, at 10°S, the transport section was set between 34°W to 36°W, at 14°S, between 37°W to 39°W and at 18°S, between 35°W to 39.5°W. The wider section at 18°S is due to an extended continental shelf, a factor that determines a less confined surface flow on that latitude. Although the calculated transport is depended on the extension adopted, and that does not attain to a very strict criteria, we have observed that by promoting small variations on the length of the sections, the relation between the fluxes tends to remain constant. The mean meridional transport values are presented for both components of the flow and are separated in two vertical layers, here named surface (0-100 m) and sub-surface (100-500 m).

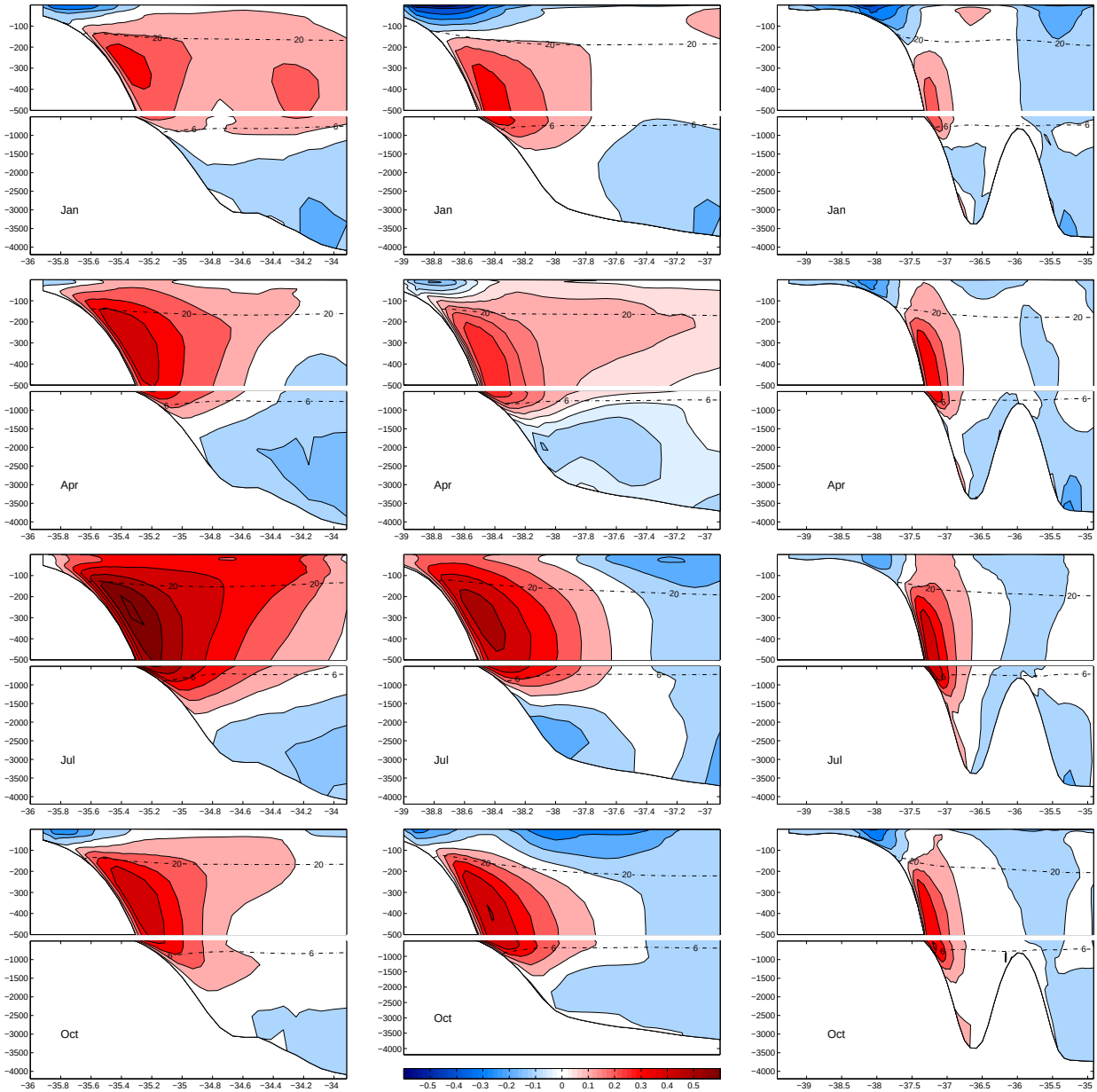

Figure 2.9: Mean meridional velocity at 10°S (left), 14°S (middle), and 18°S (right) for selected months, from top to bottom: January, April, July, and October. Red (blue) shades represent positive northward (negative southward) flow. The isotherms of 20°C and 6°C indicate the interfaces between TW/SACW and SACW/AAIW, respectively. The contour interval is 0.1 m s^{-1}.

To evaluate the onshore transport entering the EBM, mostly through the SEC flow, the zonal transport was calculated on two segments along 34°W, a northern segment from 10°S to 14°S and a southern segment from 14°S to 18°S. For these meridional sections, we present the net transport integrated over the two vertical layers defined above.

Based on the analysis of the transport summarized in Figure 2.10 (left panels), we observe that at the surface layer, the southward transport presents a flow increment towards higher latitudes, with mean annual values of 0.5 Sv (10°S), 2.4 Sv (14°S) and 2.8 Sv (18°S). The annual surface transport is dominantly towards the north, at 10°S, with a net transport of 2.7 Sv and dominantly towards the south at $18°S$, with a net transport of 1.0 Sv. This suggests that the BC appears as the dominant surface boundary current at 18°S, while at 10°S, the NBC/NBUC system is the main dominant surface feature. At the middle section, 14°S, the resultant annual surface transport (net of 0.4 Sv) is slightly towards the south. The seasonal pattern however suggests an alternate dominance of the circulation throughout the year.

At the sub-surface layer (Figure 2.10, right panels), the northward flow is clearly dominated by the NBUC transport, carrying SACW toward equatorial regions. This transport presents an increment of 6.6 Sv, varying from 8.5 Sv at 18°S to 15.1 Sv at 10°S. A steady latitudinal transport increment is observed on the southward transport. In general, the southward sub-surface transport is lower than the surface layer transport (Figure 2.10, left panels), except at 18°S, where it gets slightly stronger, indicating a deepening of the BC flow toward higher latitudes. The net transports at the sub-surface layer is always northward oriented, presenting an increment of 9.1 Sv from the southern section to the northern section.

At 10°S, the NBC/NBUC is the dominant dynamical feature. The annual variability of the transport presents a similar behavior between the surface and the sub-surface layers and a marked seasonal signal. The peak transport occurs in July and is coherent with the largest zonal inflow at 34°W presented in Figure 2.11. The southward flow,

which for most of the year transports under 1 Sv, also presents a marked seasonality, reaching a peak of 2 Sv at the end of the year. A question still opened is that if such transport could be ascribed to the origin of the BC.

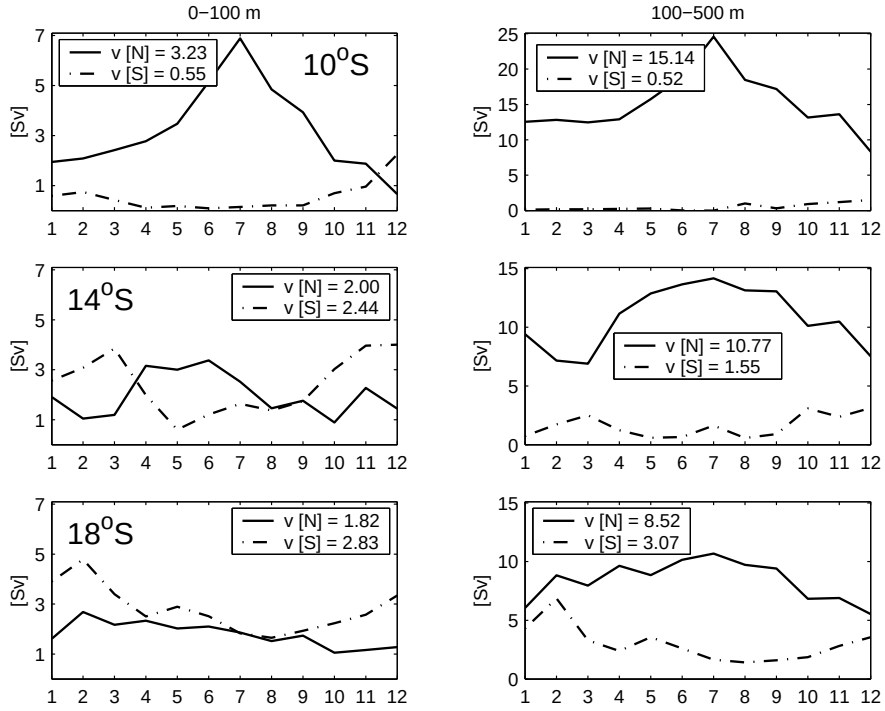

Figure 2.10: Annual cycle of the monthly mean transport (Sv) estimates along the zonal sections at 10°S (top panels), 14°S (middle panels) and 18°S (bottom panels). Northward (southward) transport is positive (negative). The left panels represent the surface layer (0-100 m) and the right panels represent the sub-surface layer (100-500 m). The annual mean transports for each direction are indicated inside the boxes. $1Sv = 10^6 m^3 s^{-1}$.

By applying an approximate transport balance, considering the 0-500 m water column, we may infer that about two thirds of the SEC that passes through the northern segment (Figure 2.11) feeds the NBC/NBUC. For instance, the annual mean zonal inflow entering the northern segment is 8.8 Sv and the increment in the northward transport from 14°S (12.8 Sv) to 10°S is of 5.6 Sv, reaching a total of 18.4 Sv. The remaining one third of the SEC zonal transport goes to the BC flow, whose increment in the southward transport from 10°S (1.1 Sv) to 14°S is about 2.9 Sv, reaching a total value of 4.0 Sv.

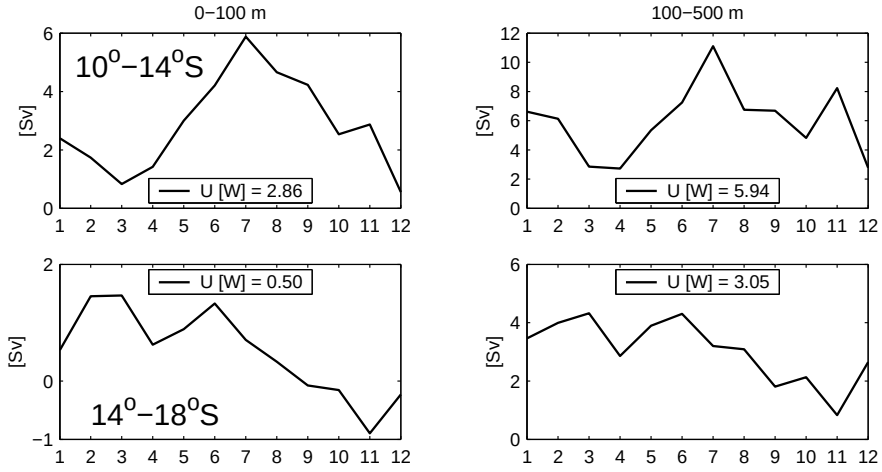

Figure 2.11: Annual cycle of the monthly mean net transport (Sv) estimates along the two meridional sections at 34°W. The top panels represent the northern segment (14°S to 10°S) and the bottom panels represent the southern segment (18°S to 14°S). Westward transport is positive. The left panels represent the surface layer (0-100 m) and the right panels represent the sub-surface layer (100-500 m). The annual mean net transport is indicated inside the boxes.

At 14°S, the transport cycle along the year presents a different character from the surface to the sub-surface layer. At the surface layer, a bimodal seasonal signal suggests an alternate dominance of the circulation, with the NBUC flow dominating from April to September and the BC flow dominating from October to March. Therefore, periods of maximum mean transport of the BC are associated to minimum transport of the NBUC. For August and September the dominance is not clear. At the sub-surface layer, the NBUC resembles a normal distribution, with the maximum mean occurring in July. In this layer, the southward transport shows an increment trend in December and a secondary peak in March, in agreement with the top layer behavior.

The 18°S section is the first section to present a clear dominance of the BC flow, at the surface layer, throughout the year. This flow presents a annual mean of 2.8 Sv, reaching as much as 5 Sv on February. At the sub-surface layer, the NBUC, although weaker when compared to the sections further north, is still dominant along the year.

Again, by applying an approximate transport balance, considering the 0-500 m water column, we may have an estimate of the SEC zonal inflow through the southern segment (Figure 2.11). The annual mean zonal inflow from 18°S to 14°S is 3.6 Sv. The increment in the northward transport from 18°S to 14°S is 2.4 Sv, reaching an annual value of 12.8 Sv at 14°S. The BC flow presents a flow increment of 1.9 Sv, from 14°S to 18°S, reaching a total value of 5.9 Sv at 18°S. Although this estimate shows an unbalance of the order of 0.8 Sv, the results suggest that at this latitude range, the SEC divergence shows the tendency to feed evenly both the northward and the southward flows.

Furthermore, the EBM presents an intense spatial variability, presenting many circulation cells, whose interaction with the main field was also registered on our transport estimates. This spatial variability will be discussed on the next section.

2.5 Spatial variability and dynamical zones

Aiming to look at the EBM spatial variability, mean temporal fields were computed for the sea surface height and for the flow pattern, at both the surface (comprising mostly the TW) and sub-surface (comprising mostly the SACW) layers (Figure 2.12). For instance, the mean field for January is dominated by an irregular flow pattern, where a succession of cyclonic and anticyclonic mesoscale gyres promotes intense cross-shelf water exchanges.

Considering the dynamical structures observed on a spatial and a seasonal perspective, we may divide the EBM in three dynamical zones. The northern zone, from 8°S to 13°S is marked by a cyclonic circulation cell with a low sea level signature in the center. The life cycle of this feature is very clear on the plots for July and October (Figure 2.12a). On an annual basis (not all months are shown), this structure starts to develop in May, gets very intensified and almost stationary from June to September

and loses its signature gradually in October and November.

The middle zone, located from 13°S to 16°S (on the oceanic zone comprised between the cities of *Salvador* and *Ilhéus*) is characterized by two distinct and well defined flow regime during the year. From October to March, the main flow is dominated by the southward flowing BC (see Figure 2.10 for the mean monthly transports and Figure 2.12b,c for the flow fields for January and October), while from April to September, the NBUC northward flow is dominant (see Figure 2.12b,c for the mean monthly fields for April and July). A less marked transitional flow pattern is revealed in April, August and September. Its important to remind that for the BC, most of the flow is confined to the top 100 m. The shelf width in this region is very narrow and the coastal circulation reveals to be closely tied to the oceanic mesoscale processes, with intensification or flow reversals being associated to these features. The knowledge of such variability is particularly important here since the region between the bays (BTS and CMB in Figure 2.1) is very relevant to fishery and oil activities.

The southern zone, from 16°S to 20°S, is marked by an extended and irregular shelf, developed between two major banks, the *Royal Charlotte* Bank (16°S) and the *Abrolhos* Bank (Figure 2.1). This irregular topography constraints and alters the flow, inducing spatial variability in physical, chemical and biological features over the shelf [Knoppers et al., 1999] and in adjacent oceanic waters.

Pereira et al. [2005] found an evidence of cross isobath residual barotropic currents due to tide interaction with topography. The authors reported that this process was particularly important on the southern flanks of the Abrolhos banks, where the tidal ellipses associated to the northern propagation of the barotropic tide were perpendicular to the slope of the flanks. The result for this interaction was the generation of upwelling favorable areas on the southern part of the flank and downwelling favorable areas on the northern flanks. Upwelling and downwelling were also modeled along the flanks on the Royal Charlotte bank, although not as intense as those found on the sides of Abrolhos

bank [Pereira et al., 2005]. Our model includes no tidal forcing and relatively cooler and fresher water were a recurrent feature on the shallow areas around Abrolhos bank, suggesting to be associated to upwelling process. Additionally, the surface flow is southward oriented throughout the year (Figure 2.12b), an indication of a perennial BC flow at this latitude. From September to April, a flux divergence, shifting between 17° to 19°S with resultant flow towards the south, represents an intensification on the BC flow.

When considering the three zones together, the flow patterns on the EBM appear to be in close agreement with the annual pattern for the trade winds, the prevailing wind system on the tropics. The trade winds are associated to the dynamics of the high pressure South Atlantic Anticyclone, blowing from east and northeast during spring and summer (October to March), when the South Atlantic Anticyclone cell is displaced towards the south, and from southeast during autumn and winter (April to September), when the anticyclone is at its northernmost position [Nimer, 1989]. Accordingly, Rodrigues et al. [2007] state that positive (negative) wind stress curl produces an anomalous anticyclonic (cyclonic) circulation, whose southward (northward) component near the western boundary causes the SEC bifurcation to occur at a lower (higher) latitude during austral spring /summer (winter) months. Therefore, and in agreement with Rodrigues et al. [2007], our results show that during austral summer, when the SEC bifurcation occurs at a lower latitude, an intensification on the southward BC transport is observed, while during austral winter, when the SEC bifurcation occurs at a higher latitude, an intensification of the northward NBUC transport occurs.

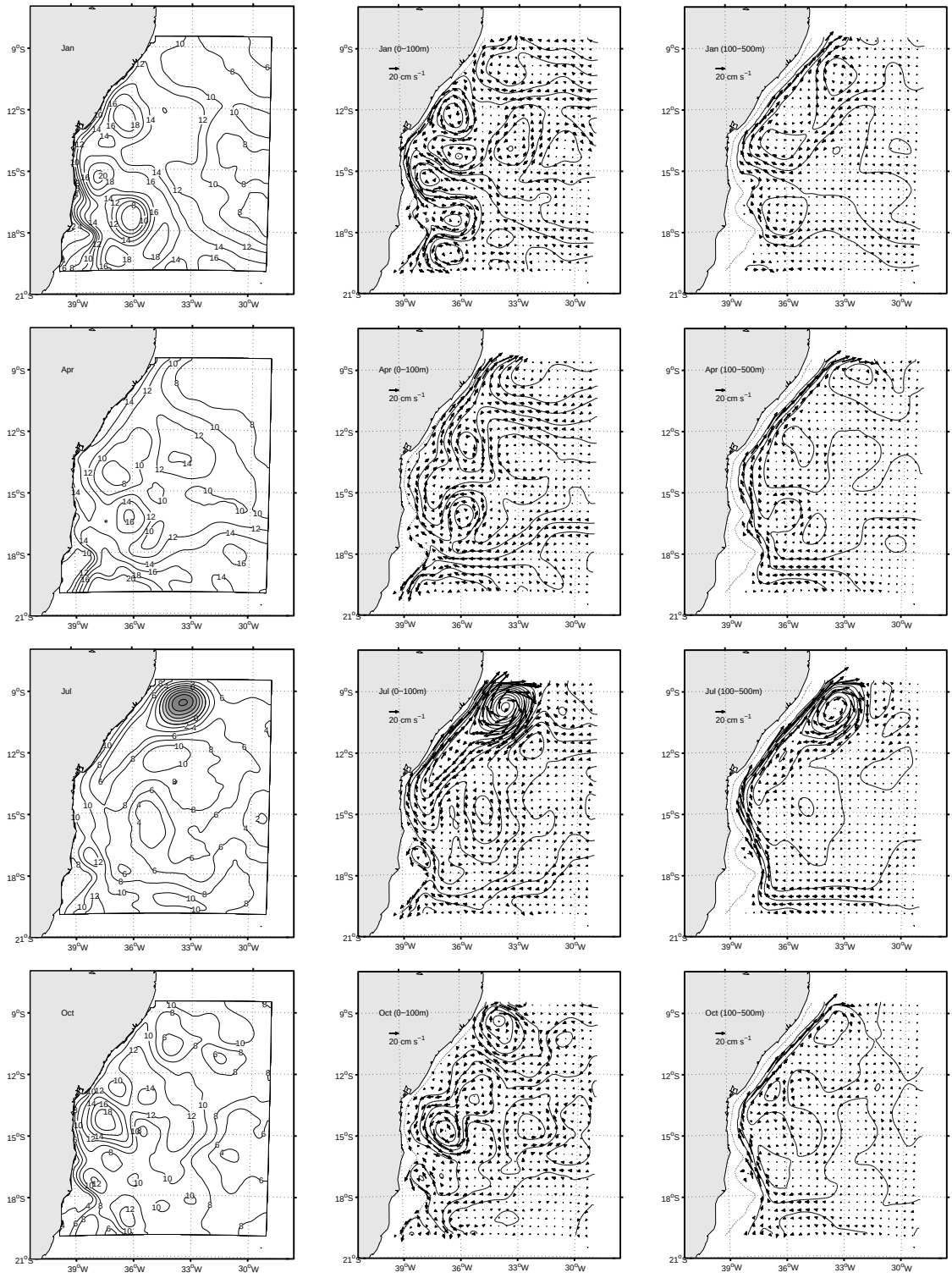

Figure 2.12: Monthly mean horizontal distribution of (a) the sea surface height(cm) and the integrated flow field for two distinct vertical layers (b) 0-100 m and (c) 100-500 m. From top to bottom, months are January, April, July and October. Superimposed solid contours on (b) and (c) represent the stream function patterns. The dotted line on those plots indicates the 200 m isobath.

2.6 Eddy interactions on the Eastern Brazilian Margin

The model results reveal an intense mesoscale activity along the EBM. These mesoscale features coexist with the large-scale circulation, may evolve into eddies and, in such cases, have a certain life time and a translation character. In this section, we discuss the behavior of a cyclonic and an anticyclonic eddy, detached from the main flow along a modeled annual cycle. Although mesoscale features are recurrent in all years of the model results, here and for a qualitative analysis, we only discuss the model results for the fifth MG year cycle, as reference.

We start our description with the cyclonic eddy (Figure 2.13), formed at the offshore region just north of the Abrolhos Bank (18°S). The geneses of this feature involves the interaction with two neighboring anticyclonic eddies (Figure 2.13a). The most important contribution comes from the northern eddy, which approaching from the upper limit of the Royal Charlotte Bank (16°S), favors an intense zonal flow. Due to local bathymetric constraints, this eddy plunges parcels of shelf waters toward deep waters (Figure 2.13a). On its origin, the cyclonic eddy incorporates cooler, coastal upwelled water (surface temperature in the coastal vicinity over the *Abrolhos* Bank is around 24°C, whereas the adjacent oceanic waters is around 28°C). After being formed, the cyclonic eddy gets individualized and remained almost stationary for more than a month (Figure 2.13b). After so, it shows a translation character and rapidly propagates northward. At this point, the feature experiences a reorganization, assuming an elliptical shape (Figure 2.13c), being finally observed at the northern part of the EBM on the mid of June (Figure 2.13d). A composite altimetric image from AVISO on mid April 2004, and the calculated geostrophic field associated to it (Figure 2.13e), which resembles the geneses presented in Figure 2.13a, is used to illustrate the occurrence of such process in the region, showing compatible length and time scales.

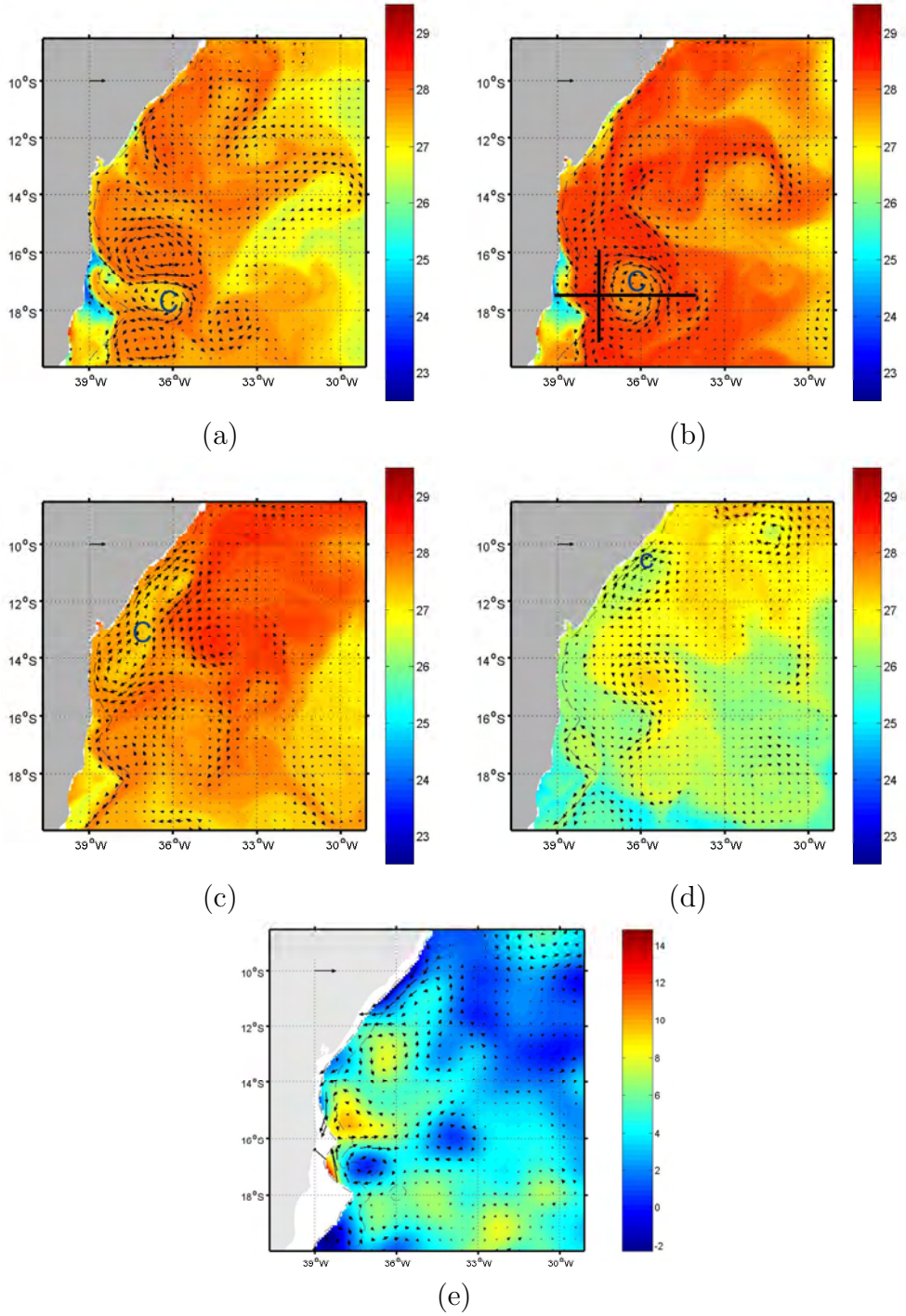

Figure 2.13: The geneses and life cycle of a modeled cyclonic system (signed with the letter C) on the EBM during an annual cycle and based on the 10 days averages of the horizontal velocity and temperature distribution at 10 m. (a) mid of January, (b) mid of February, (c) end of April, (d) mid of June. (e) A composite altimetric image from AVISO data set and its calculated geostrophic field distribution for mid of April 2004. The vector scale is 1 m s^{-1}.

The second pattern described here is related to the anticyclonic eddy (Figure 2.14). The formation of this feature was traced back to August, at around 12°S (Figure 2.14a). The feature propagates southward, following the main flow for the period of a month or so (Figure 2.14b), when it then interacts with the shelf region and appears better individualized and intensified during the period of October/November (Figures 2.14c,d). In analogy to what was presented for the cyclonic feature, a composite altimetric image for the mid of September 2004 with the associated calculated geostrophic distribution (Figure 2.14e), presents a well defined anticyclonic eddy, north of 16°S, adding physical evidence to our model results. It is important to emphasize that, for either cases, our description is focused on the major feature and its related translation pattern. Less important features, sometimes presenting erratic patterns have also been observed.

On our model results, a typical southward extension for the anticyclonic feature is coincident with the region limited by the northern flank of the *Abrolhos* Bank, which is also the geneses region for the cyclonic feature. The translation patterns appear to be temporally connected to the intensification of the main seasonal EBM flow patterns, with the cyclonic northward translations occurring preferentially in the first half of the year (when the NBUC starts to intensify) and the anticyclonic southward propagation occurring in the second half of the year (when the BC starts to intensify).

On their pathways, these features interact with the near-shelf region. Their dynamical structure during such events, the cyclonic eddy during mid February (Figure 2.13b) and the anti-cyclonic eddy during mid November (Figure 2.14d), are explored in two specific sub-sections. Our aim here is to foster new ideas on the EBM near shelf-dynamics, specially regarding the impacts of the remote forcing on the local circulation.

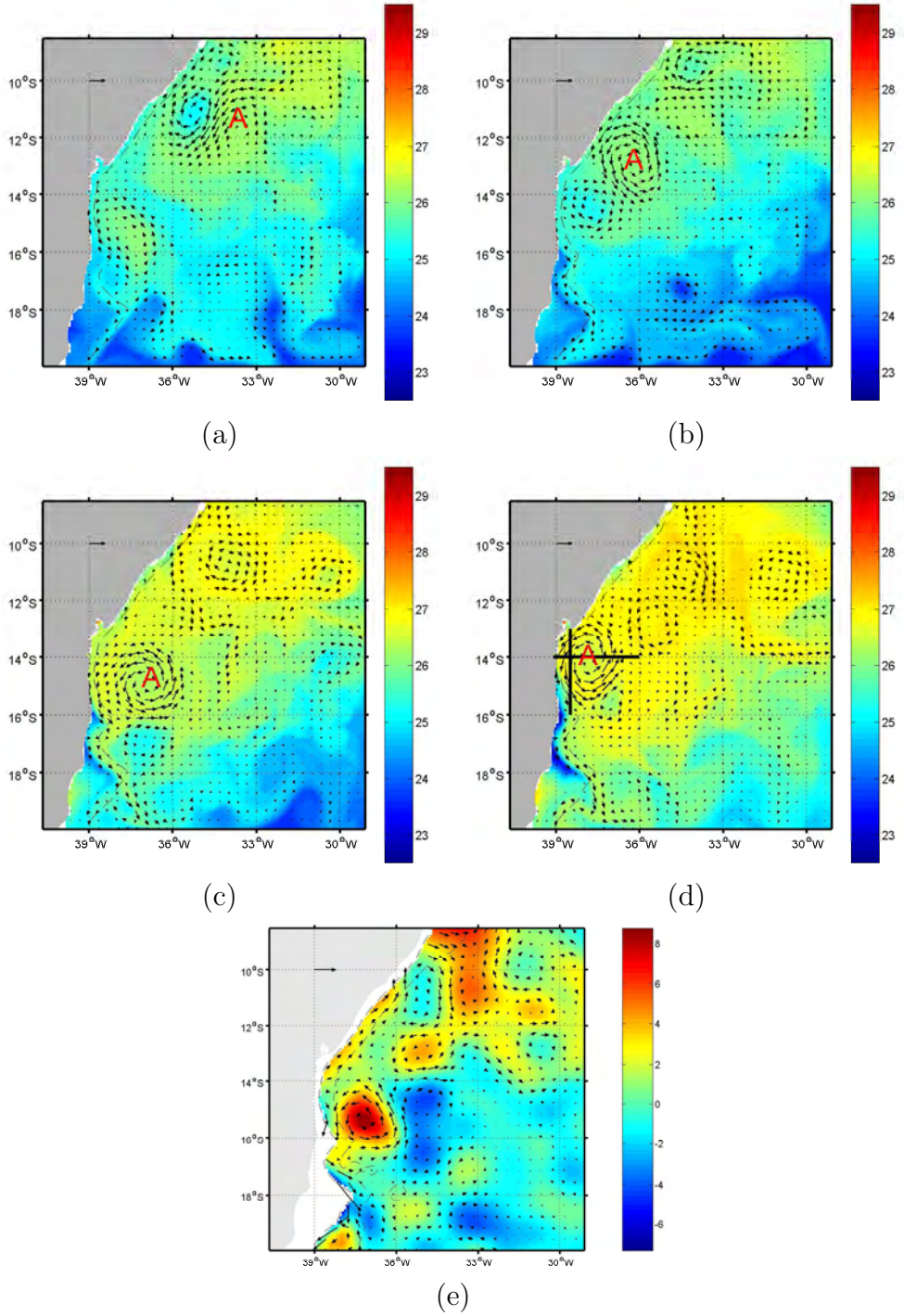

Figure 2.14: The geneses and life cycle of a modeled anti-cyclonic system (signed with the letter A) on the EBM during an annual cycle and based on the 10 days averages of the horizontal velocity and temperature distribution at 10 m. (a) beginning of August, (b) mid of September, (c) end of October and (d) mid of November. (e) A composite altimetric image from AVISO data set and its calculated geostrophic field distribution for mid September 2004. The vector scale is 1 m s^{-1}.

Furthermore, Campos [2006], invokes a possible northward propagation behavior for the cyclonic *Vitória eddy*. Our MG domain (Figure 2.2) does not extends south of the *Abrolhos* Banks, where the *Vitória eddy* has been experimentally reported [Schmid et al., 1995]. An extra experiment set however, with a larger domain (not shown), has shown evidences of a recurrent *Vitória eddy*, south of the *Abrolhos* Banks as well as the mesoscale dynamics described above. According to our analysis, these features may not be referred to a northward propagation of the *Vitória eddy*, but as mesoscale features, formed north of 19°S, that indeed present a seasonal northward propagation character.

2.6.1 Snapshot over a cyclonic eddy

On mid February, a mesoscale cyclonic eddy appeared well developed, centered at $\sim 17.25°$S and 36.25°W (Figure 2.13b), on the offshore waters adjacent to the *Abrolhos* bank. At that time, the eddy was cyclonic (clockwise), associated with a negative sea surface height reaching up to 11 cm on the core. it had a 130 km diameter, remaining stationary for a few days. At 10 m depth, it presented maximum cross-shore (u) velocity component of 0.85 m/s eastwards at its northern limit (16.25°S) and of 0.95 m/s westwards at its southern limit (18.25°S). The alongshore velocity component (v) reached 0.83 m/s southwards at the eastern limit (35.25°W) and 0.71 m/s northwards at the western limit (37.25°W).

Figure 2.15 shows a latitudinal (top panels) and meridional (bottom panels) section of the velocity structure and the associated hydrographic properties. The isotherms (Figure 2.15b) and isohaline contours (Figure 2.15c) are tilted upwards on the center of the eddy, suggesting an eddy induced upwelling, whose effect extends over the 500 m depth. On the coast side of the eddy, a prograding front, noticed on the hydrographic sections, suggests that offshore water is brought to the shelf domain, a possible combined effect of the coastal upwelling process and the cyclonic translation. The divergence of the surface layers also favors the southwards near-shelf flow (Figure 2.15a), inducing an intense zonal flow and a sharp flow gradient with the cyclonic eddy itself.

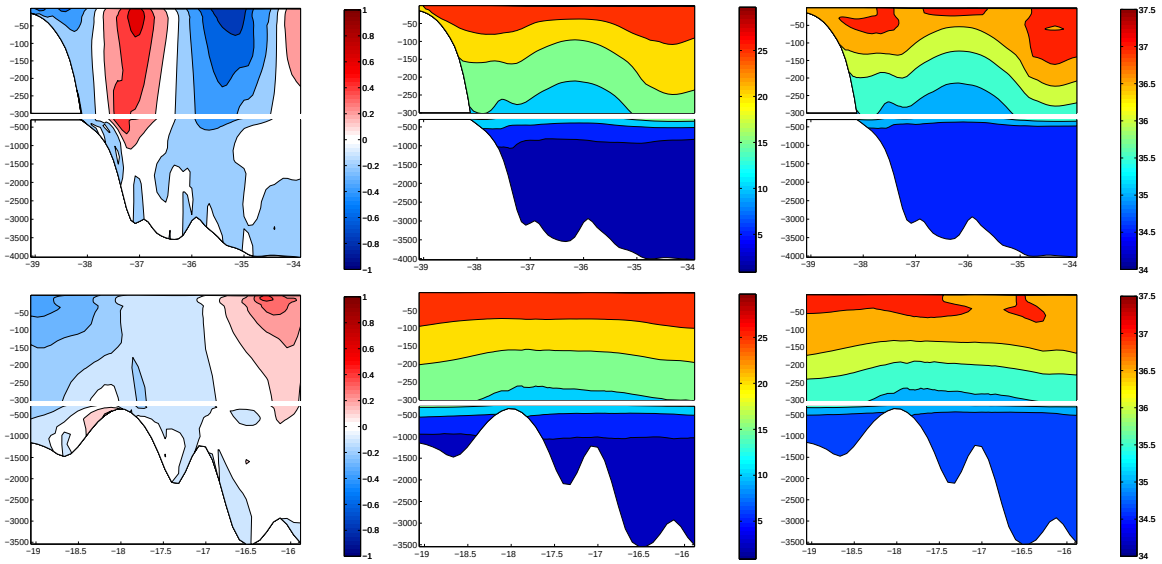

(a) (b) (c)

Figure 2.15: Latitudinal (top) and Meridional (bottom) sectional structure for Velocity (a), Temperature (b) and Salinity (c) along a modeled cyclonic (clockwise) eddy on the EBM, on mid February. The location of these sections are represented in Figure 2.13b.

2.6.2 Snapshot over an anti-cyclonic eddy

On mid November, a mesoscale eddy, appeared at $\sim$ 14.00°S and 37.75°W, at the vicinity of *Baía de Camamu* and *Baía de Todos os Santos*, the two major coastal systems on the EBM (Figure 2.14d). This eddy was anti-cyclonic (anti-clockwise), reaching a positive sea surface height of 25 cm at the core. It presented an elliptical shape on surface, with a minor latitudinal axis of $\sim$ 175 km and a major longitudinal axis of $\sim$ 250 km. At 10 m depth, the velocity field extended to a diameter of $\sim$ 270 km, and assumed a more regular shape. The eddy presented maximum cross-shore (u) velocity component of 0.8 m/s, westwards at its northern limit (13°S), with highest intensity over the shelf. At its southern limit (15°S), the highest velocity was also of 0.8 m/s eastwards, around 38.25°W. The alongshore velocity revealed a pronounced asymmetry, with the alongshore (v) component, reaching 1.2 m/s, southwards, over the shelf, at the westernmost limit (38.85°W) and 0.8 m/s, northwards, at the eastern limit(37.00°W).

The sections presented in Figure 2.16 for the latitudinal (top panels) and meridional (bottom panels) axis of the eddy reveal some possible connections of the anti-cyclonic feature with the regional dynamics. The isotherms (Figure 2.16b) and isohaline contours (Figure 2.16c) are tilted downwards in the center of the eddy, suggesting a downwelling process, whose effect extends to depths over 200 m. On the near coast side of the eddy, an asymmetric alongshelf flow structure and a pronounced near coast tilting up for the hydrographic properties are noticeable, suggesting water renewal, a possible result of the meander coupling with the coastal dynamics.

Connections of eddies with upwelling coastal system have been studied on the Southeastern coast of Brazil [Calado et al., 2006]. Asymmetries on the eddy structure were associated to such interactions. Feedback mechanisms with the coastal processes are likely to happen. The very intense alongshore and sharp flow gradients associated to the meandering structures, may be enhancing shelf edge upwelling, that in turn, contributes to maintain the flow structure gradient.

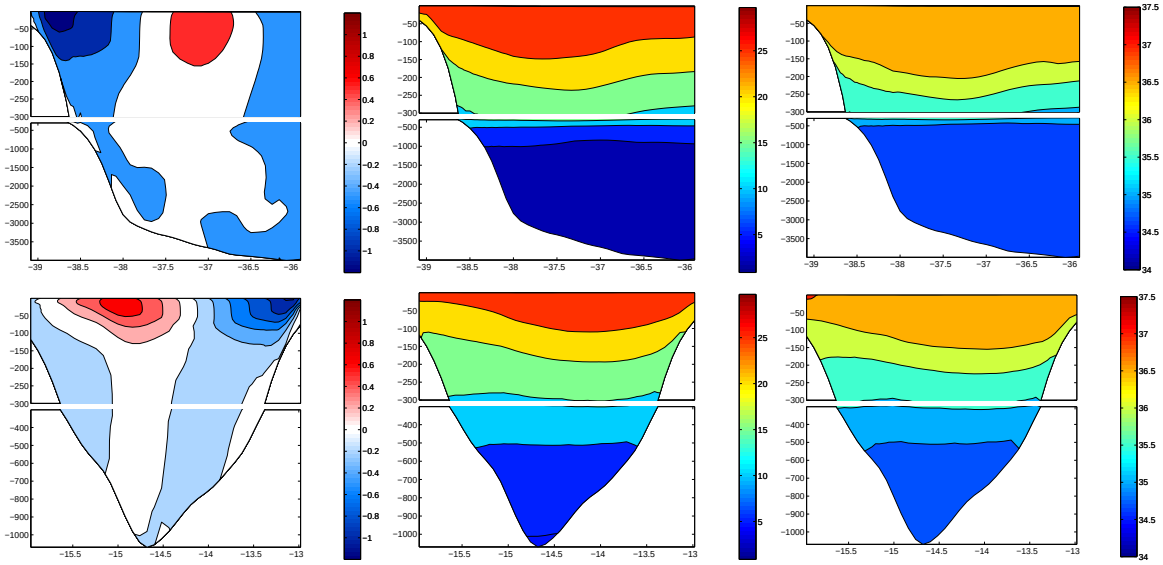

(a) (b) (c)

Figure 2.16: Latitudinal (top) and Meridional (bottom) sectional structure for Velocity (a), Temperature (b) and Salinity (c) along a modeled anti-cyclonic (anti-clockwise) eddy on the EBM, on mid November. The location of these sections are represented in Figure 2.14d.

2.7 Concluding remarks

In this work, an effort was done to evaluate the main circulation patterns of the Eastern Brazilian Margin (EBM), focusing on its seasonal variability and on the interaction between mesoscale features, the mean flow and the associated coastal region. The circulation in the area, has shown to be markedly influenced by the large-scale circulation driven by the South Equatorial Current (SEC) divergence. The SEC represents the northern limb of the South Atlantic Subtropical Gyre, a large-scale feature, that if not specified properly at the boundary, imposes the first problem for a regional circulation model. To cope with this difficulty, we adopted the nesting capability integrated into the Regional Ocean Modeling System (ROMS), retaining on the regional solution the connections and forcing from the large-scale circulation.

In order to validate our modeling system, in a region where the data is scarce and irregularly sampled on space and time, we made use of eddy kinetic energy estimates from satellite altimetry. Our validation procedure revealed that for the EBM zone (8°S to 20°S) there is a reasonable agreement between the mean model outputs and the satellite data. On higher energetic zones though, such as the low latitude equatorial zone or the Brazil/Malvinas Confluence zone, the model had the tendency to underestimate the ocean variability. The modeled results were also compared with the few observations available for the region and the transports obtained were compatible with those found in the literature. Based on the results above, we believe that the nesting technique adopted here have shown to be adequate and realistic to study the circulation on the EBM.

The EBM not only has a complex dynamics, but also hosts some of the most important coastal and biological systems along the Brazilian coast, such as the coral reef aggregation on the Abrolhos Bank region or the two major bay systems: *Baía de Todos os Santos* and *Baía de Camamu*. Apart from Stramma et al. [1990] and Rodrigues et al. [2007], and prior to this work, the EBM dynamical connectivity was virtually unknown.

The EBM is divided into three zones, according to their distinct seasonal dynamical features. These were geographically defined as the northern zone (8°S to 13°S), the middle zone (13°S to 16°S) and the southern zone (16°S to 20°S). The results have shown that these zones are seasonally connected either by the mean flow or by the mesoscale variability on the flow.

The permanent mean flow is deeply influenced by the divergence of the southern branch of SEC, which is responsible for feeding the major western boundary currents, known as the Brazil/North Brazil Current system. For the surface layer (0-100 m) and at the northern zone, the North Brazil Undercurrent (NBUC) is the main dynamical permanent feature (annual mean transport of 3.2 Sv), while the Brazil Current (BC) is just a thin flow confined to the top few meters (annual mean transport of 0.5 Sv). As we move southwards, the BC deepens and its transport is intensified. On the middle zone, the dominance of the surface layer circulation seasonally alternates between the southward BC flow (annual transport of 2.4 Sv) and the northward NBUC flow (annual transport of 2 Sv), while around the Abrolhos Bank, on the southern zone, the BC appears as the dominant surface feature (annual transport of 2.8 Sv) and has a perennial character.

On subsurface waters (100-500 m), the NBUC connects the EBM continuously, with the annual mean transport increasing northwards from 8.5 Sv (18°S) to 15 Sv (10°S), while the southward BC flow increases in a reverse manner, from 0.5 Sv (10°S) to 3 Sv (18°S). Considering the surface and the sub-surface layers together and on an annual basis, our results also show that the SEC has a different contribution into the BC/NBC system according to the region. In the northern part of the domain (10°S to 14°S) only 1/3 of this zonal flow feeds the BC, while the remaining is incorporated into the NBUC flow. In the southern part of the domain (14°S to 18°S) this relation reaches an almost evenly balance.

When considering the three zones together, the flow patterns on the EBM appear to be in close agreement with the annual cycle for the trade winds, the prevailing wind system for the tropics. Our results show that during austral spring and summer (when easterly and northeasterly winds prevail), the SEC bifurcation occurs at a lower latitude, and an intensification of the southward BC transport is observed. During austral autumn and winter (when southeasterly winds prevail), the SEC bifurcation occurs at a higher latitude, and an intensification of the northward NBUC transport occurs. Our results are in agreement with the pattern proposed by Rodrigues et al. [2007] for the SEC divergence.

The regional simulation reveals intense mesoscale activities. Well defined cyclonic and anticyclonic eddies detached from the main flow are seen translating throughout the domain along the year. The translation of these features are connected to the seasonal main EBM flow, with cyclonic (anticyclonic) eddies preferably translating northward (southward) along the first (second) semester of the year. The physics involved on this dynamics are far beyond the scope of this work and continues as an open issue, which should be properly addressed in a future work.

Modeling evidences of interactions with the near-shelf dynamics are presented for both cases. Such direct connections have never been reported on the regional oceanographic literature. Considering that tropical shelves governed by western boundary currents are the least productive ocean margins of the world, unless land run-off and eddy induced shelf-edge upwelling become significant [Walsh, 1988], those interactions, if experimentally proved, may have environmental relevance on the oligotrophic EBM dynamics.

Chapter 3

Physical setting, hydrography and circulation of *Baía de Camamu*. Field results covering dry and rainy conditions.

3.1 Introduction

Baía de Camamu (CMB) is an important fishing, mining and touristic site located at the central coast of the state of Bahia (14°S; 39°W) on the Eastern Brazilian Margin (EBM), Figure 3.1. The CMB is a shallow system, mostly well preserved [Hatje et al., 2008] that occupies a flooding area of 384 km^2, being surrounded by small cities and extensive mangrove vegetation [Oliveira, 2000].

Baía de Camamu presents numerous small islands and several small-scale fisheries communities whose population is engaged on artisanal fishing [Souza and Petrere-Jr, 2008] and subsistence agriculture practices. On the shelf zone adjacent to CMB entrance, coral structures, such as those described on classical works (e.g. Spix and Martius [1828]) still thrives while on the hinterlands, remanent of the Brazilian Atlantic Rain Forest are found. In the municipality of *Camamu*, a long lasting tradition

of wood boat building is still active, while in other watershed surrounding zones, such as in *Barra Grande*, touristic activities flourishes.

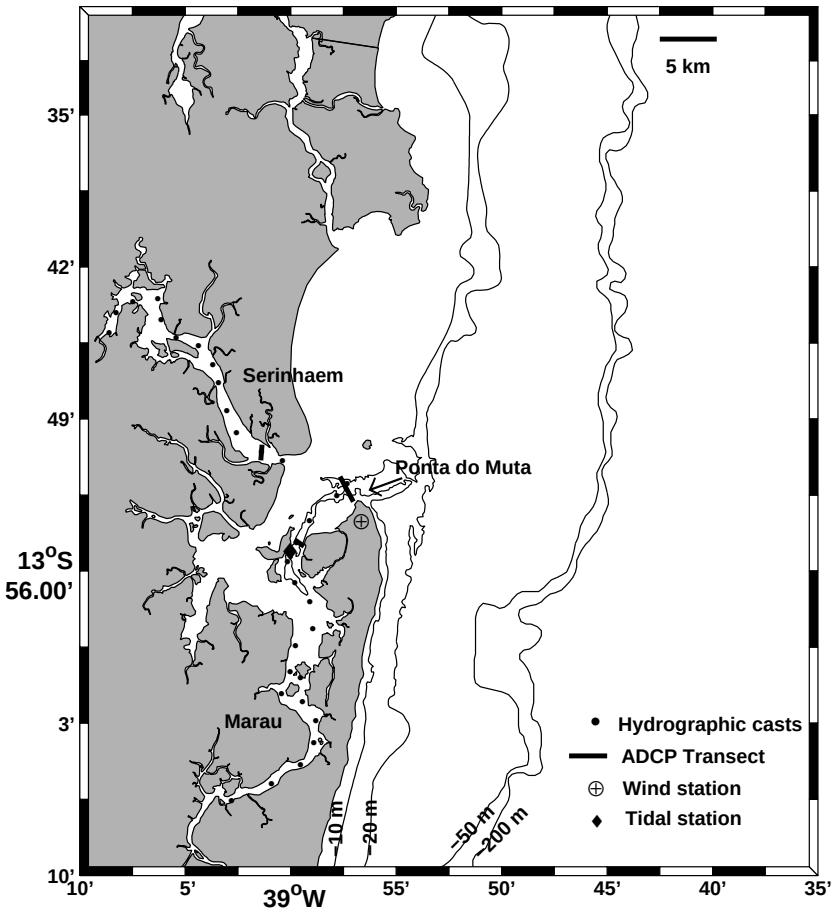

Figure 3.1: Map of *Baía de Camamu*, depicting its bathymetric distribution and sampling strategy.

Nevertheless, CMB occupies the central region of *Camamu* Basin, a marginal sedimentary cretaceous basin that extends from the coastal plains to the 2000 meters isobath, for about 130 km along the EBM. This sedimentary basin is limited on North by the *Jacuípe* Basin and on South by *Almada* Basin, occupying an area of 15000 km^2 [Souza-Lima et al., 2003], granting *Camamu* Basin a great economic potential on oil and gas reserves [ANP, 2009]. In the past few years there has been increasing attention on CMB oil reserves and recently eighteen areas on its adjacent continental shelf were offered for concession during international auctions, including six areas located in

shallow waters located a few kilometers from the coast. Commercial gas exploration have started on 2007 [ANP, 2009]. The local residents fears of episodic or systematic contamination of *Baía de Camamu* by such activities while numerical simulations performed by Amorim [2005] predict that oil spill from such oil fields, in the worst scenario, could reach the bay within one day.

Despite the social, environmental and economic values of CMB, there is still a lack of scientific references regarding its basic climatology, physiography and hydrodynamics, which are important keys for establishing environmental precautionary plans involving oil and gas activities. In order to address this deficiency and basing on a comprehensive and original sampling effort, this work aims to provide the first time description of the physical oceanography of *Baía de Camamu* summarizing the physical setting and investigating the water dynamics along two distinctive sampling periods, covering dry and rainy conditions. By doing so, we give a contribution on the multidisciplinary discussion regarding its maritime planning and preservation.

This work was organized with the following structure. Following the introduction (section 3.1), we present the regional physical setting of *Baía de Camamu* (section 3.2), which summarizes the physiography (section 3.2.1), pluviometry (section 3.2.2), fluviometry (section 3.2.3) and regional wind field (section 3.2.4). Section 3.3 provides the sampling strategy and some data processing procedures. The field contribution of this work comprises the tidal characterization and an analysis of sea level variabilities on inner *Baía de Camamu* (section 3.4), an evaluation of the pluviometric and discharge conditions concurrent field surveys (section 3.5) and the field data analysis, covering a dry (September 2004) and a rainy (July 2005) sampling effort (section 3.6). A summary and a discussion of the major results is presented in section 3.7 while the concluding remarks is presented in section 3.8. Finally, an appendix provides a *Baía de Camamu* discharge estimate, based on instantaneous basin point sources, soil composition and relative sub-basin sizes.

3.2 Regional settings of *Baía de Camamu*

Scientific references for *Baía de Camamu* are scarce, the majority being disperse on unpublished, hard-to-access technical reports. In this section we summarize the physical background setting, adding new interpretation to the available information. This information is the basis for the interpretation of our original survey efforts.

3.2.1 Physiography

Baía de Camamu forms a complex and shallow physiographic system that receives contribution from many tributaries. Its watershed has a mean depth of 5 m, distributed on three major connecting channels (Figure 3.2). On the north region, the *Serinhaém* river occupies a flooding zone of 106 km^2. The central bay zone is marked by low water depths (3.3 m mean) and narrow tributaries (*Igrapiúna*, *Pinaré* and *Sorojó* rivers), which, together, occupy a flooding area of 158.3 km^2. On the south region the *Maraú* river occupies a flooding zone of 119.4 km^2. Mangrove surrounds the mean tributaries almost evenly, covering about 39% of the flooding region at the central tributaries, 43% at the *Maraú* system and 48% at the *Serinhaém* system [Amorim, 2005].

The CMB watershed connects with the adjacent continental shelf through one main channel ∼6400 m wide, oriented SW-NE from *Ponta do Apaga Fogo* (SW) to *Ponta do Mutá* (NE). This main channel has around 15 m deep on its eastern and deeper side. On its western portion the bottom topography is very irregular, being marked by the presence of numerous rocks and sand banks as shallow as 3 m. From its deeper portion, the ∼6400 m wide entrance channel is reduced towards the interior of the system, being ∼800 m wide at *Serinhaém* channel entrance, ∼2200 m wide towards *Maraú* channel and ∼1300 m wide towards the central region. Among all the CMB tributaries, only the *Maraú* and the *Serinhaém* present well defined channels. The *Maraú* has a mean depth of 6.2 m but its mean channel may reach a maximum of 37 m depth. The *Serinhaém* has a mean depth of 7.3 m but on its right margin the depth reaches 25.2 m. The central zone tributaries are very shallow, with depths lower than 7 m.

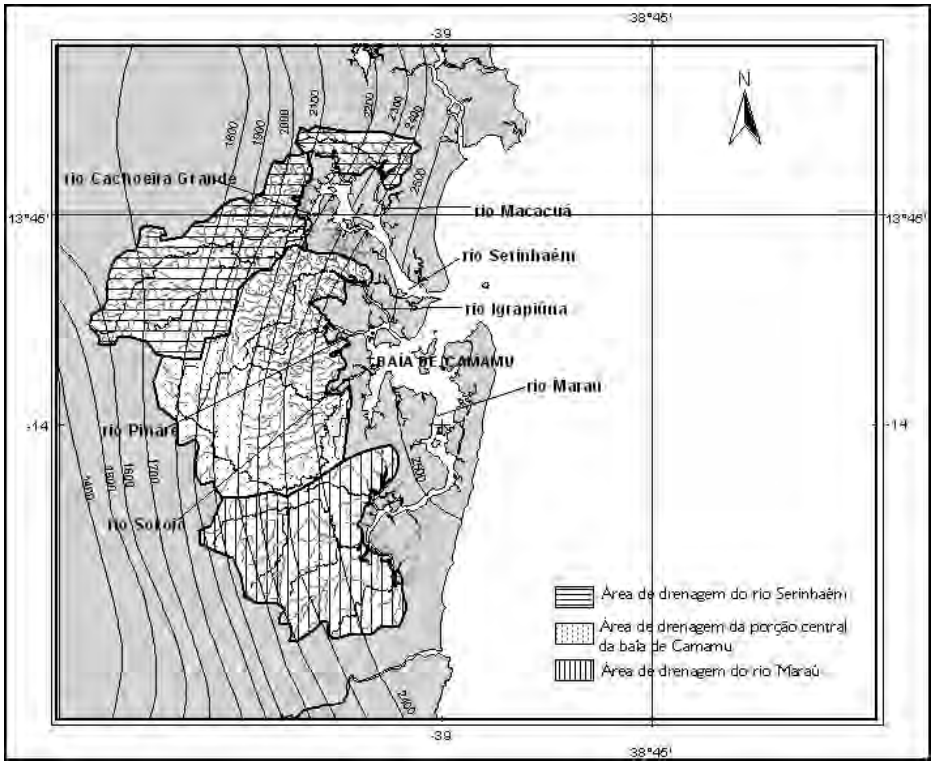

Figure 3.2: Drainage basin of the main *Baía de Camamu* tributary system. The *Serinhaém* system, at the north, the *Igrapiúna*, *Sorojó* and *Pinaré* systems at the central bay zone and the *Maraú* channel, at the south. Representation, at 1:100.000, based on the digital cartographic database from SEI [2000]. Isocontours are precipitation curves based on SRH [2003].

The adjacent continental shelf has a mean width of 16 km close to the bay entrance and 12 km off to the *Peninsula Maraú*, the elongated sedimentary barrier that separates the bay from the ocean. North of the main bay entrance there is a shallow (10 m depth) embayment where a continental shelf of 27 km width is observed. In average, the shelf breaks at 70 m depth. The bottom of CMB is covered by recent siliciclastic muds from continental origin, with variable organic content. This composition extends toward to the North portion of the *Peninsula Maraú*, while on its oceanic region quartz sand and biodetritic material from coral algae structures are abundant [Amorim, 2005].

3.2.2 Pluviometry

The latitudinal extensive coastal zone of the state of *Bahia* is characterized by a tropical and humid climate whose pluviometry is typically marked by high precipitation during Autumn and Winter. Spatially, the regime trends to a more uniform distribution towards the south [Araújo and Rodrigues, 2000]. To provide a regional characterization of the CMB precipitation data series from two pluviometric stations were used, The *Camamu* (13°55.8′S; 39°06′W) and *Ituberá* (13°48′S; 39°10.2′W) stations (Figure 3.1), maintained and provided by the Brazilian national water agency - ANA [ANA, 2009]. These data series cover daily information of 24 years (1964-1988) at the *Camamu* station and of 40 years (1964-2004) at the *Ituberá* station.

The *Camamu* station is located on the CMB central region and can be representative of the main watershed precipitation. The *Ituberá* station is located 20 km from the first station, at the *Cachoeira Grande* river which is the main tributary of *Serinhaém* system. This second station was included to provide information on the spatial rain distribution and by being located close by the only fluviometric station to monitor a discharge into CMB as will be discussed on section 3.2.3. Based on the investigation of these data series the pluviometric regime at the CMB region presents a marked seasonal signal and can be divided into a rainy period, from March to July, and a dry period, from August to February (Figure 3.2.2).

Camamu station presents an annual mean precipitation of 2570±538 mm, with monthly mean precipitations of 244 mm during the rainy period and of 194 mm during the dry period, which is about 26% lower. Extreme mean values at this station ranges between 163 mm in September and 266 mm in July. Despite the closeness, *Ituberá* station presents a annual mean precipitation of 2020±342 mm, about 27% lower than at *Camamu* station. The seasonal monthly mean precipitation are 195 mm during the rainy and 150 mm during the dry periods and the extreme values are 137 mm in October and 219 mm in March.

Besides the seasonality, with about a quarter less precipitation on the dry period. The pluviometric data also reveals a considerable spacial variability between the two stations. This behavior is a climatic characteristic along the Eastern Brazilian Margin, marked by a humid coastal fringe in contrast to an arid interior only few kilometers inland.

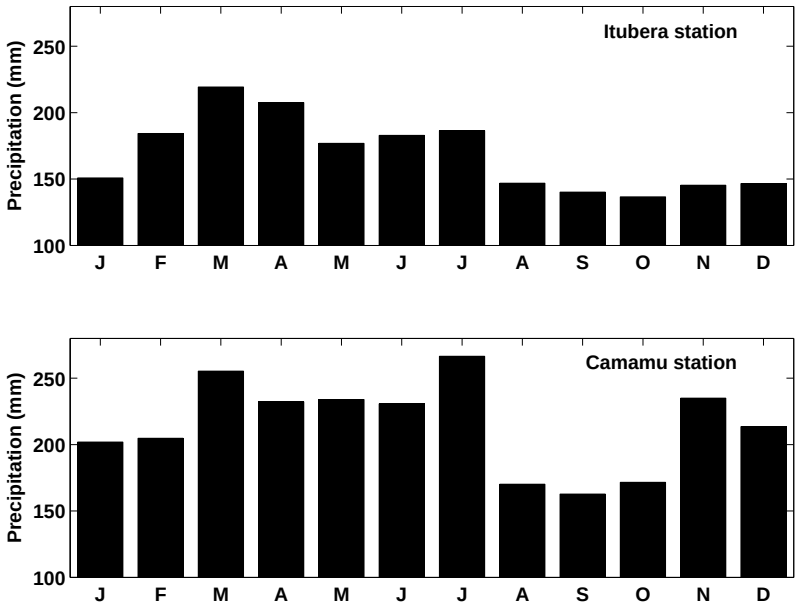

Figure 3.3: Monthly mean precipitation on the *Ituberá*and Camamu pluviometric stations. Based on daily data series for 24 years (1964-1988) at the *Camamu* station and for 40 years (1964-2004) at the *Ituberá* station.

3.2.3 Fluviometry

Baía de Camamu drainage basin covers 1450 km^2, distributed between three sub-basins at its north, central and south portion (Figure 3.2). The north sub-basin covers approximately 473 km^2 and have the *Serinhaém* river as its main tributary. On the central sub-basin the major tributaries are the *Igrapiúna*, *Pinaré* and *Sorojó* rivers which, together, drain an area of 573 km^2. The *Maraú* river drainage basin of 404 km^2 is the south sub-basin tributary.

Water discharge data into the CMB are restricted to the *Ituberá* fluviometric station ($13°47,1'$S; $39°10,58'$W) operated by the Brazilian national electric energy agency - ANEEL [ANA, 2009], Figure 3.1. The *Ituberá* fluviometric station registers daily runoff for the *Cachoeira Grande* river, one of the main *Serinhaém* river tributary, whose drainage basin covers 310 km^2. Due to the lack of complimentary data sources along the *Camamu* basin, the *Cachoeira Grande* was taken as reference for the main *Camamu* Bay fluviometric regime, a proxy, as one considers the pluviometric gradient along the region (section 3.2.2), which among other factors, determines the surface runoff. On our analysis, we use a 33 years series of daily fluviometric data (from 1969 to 2002).

The annual mean discharge at *Ituberá* station is of 5.80 m^3.s^{-1}. The monthly mean value presents high temporal variability, oscillating from a minimum of 5.1 m^3.s^{-1} in January to a maximum of 6.9 m^3.s^{-1} in July. Considering the seasonal cycle previously established, the rain period, from March to July, presents a mean discharge of 6.04 $\pm$ 3.00 m^3.s^{-1} while the dry period, from August to February, presents a mean discharge of 5.60 $\pm$ 3.15 m^3.s^{-1}, Figure 3.4. These values are equivalent to a time permanence of 35% for the dry period and, of 43% for the rain period (Figure 3.5) and does not shows a marked seasonality. Furthermore, the mean of the maximum daily discharge oscillated from 8.6 m^3.s^{-1} in May (on the rain period) to 12.3 m^3.s^{-1} in December (in the dry period), suggesting the relevance of short events on the fluviometric regime (Figure 3.4).

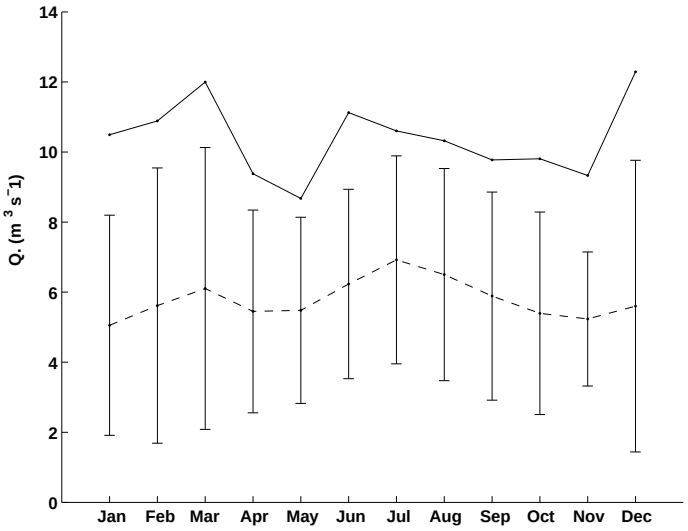

Figure 3.4: Annual mean *Cachoeira Grande* fluviogram, based on the *Ituberá* fluviometric station data [ANA, 2009]. Dotted line represents the monthly mean discharge while solid line represents the maximum daily mean discharge. Vertical bars are the standard deviation of the mean.

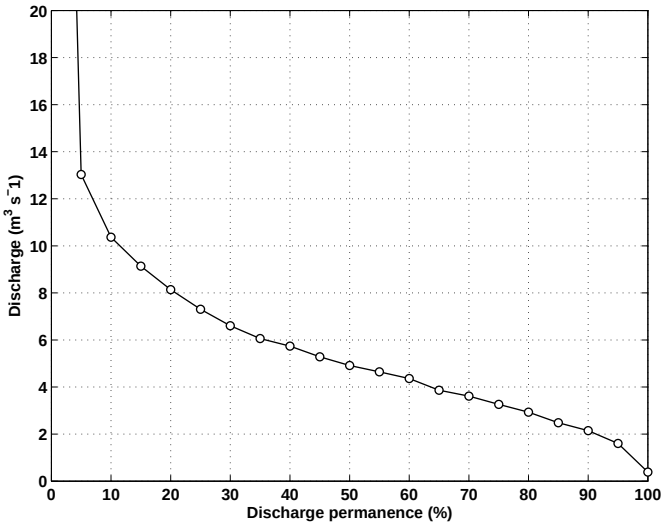

Figure 3.5: Permanence (flow duration) curve for the *Ituberá* fluviometric station.

Typical *Baía de* Camamu inflow were virtually unknown previous this estimative. Based on the methodology presented in (section 3.9) the mean discharge into *Baía de Camamu* was estimated of 51 m^3 s^{-1} for the dry period and 55.7 m^3 s^{-1} for the rain period. Although conservative these establishes a reference for the CMB inflow.

3.2.4 Regional wind field

The largest variability found on the ocean-atmosphere interaction of the Western South Atlantic are related to the seasonal cycle. As a response, the ocean surface circulation reflects the seasonality of the wind field cycle, marked by the trade wind patterns, and the dynamics of the Intertropical Convergence Zone (ITCZ) [Stramma and Schott, 1999].

The trade winds are the prevailing wind system on the tropics, being associated to the dynamics of the high pressure South Atlantic Anticyclone, blowing from East and Northeast during Spring and Summer (October to March), when the South Atlantic Anticyclone cell is displaced towards the South, and from Southeast during Autumn and Winter (April to September), when the anticyclone is in its Northernmost position [Nimer, 1989]. The ITCZ, changes its position seasonally, coming closer to the Eastern Brazilian Margin on Autumn and Summer; higher precipitation and weaker winds are regionally associated to the ITCZ. [Dominguez, 2004].

The results from a 32 years mean (1972-2004) of the global wind model reanalysis from the National Center of Environmental Prediction [NCEP, 2005] presented on Figure 3.6, reflects the regional wind field seasonality during the dry (August to February) and rain (March to July) periods. The wind on the regional *Baía de Camamu* zone blows preferably from East, during the dry period, with intensities varying from $2.7 m.s^{-1}$ near the coast, increasing offshore and northwards to a mean intensity of $4.0 m.s^{-1}$ (East of 38°W and North of 13°S). On the rain period, the wind blows preferably from the Southeast, with a similar spatial behavior but with about 14% less intensity than on the dry period. The mean intensities varied from about $2.3 m.s^{-1}$ near the coast to $3.5 m.s^{-1}$ East of 38° W and North of 13° S.

Another important intervenient factor on the regional scale is the influence of atmospheric cold fronts. Those are resultant from the northward progression of polar masses

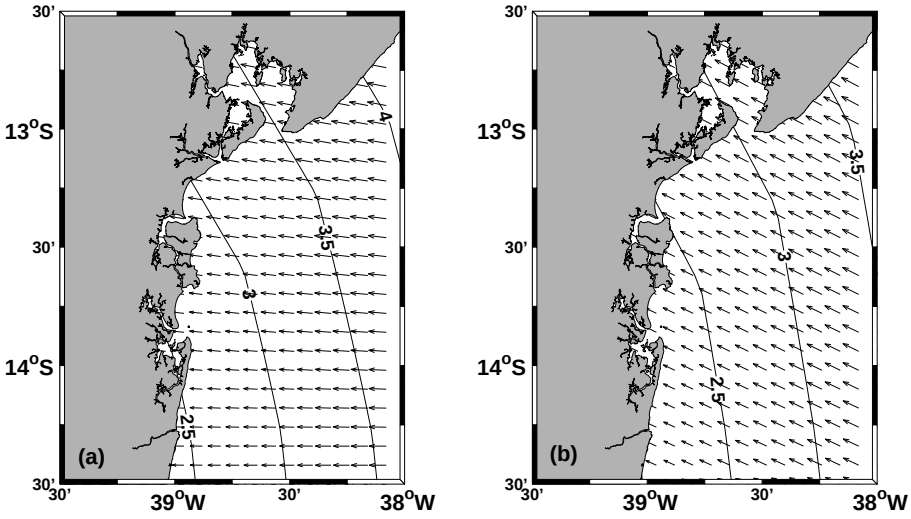

Figure 3.6: Mean wind field on the regional vicinity of *Baía de Camamu* (14°S) and *Baía de Todos os Santos* (12.5°S), on the Eastern Brazilian Margin. On left, representation for the dry period (August to February) and on right, representation for the rain period (March to July). Results from a 32 years mean (1972-2004) of the global wind model reanalysis from the U.S. National Center of Environmental Prediction [NCEP, 2005]

.

originated on higher latitudes. On summer, the cold fronts tend to be weaker, have a lower pressure gradient, and a NE orientation, being deflected offshore and rarely crossing the tropics. On the other hand, during the winter the cold fronts may have a pronounced pressure gradient and reach latitudes lower than 10°S [Dominguez, 2004].

3.3 Sampling strategy and methods

The dominant physical forcing driving the estuarine circulation and mixing are related to the tidal forcing on the ocean boundary, to freshwater discharge at the riverine interface and to gravitational circulation resultant from along-estuary gradients in density [O'Callaghan et al., 2007]. Since *Baía de Camamu* presents a complex geometry and is influenced by many tributaries along its watershed, the establishment of a sampling strategy is not a trivial task. On one hand, the intention to evaluate its spatial variability demands a spatial and broad sampling effort. On the other hand, to keep the analysis as synoptical as possible and to cope with sampling limitations, a limited number of sites must be chosen.

To achieve a comprehensive but not extensive survey of CMB, the dynamical and hydrographic structure were sampled along two sampling periods, covering seasonal dry and rainy conditions. Across-channel transects lines were located at CMB major tributaries, at Ponta do Mutá (the estuarine-shelf interface) and at *Maraú* and *Serinhaém* channels (Figure 3.1). Based on this sampling strategy twelve semi-diurnal tidal cycles were monitored during the 2004 dry period ($21^{\underline{st}}$ to $29^{\underline{th}}$ September) and the 2005 rainy period ($20^{\underline{th}}$ to $29^{\underline{th}}$ July). Therefore, each channel was sampled on a neap and spring tidal regime, in each survey. Furthermore, along-system hydrographic profilers were conduced along the *Maraú* and *Serinhaém* channels in order to evaluate the spatial structure and variability along neap and spring (Figure 3.1).

The dynamical structure was hourly profiled along the three transversal transects with a workhorse 600 kHz bottom-tracking acoustic doppler current meter profiler (ADCP) based on 1 m thick vertical cells. The vertical water properties (temperature, salinity and turbidity) were sampled with a SBE 19 plus seabird CTD profiler, with a vertical resolution of 25 cm and a frequency of 4 Hz. On the across-channel transect line, the CTD casts were positioned on two stations (Cast 1 and 2) located on both channel sides, symmetrical to the main channel axis (Figure 3.13 and 3.17). On the along-system hydrographic sampling, the casts were set along the channel main axis (Figure 3.1).

To better represents the hydrography the vertical profilers measurements were averaged at fixed stratum of non-dimensional depth [Miranda et al., 2002], since the stretching and contraction of the water column during a complete tidal cycle may cause distortions in the representation of the local depth. Turbidity readings were calibrated against Suspended Particulate Material (SPM) concentrations determined from ten triplicates of surface and bottom water samples collected along the Serinhaém river longitudinal transect. All regressions were significant at the 95% confidence level with correlation coefficients (r^2) of 0.9 and 0.84 for dry and rainy period, respectively.

Sea level oscillations are studied based on three data series obtained with a pressure sensor set on the borders of Maraú channel, at the harbor of *Companhia Baroid*, at $13°54,9'$ S; $39°00,9'$ W, Figure 3.1: i) a dry period between 2002/12 and 2003/02; ii) a rainy period between 2003/05 and 2003/06 and iii) a larger period (2004/12 to 2006/01) covering one year of observations. Although these data series cover two dry and two rainy periods they are not simultaneous to the hydrographic campaigns. Wind time series were sampled simultaneous to sea level with a Wind Sentry RM Young anemograph located at the *Maraú Península*. The anemograph was set to operate at 10 hz, with a 15 minutes interval at a 18 m height platform. The data was post-processed to fit a 10m height wind level. Altogether, these represent the most extensive oceanographic data collecting effort ever conducted at CMB. The complete sampling map is depicted in figure 3.1.

3.4 Sea level variability and the local wind.

Baía de Camamu is subject to microtidal regime on neap, with a maximum amplitude of 189 cm, and to mesotidal regime on spring, when the amplitude reaches a maximum of 266 cm (Table 3.1). Seasonally, the sea level height varies from a minimum of 80 (83) cm to a maximum of 213 (216) cm along the dry (rainy) periods. The longer period record reveals a sea-level variation from a minimum of 47 cm to a maximum of 266 cm presenting a difference of about 60% from the extreme values found on the previews series (Table 3.1). Such variability is of environmental relevance, determining the tidal wave excursion on the flooding zones which, in conjunction with topography and geomorphology, controls the mangrove colonization.

Table 3.1: Minimum (H_{min}) and maximum (H_{max}) tidal amplitude at neap and spring tides. Data from the three tidal series, registered at *Baroid company* harbor, *Baía de Camamu*.

Series	**Record Period**	**Neap tide**		**Spring tide**	
		$\mathbf{H}_{min}$ (cm)	$\mathbf{H}_{max}$ (cm)	$\mathbf{H}_{min}$ (cm)	$\mathbf{H}_{max}$ (cm)
Dry	2002/12/16 - 2003/02/03	80	188	140	213
Rainy	2003/05/25 - 2003/06/24	83	158	112	216
Longer	2004/12/24 - 2006/01/18	47	189	124	266

The harmonic analysis of the large sea-level record was performed after Pawlowicz et al. [2002] resulting in 67 tide components. Based on these components we found that 98% of the sea-level oscillations are forced by astronomical tides. The relative rate between the amplitudes of the main diurnal and semi-diurnal tidal components (Table 3.2) reveals a semi-diurnal tidal modulation dominance (Form number F_n=K_1+O_1/M_2+S_2=0.10 [Defant, 1960]).

The tidal prism is a proxy of the estuarine flushing capacity, being higher in mesotidal than on micro-tidal estuarine systems [Miranda et al., 2002]. The tidal prism was estimated by integrating instantaneous volume transport from hourly current meter

Table 3.2: Amplitude (A) and Greenwich phase (Gw°) of the main harmonic components obtained from the harmonic analysis of the one year sea-level register. The amplitude and phase error (ϵ) are predicted with 95% confidence level.

Component	**A $\pm$ ϵ (cm)**	**Gw $\pm$ ϵ (°)**
O_1	6.32 $\pm$ 0.22	130.73 $\pm$ 2.22
K_1	3.89 $\pm$ 0.24	217.03 $\pm$ 3.29
M_2	74.69 $\pm$ 0.45	117.40 $\pm$ 0.32
S_2	27.77 $\pm$ 0.41	136.15 $\pm$ 0.89

sections, along the flooding tide period of 6.5 h. As one would expect, the tidal prism is considerably higher on spring than on neap, being almost three times larger on the Maraú and approximately double on the Serinhaém (Table 3.3), denoting the high flushing variability between spring and neap. Furthermore, the tidal prism is about 30% larger at Maraú ($145.2\times10^6.m^{-3}$), than at Serinhaém ($112\times10^6.m^{-3}$) at spring, and about 7% lower on the Maraú ($55.0\times10^6.m^{-3}$ than at the Serinhaém ($59.2\times10^6.m^{-3}$) at neap.

Table 3.3: Tidal prism estimative at Serinhaém and Maraú channels. Results based on the local data from September 2004 and June 2005 field survey.

River channel	**Tidal Prism (10^6 m^3)**	
	Neap tide	**Spring tide**
Maraú	55.0	145.2
Serinhaém	59.2	112.0

The tidal asymmetry, determined by the relation between the flood and ebb times is a hydraulic characteristic of particular importance on sedimentary dynamics. On the least lasting event, the flow velocity tends to be higher and so, the flow capacity to transport sediments tends to be increased. Based on this relation, calculated for the Maraú channel (Figure 3.7), we observe that the flood and ebb periods were almost equivalent, with the flood time being about 2% higher than the ebb time. The data also reveals that the flood/ebb relation is maximum for low tidal heights and shows the

tendency to lower as the tidal heights gets higher. This behavior suggests that *Baía de Camamu* may work as a sediment exporter (importer) during neap (spring) periods, when the tidal heights are typically lower (higher).

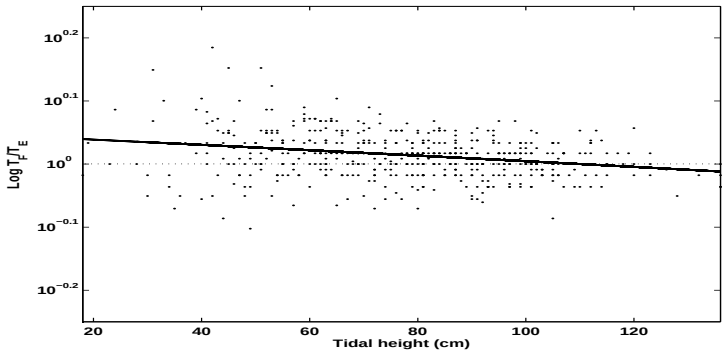

Figure 3.7: Tidal asymmetry based on the rate between the flood time (T_F) and the ebb time (T_E) calculated from the sea-level records obtained at *Baroid* company harbor (Table 3.1).

The estuarine residence time is closely connected to the estuarine sub-inertial circulation. Residual sea-level oscillations is one of the main mechanisms to control the sub-inertial circulation and have a close relationship with the variations in the wind orientation which reflects on the local and remote wind forcing. The local wind forcing is associated to the zonal component of the wind being as higher as the alignment with the main channel while the remote wind forcing is a response to the Ekman transport dynamics caused by downwelling/upwelling favorable winds. These changes reflect the need to evaluate the seasonal wind variations [Janzen and Wong, 2002].

Local wind time series sampled during the dry period were preferentially E-NE oriented with mean intensity of 1.25 m s^{-1}. A exception are the SE winds observed in the later January and early February. During the rain period the wind shows a complete reversal, blowing preferentially from SW and are about 50% higher with a mean intensity of 1.87 m s^{-1} which can be ascribed to the higher frequency of cold front systems on the period (Figure 3.4, right panel).

In order to evaluate the sub-inertial wind forcing sea level variability inside the CMB, the wind components (zonal and meridional) and the tidal series were low-pass filtered with the digital filter proposed by Walters and Heston [1982]. The cut-off period adopted is the local inertial frequency, which, based on the relation $T_f = 2\pi/f$ where f is the local Coriolis parameter, corresponds to 50 hours. The sub-inertial CMB sea level oscillations presented a in-phase correlation with the meridional wind forcing (remote effect) for both dry and wet periods which implies that an upwelling (downwelling) favorable wind causes a decrease (increase) in the sea level, in agreement with coastal Ekman dynamics (Figure 3.4). Also, the zonal wind forcing (local effect) presents a seasonal influence on the CMB sea-level oscillations. During the dry period the zonal wind were preferentially onshore and opposed the direction of the estuarine circulation, resulting in a sea level rise (Figure 3.4 left panel). Such behavior was not observed during the wet period, when the zonal wind were preferentially off-shore (Figure 3.4 right panel). The longer sub-inertial sealevel series however (Figure 3.4 bottom panel) shows a succession of upper and lower sea level heights along the year, suggesting that other physical forcing may also be relevant on the sub-inertial sea level variabilities along the period.

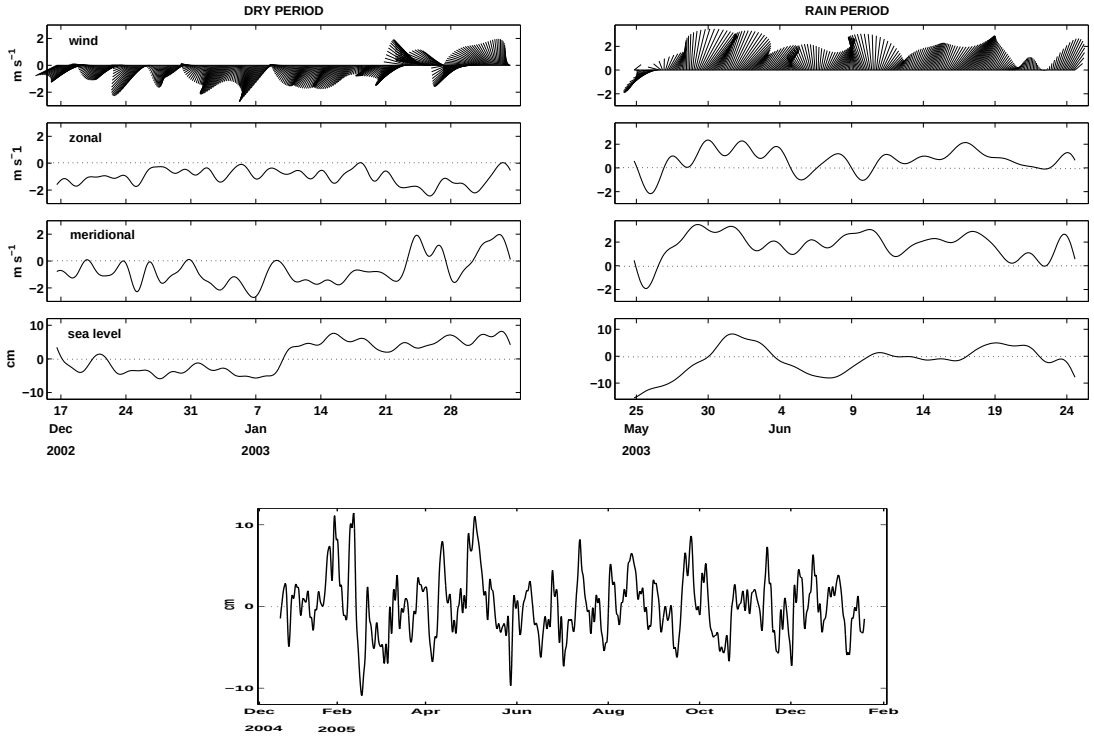

Figure 3.8: Wind time-series, sub-inertial zonal and meridional wind components and sub-inertial non-tidal sea level oscillations at *Baroid* company harbor during the dry (2002/12-2003/02) and the rain (2003/05-2003/06) periods. The bottom panel represents the one year record (2004/12-2006/01) sub-inertial non-tidal sea level oscillations. Wind positive values are northward and off-shore.

3.5 An evaluation of the dry and rainy conditions concurrent the sampling surveys.

Daily pluviometric results and concurrent daily discharge distribution from the Ituberá station along the survey period months are presented in Figure 3.9. The dry period survey covers the September 2004 data, presented on the left while the rainy period survey covers the July 2005 data, presented on the right. These results are a proxy for the pluviometric and runoff conditions along CMB over the survey periods.

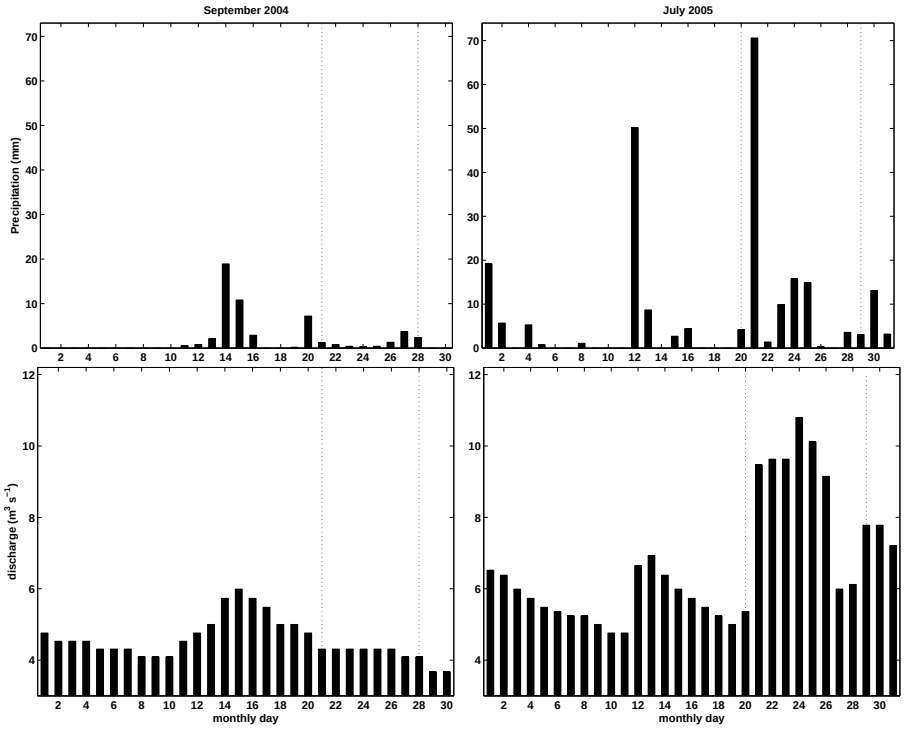

Figure 3.9: Pluviometric (top panels) and fluviometric (bottom panels) daily distribution at Ituberá stations concurrent the survey periods. The dotted lines delimits the sampling periods.

In September 2004 the total monthly precipitation was 54 mm while during July 2005 it was 238 mm (Figure 3.9 top panels). Considering the climatological distribution discussed on section 3.2.2 these are low values for the dry period (mean of 150 mm) and moderately high values for the rainy period (mean of 195 mm). Furthermore, the daily

precipitation distribution reveals a persistent rainfall during both survey periods, but distinct nature between them. In September 2004, a low precipitation (maximum of 4 mm) marked the dry survey period while most of the monthly precipitation occurred out of the sampling period. On july 2005 however, the total monthly precipitation of 238 mm was about 28% higher than the climatological mean value and an anomalous high precipitation of 70 mm, which represents almost 30% of the monthly total, was registered for the second sampling day.

As expected, the Cachoeira Grande discharge was directly influenced by the precipitation (Figure 3.9, bottom panels). During September 2004, the monthly discharge of 4.6 m^3 s^{-1} was below the climatological value of 5.8 m^3 s^{-1}. The mean discharge over the dry survey period was 4.2 m^3 s^{-1}. During July 2005, an extreme condition was registered. Despite the fact that the monthly mean discharge of 6.7 m^3 s^{-1} represents the climatological value, a high mean discharge of 9.5 m^3 s^{-1} was registered for the survey period and a extreme discharge of 10.8 m^3 s^{-1} occurred in the fourth day. The dry period survey discharge correspond to 50% time permanence for the Cachoeira Grande while the rain period amount corresponds to 8% permanence (Figure 3.5). Therefore, in seasonal terms, we may infer that the September 2004 survey was performed under typical dry condition while the July 2005 survey was performed under extreme rainy conditions.

3.6 Hydrography and flow patterns at *Baía de Camamu* main channels.

This section presents field results from the most prominent *Baía de Camamu* channels (*Maraú and Serinhaém*) and at *Ponta do Mutá* (at the bay mouth) during a typical dry condition (September 2004) and on an extreme rainy condition (July 2005). The objective is to characterize the hydrographical and dynamical structure over the sampling periods. The results are presented and discussed in this order.

3.6.1 September 2004 - Dry period, low discharge event.

The along-channel hydrographic and SPM distributions remarks the marine influence over the *Maraú* and *Serinhaém* channels in September 2004, dry period survey (Figure 3.10). On the *Maraú*, salinity higher than 30 persists for over 25 km towards the inner channel, on either spring (not shown) or neap (Figure 3.10, left). The water column stratification was weak, being always lower than 1. The spatial salinity gradient was similar on neap and spring, with a maximum of 35 and a minimum of 25 (neap) or 24 (spring). On the *Serinhaém* channel however (Figure 3.10, right panel), salinity higher than 30 persists for about 10 km, while a marked horizontal gradient of 13.8 (32.8 - 19) occurs towards the innermost channel during the spring tidal period. The vertical salinity stratification was slightly higher in the *Serinhaém* than in the *Maraú* but the differences are not sound.

The temperature field presented a homogeneous spatial distribution in both channels, with slightly warmer values on the inner zones (26.8^{o}C and 27.2^{o}C) than on the mouth (26.5^{o}C and 26.9^{o}C). Vertical variations of 0.6°C are found in the central and deeper *Maraú* channel, which also presented higher SPM, with maximum values of 22 mg l^{-1} in spring (not shown) and 11 mg l^{-1} in neap (Figure 3.10, bottom left). Higher *Serinhaém* SPM are found towards the channel mouth and reaches 18 mg l^{-1} in spring (Figure 3.10, bottom right) and 4 mg l^{-1} in neap (not shown).

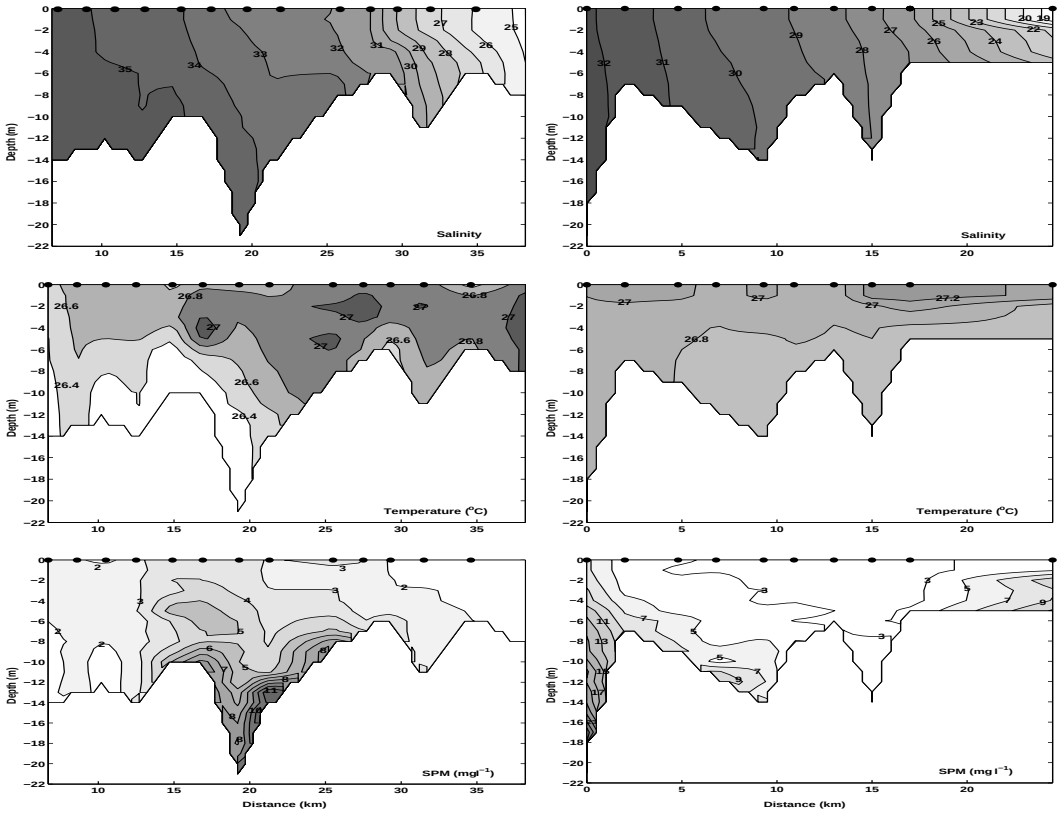

Figure 3.10: Along-channel vertical distribution for Salinity, Temperature and Suspended Particulate Matter (SPM) along *Maraú* (left panels) and *Serinhaém* (right panels) channels during the September 2004 (dry period) survey. Neap low tide and spring high tide, respectively. Distance are from the channel mouth and dots represents the CTD casts position (Figure 3.1).

Hourly currents and salinity vertical structure are represented in Figures 3.11 and 3.12 for neap and spring at the *Maraú*, *Serinhaém* and *Ponta do Mutá* channels, respectively. Ebb and flood flow presents maximum intensity on surface, gradually decreasing towards the bottom, where friction is stronger. This pattern is recurrent in every channel and in all tidal periods, except for the flood *Serinhaém* flow during spring tide, where a maximum mid-depth intensity of -0.6 m s^{-1} is found (Figure 3.12).

The mean across-channel ebb flow ranges from 0.26 m s^{-1} to 0.38 m s^{-1} during neap and from 0.78 m s^{-1} to 0.83 cm s^{-1} during spring tides. The maximum ebb transport of 26,631 m^3 s^{-1} is observed at *Ponta do Mutá* during spring while the minimum ebb

transport of 4,492 m^3 s^{-1} is observed at the *Serinhaém* during neap (Table 3.4). On flood, the mean across-channel intensities ranges from -0.28 m s^{-1} to -0.32 m s^{-1} in neap and, from -0.51 m s^{-1} to -0.72 m s^{-1} in spring. Maximum flood transport of -22,024 m^3 s^{-1} occurs at *Ponta do Mutá* during spring while a minimum flood transport of -4,091 m^3 s^{-1} is observed at the *Maraú* channel, in neap (Table 3.4).

Flow reversion shows different patterns in neap and spring tidal periods. At *Ponta do Mutá* and *Maraú*, the neap bottom currents began to reverse before the surface flow while on spring, the surface flow reverses first. The opposite is observed at the *Serinhaém* channel for spring and neap tides.

The residual flow at *Ponta do Mutá* is upstream in the central and deeper channel and downstream along the upper margins during both neap and spring tides, being associated with a residual flood transport of -90 m^3 s^{-1} for neap and -977 m^3 s^{-1} for spring tidal period (Figure 3.13 and Table 3.4). In the *Maraú* and *Serinhaém* channels, the flow structure for neap is mainly downstream, except for a reversal close to the bottom, being associated with a ebb residual transport of 502 m^3 s^{-1} and 35 m^3 s^{-1}, respectively. On spring tide however a two layer residual pattern is noticeable for both channels, while the residual transport is upstream at the *Maraú*, associated with a flood transport of -221 m^3 s^{-1}, and downstream at the *Serinhaém*, associated with a ebb transport of +329 m^3 s^{-1} (Figure 3.13 and Table 3.4).

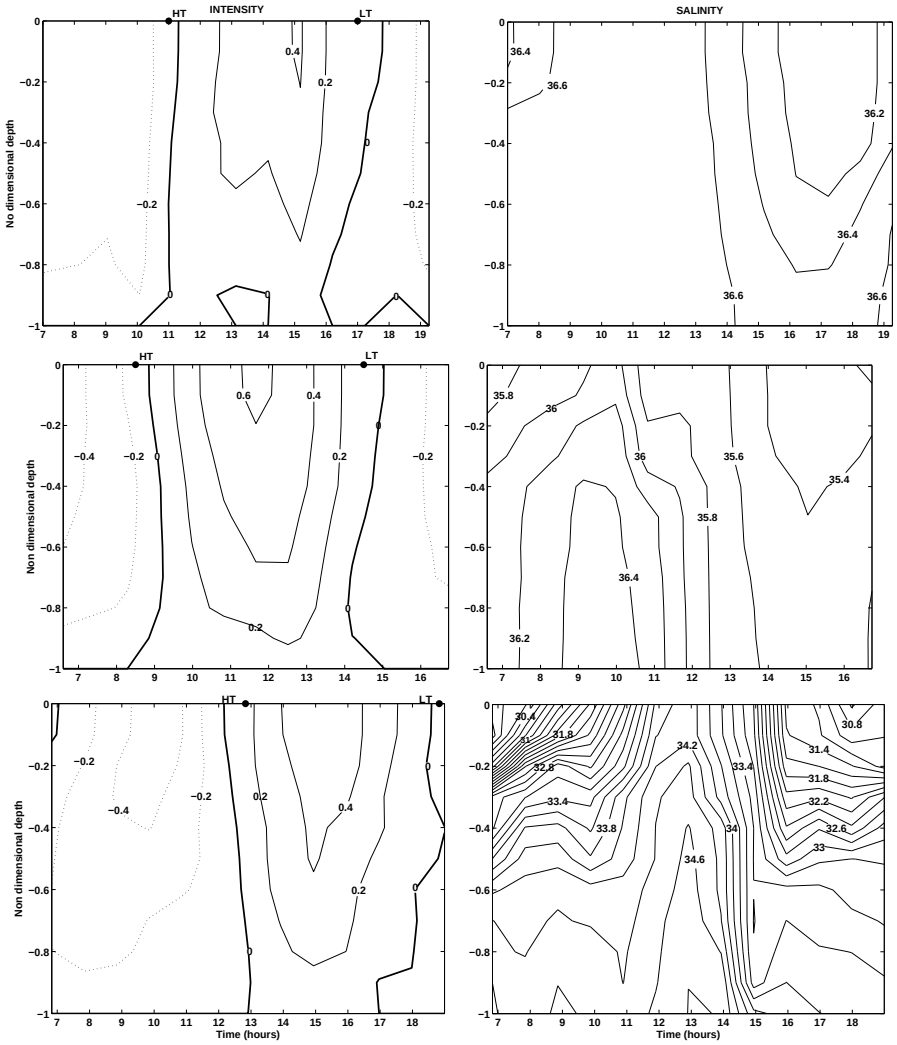

Figure 3.11: Hourly vertical structure for flow intensities (left) and salinity (right) during a dry period neap tide survey at *Ponta do Mutá* (top panels), *Maraú* (middle panels) and *Serinhaém* (bottom panels) channels. CTD cast 1 are represented for *Ponta do Mutá* and *Maraú* and CTD cast 2 at the *Serinhaém* channel. HT and LT represents high and low tidal times.

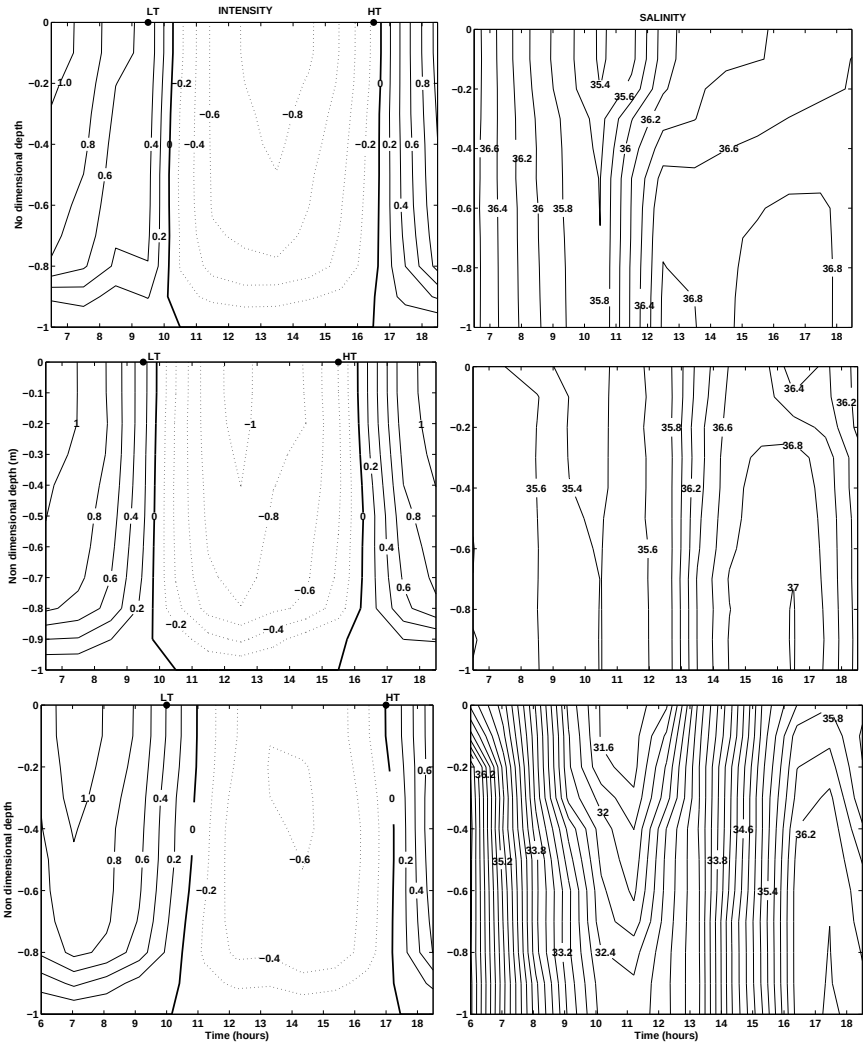

Figure 3.12: Hourly vertical structure for flow intensities (left) and salinity (right) during a dry period spring tide survey at Ponta do Mutá (top panels), Maraú (middle panels) and Serinhaém (bottom panels) channels. Above, CTD cast 1 are represented for *Ponta do Mutá* and *Maraú* and CTD cast 2 at the *Serinhaém* channel. HT and LT represents high and low tidal times.

The asymmetry between ebb and flood is very pronounced on the *Serinhaém* during spring tides. The flood flow presented a maximum intensity of -0.70 m s^{-1} and an associated transport of -7,279 $m^3.s^{-1}$ while the ebb flow reached 1.2 m s^{-1} and transport of 10,225 $m^3.s^{-1}$. The ebb residual flow of +329 m^3 s^{-1} may reflects the along-channel salinity gradient.

The vertical salinity structure varies significantly between neap and spring tidal periods, as well as, between the channels (Figures 3.11 and 3.12 right panels). The water advected toward the bay during the flood tend to occupy all the water column during the high tide, for both neap and spring tides, when the surface salinity reach its maximum value (Figures 3.11 and 3.12 right panels). During the neap tide, the whole water column presented salinity $\geq$ 36.6 during flood tide. Minimum surface salinity of 28.8 occurs at *Serinhaém* during ebb tides. During the spring tide the salinity reach a maximum of 37 near the bottom at the *Maraú* in the high tide, and a minimum surface value of 31.5 at the *Serinhaém* low tide (Figures 3.11 and 3.12 right panels).

Table 3.4: Mean across-channel velocity and transport at *Barra do Mutá*, *Maraú* and *Serinhaém* channels during the dry survey, on neap (N) and spring (S) tides. U_E, U_F, T_E, T_F e T_R represents respectively mean velocity (U) and transport (T) on high ebb (E), high flood (F) and residual (R).

Transversal Transects		U_F **(m s^{-1})**	U_E **(m s^{-1})**	T_F **(m^3s^{-1})**	T_E **(m^3s^{-1})**	T_R **(m^3s^{-1})**
Ponta do Mutá	N	-0.28	0.26	-9,352	8,867	-90
	S	-0.68	0.83	-22,024	26,631	-977
Maraú	N	-0.32	0.38	-4,091	4,915	502
	S	-0.72	0.80	-9,255	10,135	-221
Serinhaém	N	-0.32	0.35	-4,455	4,492	35
	S	-0.51	0.78	-7,279	10,225	329

During neap tide, the vertical salinity structure at the bay entrance (*Ponta do Mutá*) changes from complete mixed at high tide to a moderate stratified at low tide, when a maximum vertical gradient of 0.5 (36.1 - 36.6) is observed. On the other hand, at the *Maraú* channel the opposite is observed. A moderate stratified structure occurs during the high tide, with a maximum vertical gradient of 0.5 (35.9 - 36.4), while during the low tide a quasi homogeneous structure is observed. The *Serinhaém* channel shows a high stratified structure along most of the monitored period. Maximum vertical gradients and low salinity is observed at low tides with an extreme value of 4.6 (30 - 34.6). At high tide however, a moderate stratified structure is observed, with a maximum salinity of 34.8 near the bottom (Figures 3.11 right panels).

At spring tide, a similar behavior is observed for the *Ponta do Mutá* and *Maraú* channels. On higher flood and ebb tides a mixed structure is formed, while, a moderate stratified structure occurs on high and low tides. Maximum vertical gradient at *Ponta do Mutá* occurs during high (36.4 - 36.8) and low (35.4 - 35.8) tide, and during the high tide (36.4 - 37.0) at *Maraú* channel. A extreme salinity variation of 4.8 is observed at *Serinhaém* channel during the spring tide. Maximum salinity value of 36.4 is observed near the bottom during the high tide and the minimum value of 31.6 occur at the surface during the low tide when a maximum vertical gradient of 0.8 (31.6 - 32.4) is observed.

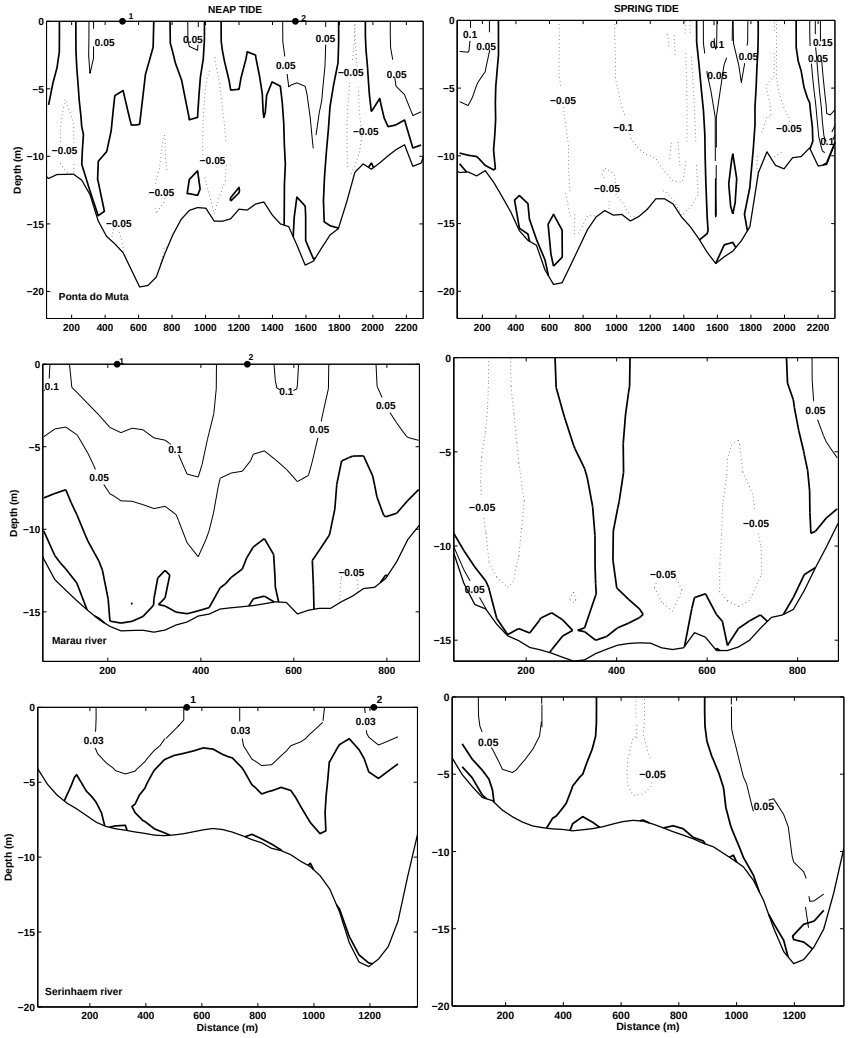

Figure 3.13: Residual flow structure over a complete semi-diurnal tidal cycle (13 h) at the *Ponta do Mutá* (top panels), *Maraú* (middle panels) and *Serinhaém* (bottom panels) across-channel transects along the dry period survey. Distance from the left margin in a continent-ocean orientation. Positive (negative) velocities indicate ebb (flood) flow. The numbers indicates the CTD casts position.

3.6.2 July 2005 - Rainy period, high discharge event.

The high discharge prevalent during the July 2005 survey (Section 3.5) is reflected on *Baía de Camamu* hydrographic conditions. The along-system salinity distribution shows a marked spatial variation. The gradient is maximum on neap tide, varying from 10 to 34 on the *Maraú* (not shown) and from 12 to 31 at the at the *Serinhaém* (Figure 3.14, right).

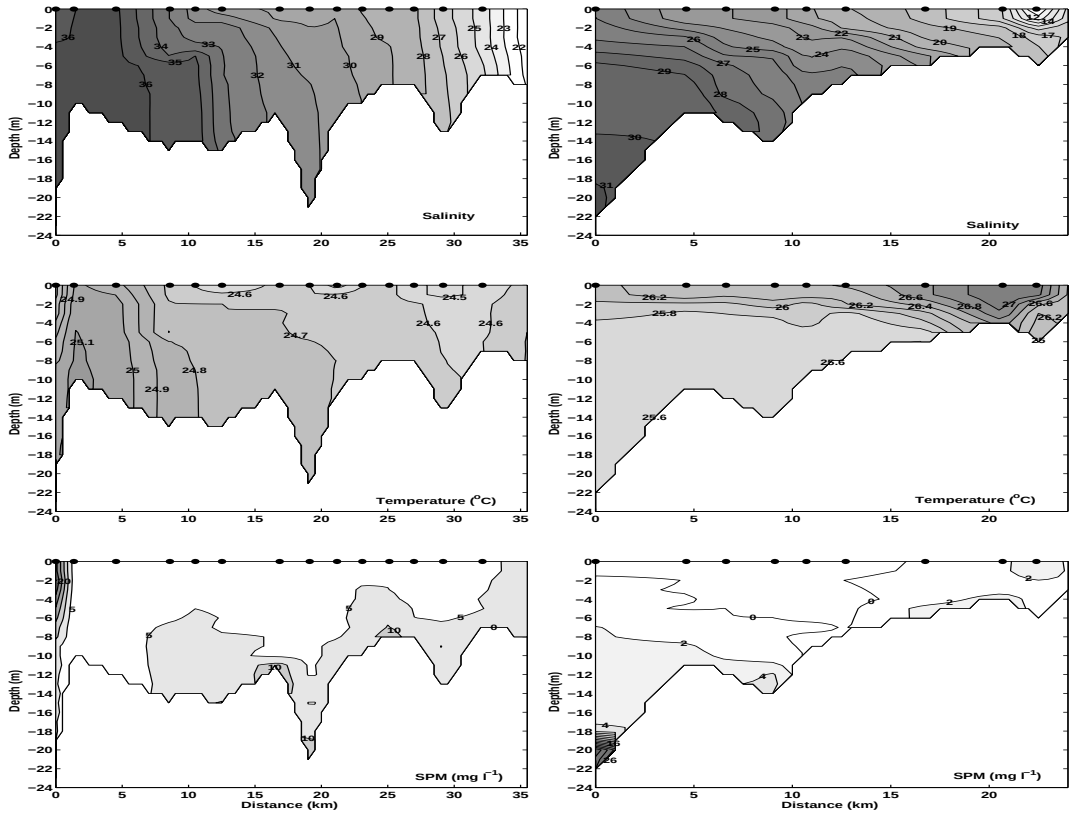

Figure 3.14: Along-channel vertical distribution for Salinity, Temperature and Suspended Particulate Matter (SPM) along *Maraú* (left panels) and *Serinhaém* (right panels) channels during the July 2005 (rain period) survey. Spring high tide and neap low tide respectively. Distance are from the channel mouth and dots represents the CTD casts position (Figure 3.1).

Although the variation is larger on the *Maraú*, the *Serinhaém* channel presented salinity lower than 30 and a marked vertical stratification along most of its extension while on the *Maraú*, a more homogeneous vertical structure is found. On Spring, the along-channel salinity gradient was lower, being of 14.2 (from 22 to 36.2) at the *Maraú*, Figure 3.14 and 15 (from 19 to 34) at the *Serinhaém* (not shown). The vertical salinity structure is well mixed at the inner *Maraú* and moderate stratified at the first 20 km, with a maximum vertical variation of 3(32-35); Vertical *Serinhaém* variations are more homogeneous, being less than 1 (not shown).

Slightly higher temperature values are found on the inner stations (values of 25.9°C on *Maraú* and 27°C on *Serinhaém*). Vertical stratification is marked along the *Serinhaém*, but the gradient is seldom higher than 0.4°C. On the *Maraú*, the vertical gradient is lower. A well marked zone of maximum turbidity is observed on either mid channels in Spring. The SPM reaches 25mg l^{-1} at the *Serinhaém* (not shown) and 10 mg l^{-1} at the *Maraú* the (Figure 3.14, bottom). High SPM values, around 20mg l^{-1} are also found at the channels entrance.

During the neap period the salinity reaches a maximum value of 36.2 near the bottom at *Ponta do Mutá* (Figure 3.15 top right panel) and the vertical salinity structure at this location varies between a complete mixed to a moderate stratified, when a maximum vertical gradient of 1.6 (33 - 34.6) at the low tide is observed. Vertical salinity structures at *Maraú* and *Serinhaém* channels are high stratified during neap tide (Figure 3.15 middle and bottom right panel). Maximum values occurred during the high tides and occupies almost the entire water column, reaching 31 at the *Serinhaém* and 35.2 at the *Maraú*, where a vertical gradient of 5.2 (30 - 35.2) is observed. During the low tides minimum salinity values of 25 and 28.8 are observed at these locations, when can be observed vertical gradients of 6 (24.8 - 30.8) and 5.8 (28.8 - 34.6), at the *Serinhaém* and *Maraú* channels, respectively.

During the spring tides the salinity vertical structures at the *Maraú* and *Serinhaém* are well mixed with slightly stratification during high tides (Figure 3.16 middle and bottom right panels). At *Maraú* maximum salinity of 35.8 is observed near the bottom during the high tide, while, a minimum value of 31.1 occur in the low tide. Maximum vertical gradient of 2.2 (31.6 - 33.8) at this location is observed during the maximum ebb velocities. The minimum salinity value of 25.6 observed during the spring tide occur at the low tide in the *Serinhaém* channel. The vertical salinity structure is well mixed, but in the high tide when a weak gradient (33 - 34) and the maximum salinity is observed. A different behavior is observed at *Ponta do Mutá*, where the vertical salinity structure is mainly moderate stratified (Figure 3.16 top right panel). Maximum vertical gradients of 1.5 (33.7 - 35.2) and 1.2 (32.8 - 34) occur, respectively, during the higher flood and ebb velocities, and the maximum salinity of 36.4 occur during the high tide, occupying almost all the water column.

The flow dynamics during a complete tidal cycle show a similar behavior than those observed during the dry period. Instantaneous ebb and flood velocities present a surface maximum decreasing toward the bottom at the three transversal transects monitored, during the neap and spring tides (Figures 3.15 and 3.16 left panels). Maximum velocities are observed during the ebbs, reaching 0.7 m s^{-1} at *Barra do Mutá* on neap tide and 1.2 m s^{-1} at *Maraú* on spring tide, where a vertical shear of 1.0 m s^{-1} is observed. During the floods the maximum velocities of -0.6 m s^{-1} and -1.2 m s^{-1} are observed at *Barra do Mutá* on neap and at *Maraú* on spring tide, respectively.

Mean ebb velocities are stronger than mean floods. High mean ebbs of 0.5 m s^{-1} and 0.77 m s^{-1} are observed, respectively, at *Ponta do Mutá* on neap and at *Maraú* on spring (Table 3.5). During the floods, mean velocities ranges from -0.28 m s^{-1} to -0.45 m s^{-1} during neap, and from -0.52 m s^{-1} to -0.71 m s^{-1} during spring. The maximum ebb transport of 22,425 occurs at *Ponta do Mutá* on the spring tide, while, the minimum flood transport of -3,635 occurs at the *Serinhaém* on the neap tide.

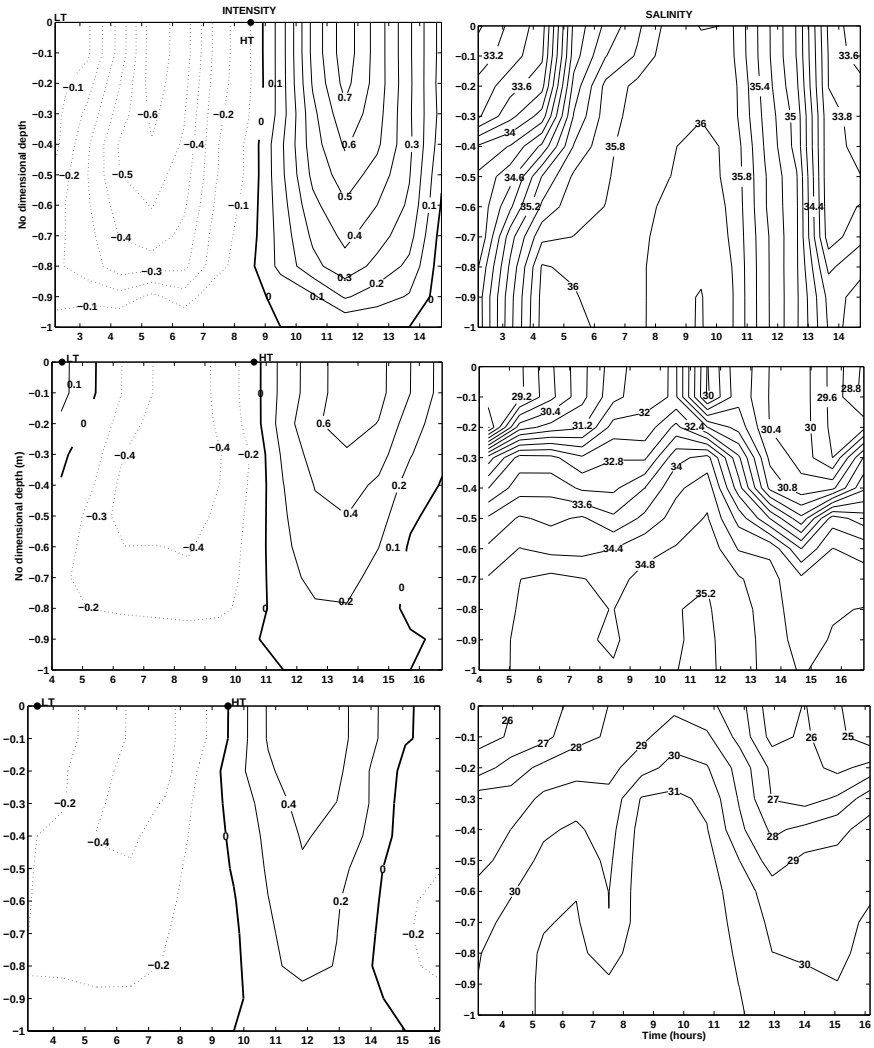

Figure 3.15: Hourly vertical structure for flow intensities (left) and salinity (right) during the rain period neap tide survey at *Ponta do Mutá* (top panels), *Maraú* (middle panels) and *Serinhaém* (bottom panels) channels. CTD cast 1 are represented for *Ponta do Mutá* and *Maraú* and CTD cast 2 at the *Serinhaém* channel. HT and LT represents high and low tidal times.

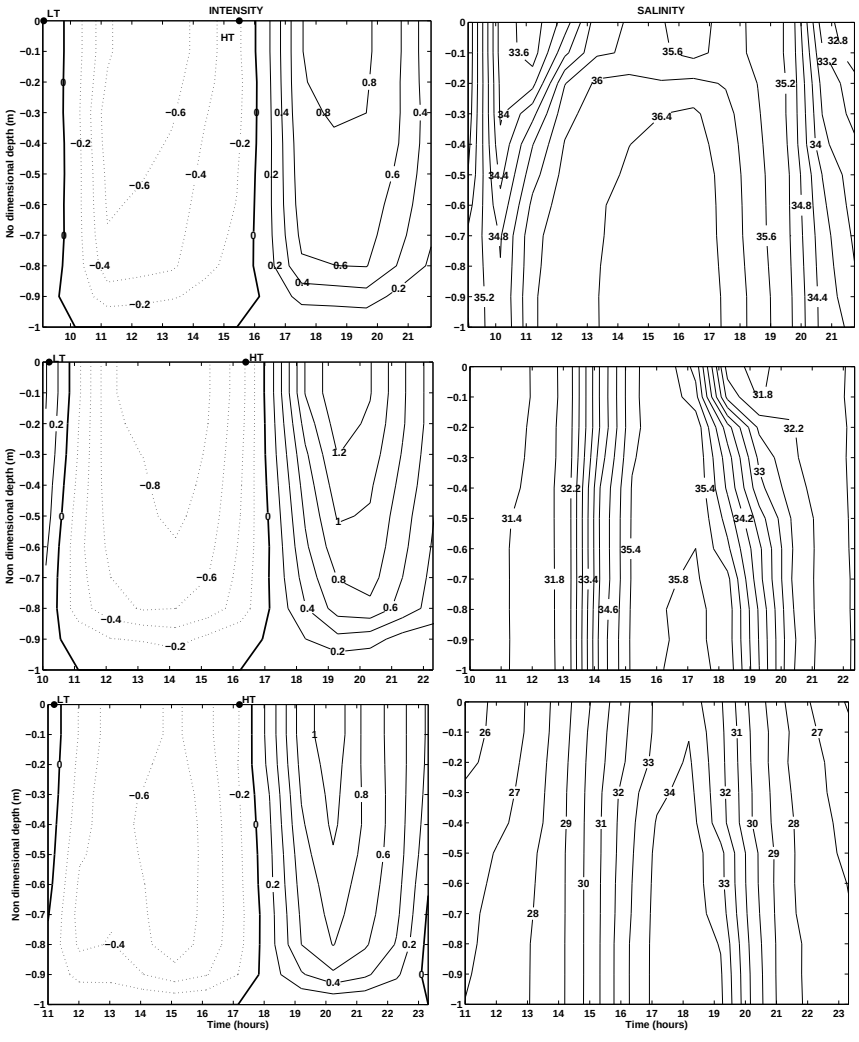

Figure 3.16: Hourly vertical structure for flow intensities (left) and salinity (right) during the rain period spring tide survey at *Ponta do Mutá* (top panels), *Maraú* (middle panels) and *Serinhaém* (bottom panels) channels. CTD cast 1 are represented for *Ponta do Mutá* and *Maraú* and CTD cast 2 at the *Serinhaém* channel. HT and LT represents high and low tidal times.

The residual velocities at *Ponta do Mutá* are mainly flood oriented and concentrates at the central part of the channel during neap and spring tides, with residual transports of -215 m^3 s^{-1} and -54 m^3 s^{-1}, at spring and neap respectively (Figure 3.17 and Table 3.5). The residual flow at *Maraú* and *Serinhaém* channels have a two layer structure at either neap and spring, being mostly ebb oriented in the first 5 m of the water column and flood from there to the bottom. On the spring tide, the flood residual flow tended to be concentrated on the middle part of the channels (Figure 3.17. A low residual transport of 21 m^3 s^{-1} is ebb oriented at the *Serinhaém* channel, while on the remaining channels, the residual was flood oriented, at either spring or neap tides.

Table 3.5: Mean across-channel velocity and transport at *Barra do Mutá*, *Maraú* and *Serinhaém* channels during the rain survey on neap (N) and spring (S) tides. U_E, U_F, T_E, T_F e T_R represents respectively mean velocity (U) and transport (T) on high ebb (E), high flood (F) and residual (R).

Transversal Transects		U_F **(m s^{-1})**	U_E **(m s^{-1})**	T_F **($m^3 s^{-1}$)**	T_E **($m^3 s^{-1}$)**	T_R **($m^3 s^{-1}$)**
Ponta do Mutá	N	-0.45	0.50	-13,377	15,298	-215
	S	-0.56	0.67	-19,427	22,425	-54
Maraú	N	-0.33	0.35	-4,230	4,473	-70
	S	-0.71	0.77	-9,107	10,537	-168
Serinhaém	N	-0.28	0.38	-3,635	4,849	21
	S	-0.52	0.73	-6,870	9,389	-76

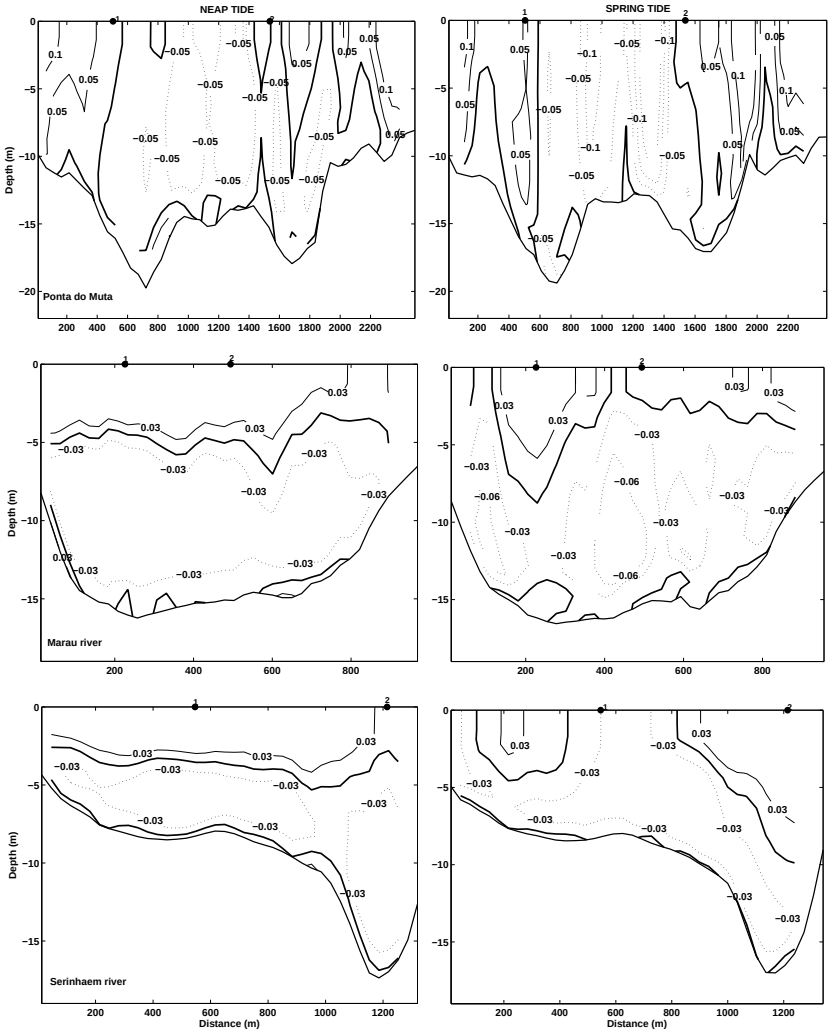

Figure 3.17: Residual flow structure over a complete semi-diurnal tidal cycle (13 h) at the Ponta do Mutá (top panels) and Maraú (middle panels) and Serinhaém (bottom panels) across-channel transects during the rain period survey. Distance from the left margin in a continent-ocean orientation. Positive (negative) velocities indicate ebb (flood) flow. The numbers indicates the CTD casts position.

3.7 Summary and discussion

Baía de Camamu presents a semi-diurnal tidal modulation dominance (Form number, $F_n = 0.10$ [Defant, 1960]), being subject to microtidal regime on neap and to mesotidal regime on spring (section 3.4). Such variability determines the tidal wave excursion on the flooding zones and a high flushing variability, being of relevance to the mangrove colonization, sediment dynamics and to water quality within the system (section 3.4).

To evaluate the spatial variability of the complex CMB estuarine system, its dynamical and hydrographic structure were surveyed along the main channels, covering September (2004) and July (2005) conditions. Basing on the pluviometric and fluviometric data concurrent the survey period (section 3.5) and on the regional pluviometric (section 3.2.2) and fluviometric (section 3.2.3) regimes, we found that September (2004) survey was performed under typical dry pluviometric condition while the July (2005) survey occurred under extreme rainy conditions. By using the *Cachoeira Grande* fluviometric regime as reference (section 3.2.3), the dry period survey discharge correspond to 50% time flow permanence while the rainy period amount corresponds to 8% time flow permanence (section 3.5), denoting to be an extreme event.

The along system hydrographic structure remarks the strong marine influence along the September, 2004, dry period survey (section 3.6.1) or alternatively, a distinguished runoff signature, prevalent on the July 2005, rainy survey (section 3.6.2). In September 2004, salinity higher than 30 persists for over 25 km towards the inner *Maraú* channel, the water column stratification is weak and the spatial salinity gradient was similar on neap and spring tides, with a maximum of 35 and a minimum of 24 in spring (section 3.6.1). In july 2005, the *Maraú* along-system salinity distribution shows a marked spatial variation and the gradient reaches a maximum of 24 (from 10 to 34) in neap, although a nearly homogeneous vertical structure remains. In Spring, the along-channel salinity gradient of 14.2 (from 22 to 36.2) is found along the *Maraú* channel (section 3.6.2).

In the *Serinhaém*, salinity higher than 30 persists for about 10 km in September 2004, although a gradient of 13.8 (19 - 32.8) occurs towards the innermost channel during the spring tidal period (section 3.6.1). In the July 2005, the *Serinhaém* channel presented salinity lower than 30 and a marked vertical stratification along most of its extension. The spatial gradient reaches a maximum of 19 (12 to 31) in neap. In spring, the along-channel salinity gradient was lower, being of 15 (19 to 34) at the *Serinhaém* (section 3.6.2).

One of the most accepted classification of estuary systems is based on the Hansen and Rattray's stratification and circulation diagram [Hansen and Rattray, 1966] that allows the characterization of an estuary based on non-dimensional parameters, related to the salinity (stratification) and dynamical (circulation) structure.

By considering the Hansen and Rattray's diagram, the *Serinhaém* channel may be classified as partially mixed in most of the September 2004 (red dots) and July 2005 (blue dots) conditions (Figure 3.18). Partially mixed estuaries have a tidal energy that provides a means of compensating the stratification, raising the salt wedge. The salt water is mixed upward and fresh water is mixed downward. Exceptions for this behavior are found on the right (deeper) side of the channel under neap, along the rain period (CTD Cast 2 or blue square) or, at the left (shallower) side of the channel under spring, along the dry period (CTD cast 1 or red crossed circle), when the system behaves as well-mixed estuary (Figure 3.18 and Figure 3.17, for the CTD cast location).

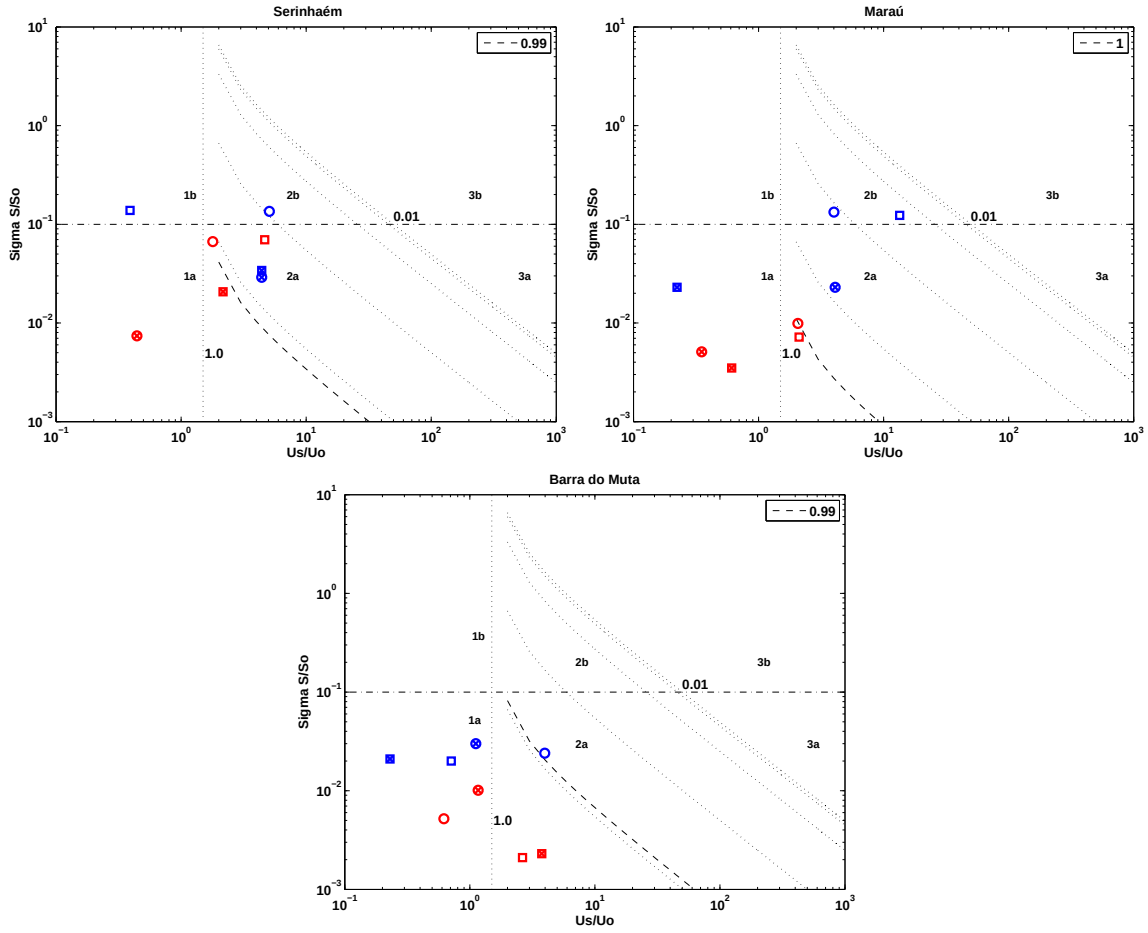

Figure 3.18: Hansen and Rattray's stratification and circulation diagram for *Serinhaém*, *Maraú* and *Barra do Mutá* channels. CTD casts 1 (2) represented as circle (square); neap (spring) tides as empty (cross) dots; rain (dry) sampling as blue (red) dots.

Well-mixed estuaries are found when either tidal forcing or water runoff are effective in promoting mixing on the water column, so that the salinity tends to be vertically homogeneous and decreases from the ocean to the river, along the channel. The net flow is weak and tends to be seaward. On the rain period, neap conditions, the net transport was seaward, at 21 m^3s^{-1} (Table 3.5) while on the dry period spring conditions, the net transport was seawards, at 325 m^3s^{-1} (Table 3.4). In the first case, the system is type 1b, while on the second is type 1a, denoting a higher stratification on the rain survey.

The spatial dynamical variance on both cases with the left (right) channel side be-

ing partially mixed along rain (dry) conditions, while the right (left) being vertically homogeneous reflects the bathymetric differences along the Serinhaém channel and, the effectiveness of turbulence, associated to higher discharge, in promoting mixture along the channel. The *Serinhaém* only gets vertically homogeneous at its deeper channel due to the increase of discharge at the rain period, being spatially non-homogeneous.

On the *Maraú* channel, the Hansen and Rattray's diagram points to vertically homogeneous conditions over spring tides and partially mixed conditions over neap (Figure 3.18). Exception to this pattern is the partially mixed condition found on the left channel side (CTD cast 1 or blue crossed circle) at the rain July (2005) survey . The *Maraú* presented lower stratification than the *Serinhaém* channel with the most stratified conditions occurring on the rain survey and neap tides (blue empty dots). The dry survey (red dots) presented conditions vertically and laterally more homogeneous than the rain period, being located on the lower left part of the diagram (Figure 3.18). The net transport was seaward on the dry period neap (502 m^3s^{-1}) and, landward on the remaining sampling periods. The Flood transport estimative however was larger than the Ebb transport in every sampling period (Table 3.4 and 3.5).

Ponta do Mutá, at the Bay entrance presents a ∼6400 m wide entrance channel being around 15 m deep on its eastern and deeper side. On its western portion the topography is very irregular with depths as low as 3 m. The Hansen and Rattray's diagram classifies this channel, at most of the sampling conditions, as vertically homogeneous (Figure 3.18). Considering the relatively large channel length, it does not shows large horizontal variability (Figure 3.18). The Flood transport estimative was larger than the Ebb transport for most of the time (except on neap, on the dry period), reaching values as high as 26,631 m^3s^{-1} on the spring dry survey (Table 3.4). Our estimative of residual flow is upwards in all monitored conditions, varying from -54 m^3s^{-1} (Table 3.5) at July (2005) spring to -977 m^3s^{-1} at September (2004) spring (Table 3.4).

3.8 Concluding remarks

In this work we summarized the regional physical setting and investigated the inner *Baía de Camamu* hydrographic and flow dynamics along two distinctive sampling periods, covering Sept. (2004) and July (2005), dry and rainy condition, respectively. By using the available fluviometric data as reference, we estimated the dry period discharge to correspond to 50% time flow permanence while the rainy period discharge corresponds to 8% time flow permanence, suggesting to be an extreme event.

This sampling effort has provided the first insight on *Baía de Camamu* structure and variability. The along system hydrographic structure remarks the strong marine influence along the September (2004) dry survey or alternatively, a distinguished runoff signature, prevalent on the July (2005) rainy survey, depicting the intense temporal variability of inner *Baía de Camamu* due to high variable discharge conditions.

The hydrodynamical structure is large depended on the freshwater inputs as well as on the tidal wave characteristics. For instance, the *Serinhaém* channel behaves mostly as a partially mixed system, only getting well mixed at its deeper channel side due to the freshwater discharge at the rain period or alternatively, to spring tidal forcing on the shallower side, on the dry period. On the Maraú, the tidal wave influence is evident. Vertically homogeneous conditions are prevalent over spring tides while partially mixed conditions are prevalent over neap tides. Lower stratification are prevalent on the *Maraú* than on the *Serinhaém*. *Ponta do Mutá*, at the bay mouth behaves mostly as a vertically homogeneous system and does not shows large horizontal variability, considering its relatively large length.

Therefore, besides the intense temporal variability related to the high variable discharge, Baía de Camamu also depicted a very marked spatial variability, evident on the distinguished dynamical character found for *Maraú*, *Serinhaém* and Ponta do Mutá channels.

3.9 Appendix: Basin discharge estimate based on instantaneous point sources, soil composition and relative sub-basin areas.

Typical *Baía de Camamu* inflow values were estimated from the *Cachoeira Grande* discharge series data and from instantaneous runoff values, collected at point sources distributed around the drainage area (Figure 3.2) on Feb. 13 and 19, 2000 CRA [2000]. The point sources included river *Cachoeira Grande* and smaller tributaries such as the *Jatiman*, *Piabas* and *Cachoeira do Barro*, at the *Serinhaém* sub-basin and river *Igrapiúna*, at CMB central sub-basin (Table 3.6).

Table 3.6: Point source discharge and time permanence along *Baía de Camamu* drainage basin . The time prevalence for each point source was estimated by correlation with the *Ituberá* flow permanence curve (Figure 3.5), defining the local permanence coefficient, K=$Q_{90}(Itubera)/Q_{90}(local)$. Reference discharge was monitored on Feb., 13 and Feb., 19 of 2000.

Point Source	**Discharge** ($\mathbf{m^3.s^{-1}}$)	**Date** (Feb, 2000)	**Time Preval. (%)**	**K**	Q_{90} ($\mathbf{m^3.s^{-1}}$)
Cachoeira Grande	5.24	(13)	48	0.40	2.10
	5.00	(19)	49	0.42	
Jatiman	0.91	(13)	48	0.40	0.37
Piabas	0.47	(13)	48	0.40	0.19
Cachoeira do Barro	0.49	(19)	49	0.42	0.21
Igrapiúna	1.56	(19)	49	0.42	0.66

The time prevalence of each point source was estimated by correlation with the *Ituberá* permanence curve (see Section 3.2.3), defining a local permanence coefficient, K=$Q_{90}(Itubera)/Q_{90}(local)$. The local discharge estimative, Qn, is thus the result of the product between K and the local discharge value ($Qn = K * Q_{local}$), for any given period. On the *Cachoeira grande*, the runoff of 5.24 $m^3.s^{-1}$ and 5.00 $m^3.s^{-1}$, corre-

sponds to a flow permanence of 48% and 49% respectively, while the discharge with 90% time permanence corresponds to 2.10 $m^3.s^{-1}$ (Section 3.2.3).

Specific discharge was estimated by considering the type of soil on every sub-basin area (Figure 3.19). For instance, an area covered by clay soils may have an specific discharge 50% larger than an area covered by latosol. The latosol zones however were typically larger than the clay soil zones and an adjustment curve, relating the area and runoff distribution on those zones was also established (Figure 3.20).

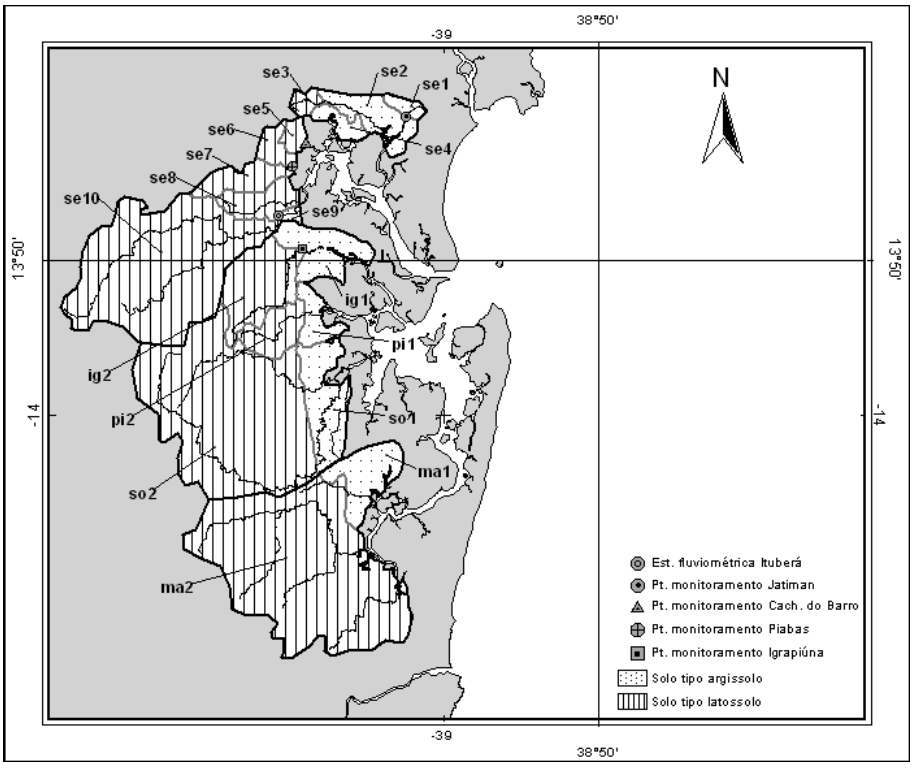

Figure 3.19: Soil sectorization of *Baía de Camamu* major tributaries basin, based on SRH [2003] geographic database. On map is also represented the *Ituberá* fluviometric station[ANA, 2009] and the runoff point sources, used to estimate the total discharge.

By following this methodology, the mean discharge at each *Camamu* sub-basin, was estimated as a composition of the runoff estimative (related to the reference station), soil composition and relative drainage area sizes (Table 3.7). The mean discharge at the *Serinhaém* basin is estimated at 18.1 $m^3.s^{-1}$ on the rain period, which is about 9% larger than the dry period discharge of 16.5 $m^3.s^{-1}$ (Table 3.7). At the central bay zone, the total discharge on the rain period sums 25.5 $m^3.s^{-1}$, against 23.3 $m^3.s^{-1}$ on the dry period. On this zone, the largest contribution comes from the *Sorojó*, that drains an area of 392.30 km^2 (about 70% of the drainage), 84% over latosol and have an estimated discharge of 12.6 $m^3.s^{-1}$ on the dry period and 13.7 $m^3.s^{-1}$ on the rain period (Table 3.7).

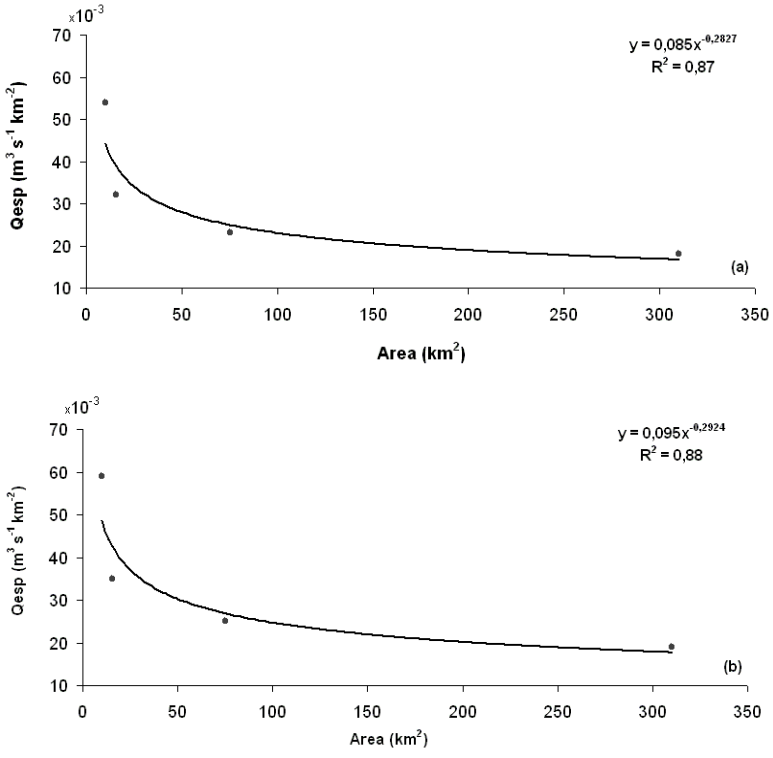

Figure 3.20: Specific discharge distribution for lotosol zones, relates runoff to drainage basin area. In (a) distribution for the dry period (August to February) and in (B) distribution for the rain period (March to July).

The *Maraú*, at the south bay zone, presents mean discharge of 11.20 $m^3.s^{-1}$ on the dry period and, 12.1 $m^3.s^{-1}$ on the rain period (Table 3.7). On this sub-basin, the clay soil zones, that covers about 14% of the total drainage basin are responsible for about 49% of the total runoff (Mean of 5.5 $m^3.s^{-1}$ for the dry period and, 6.06 $m^3.s^{-1}$ on the rain (Table 3.7). Finally, the total CMB discharge was estimated on 51 $m^3.s^{-1}$ on the dry period and, 55.7 $m^3.s^{-1}$ for the rain period. These are conservative values but establishes a reference for the seasonal *Baía de Camamu* inflow.

Table 3.7: Seasonal mean runoff for the main *Baía de Camamu* tributaries. The runoff was estimated as a composition of point discharge data (related to the reference station), sub-basin soil composition (latosol curve or clay soil specific discharge) and relative drainage area sizes. Considering the seasonal cycle where the dry period extends from August to February and the rain period extends from March to July.

System	**Sector**	**Area** (km^2)	**Method**	**Mean Q.** ($m^3.s^{-1}$)	
				Dry	**Rain**
Serinhaém	SE1	8.8	Qn (Jatiman)	0.98	1.08
	SE2	40.0	Clay soil Q	4.44	4.92
	SE3	9.2	Latosol curve	0.42	0.46
	SE4	14.49	Clay soil Q	1.61	1.78
	SE5	9.9	Qn (Cachoeira do Barro)	0.53	0.59
	SE6	15.8	Qn (Pabas)	0.50	0.56
	SE7	30.3	Latosol curve	0.98	1.06
	SE8	30.9	Latosol curve	1.00	1.08
	SE9	4.1	Clay soil Q	0.46	0.51
	SE10	310.0	Qn (Cachoeira Grande)	5.60	6.04
			Runoff Serinhaém	**16.5**	**18.1**
Igrapiúna	IG1	49.9	Clay soil Q	5.54	6.14
	IG2	75.2	Qn (Igrapiúna)	1.70	1.87
			Runoff Igrapiúna	**7.2**	**8.0**
Pinaré	PI1	21.9	Clay soil Q	2.43	2.69
	IG2	33.8	Latosol curve	1.06	1.15
			Runoff Pinaré	**3.5**	**3.8**
Sorojó	SO1	64.6	Clay soil Q	7.17	7.94
	SO2	327.7	Latosol curve	5.42	5.72
			Runoff Sorojó	**12.6**	**13.7**
Maraú	MA1	49.2	Clay soil Q	5.46	6.06
	MA2	355.6	Latosol curve	5.74	6.07
			Runoff Maraú	**11.2**	**12.1**
			Total Camamu Runoff	**51.0**	**55.7**

Chapter 4

Barotropic tidal currents on the Eastern Brazilian Margin and on inner *Baía de Camamu*, model results using ROMS.

4.1 Introduction

In the process of developing a tide-permitting model response for a coastal circulation system, tidal signals are added to a numerical model for the Eastern Brazilian Margin (EBM). The model, which is configured from the regional ocean modeling system (ROMS), a three dimensional community model designed for coastal applications [Shchepetkin and McWilliams, 2005], has two separated one-way off-line nested domains with resolution of $\sim 3km$ and $\sim 1km$ in the horizontal direction and 30 vertical sigma levels, comprising the coastal and estuarine systems in the zone between the cities of *Salvador* and *Ilhéus* and higher resolution focus on *Baía de Camamu*(Figure 4.1).

To date, no modeling or data analysis work have focused on tidal or tidal current dynamics along the EBM, on a regional basis. Local studies exists for *Baía de Todos os Santos*, such as Cirano and Lessa [2007] that finds the local circulation to be mostly

tidally driven and not varying significantly seasonally or Barroso Junior [2009] that suggests a methodology for prognostic tidal current charts, using *Baía de Todos os Santos* as a case study. *Baía de Camamu*, the second largest EBM embayment system was first investigated on a data analysis basis, in *Chapter 3*, revealing to be subject to micro tidal regime on neap and to meso tidal on spring. Such variability determines the tidal wave excursion on the flooding zones and a high flushing variability, being of relevance to the mangrove colonization, sediment dynamics and to the water quality within the system. On the Southern EBM, Pereira et al. [2005] applied a three dimensional model, suggesting that tidal currents and steep topography may enhance upwelling, increasing local primary productivity on the zone around the *Abrolhos* bank.

In many predictive tidal surface applications two dimensional models have traditionally been applied, giving adequate results. But, due to the much smaller scale variability of tidal currents, in comparison to tidal elevations, tidal currents studies over shelf and near coastal zones invokes a three dimension tidal model implementation [Prandle, 1997]. Recent applications of ROMS with this purpose includes Marta-Almeida and Dubert [2006] and Wang et al. [2008].

In the present study, the model tidal response is compared against short period tidal gauge data from stations along the EBM and to one year long *Baía de Camamu* pressure sensor data. The primary objective is to evaluate the model response by using a simple configuration (that considers constant bottom stress and homogeneous hydrographic conditions) and to investigate the nature of the barotropic tidal propagation along different spatial scales on the Eastern Brazilian Margin and towards inner *Baía de Camamu*. Secondly, its discussed the paths to follow in order to establish a realistic coastal modeling system that allows estuarine connections and some work science hypotheses to follow.

4.2 Model setting

A nested general oceanic model was configured for the Eastern Brazilian Margin, with the objective of establishing a model view of the lesser investigated regional mesoscale dynamics, retaining on the solution the connections from the large-scale circulation (*Chapter 2*). In the current experiment, a third (L2) and fourth (L3) level was set in the previous configuration to investigate the tidal propagation along different spatial scales and towards more realistic and shallower bathymetry on the shelf, near shore and estuarine inner-bay system. The oceanic general circulation model used is ROMS, a free surface, s-coordinates, hydrostatic, community model designed for coastal applications [Shchepetkin and McWilliams, 2005].

The nesting of the model domains is accomplished through the Adaptive Grid Refinement in Fortran (AGRIF), which is based on the use of pointers to successively address the variables of the different grids, keeping most of the original code unchanged (Debreu et al. [2008], Blayo and Debreu [1999]). ROMS AGRIF provides a continuous transition from the coarse resolution to the fine resolution solution [Penven et al., 2006]. As described in *Chapter 2*, the nesting between L0 and L1 is online and one-way, which allows the two grids to run simultaneously with the coarse-resolution domain providing the boundary conditions to the finer-resolution domain and not backwards. In contrast, the nesting down-scale to L2 and L3 is one-way and off-line, stoping and restarting the nested domains at a fixed time interval.

For this experiment, homogeneous conditions for temperature and salinity, with values $T = 25°C$ and S=35 psu, are applied. The L2 and L3 grids are forced at the boundaries with elevation (amplitude and phase) and tidal ellipse parameters (axis, inclination and phases) from eight major tidal constituents of semi-diurnal and diurnal frequencies (M_2, S_2, N_2, K_2, K_1, O_1, P_1, Q_1). The tide forcing is from global inverse barotropic tide (TPXO, version 6.0) [Egbert et al., 1994]. TPXO is a global model of oceanic tides that assimilates TOPEX/Poseidon orbit cycles through the inverse

modeling technique [Egbert and Erofeeva, 2002] and presents a 1/4° resolution for the South Atlantic. The tidal-permitting grid domains (grids L2 and L3) are presented in Figure 4.1.

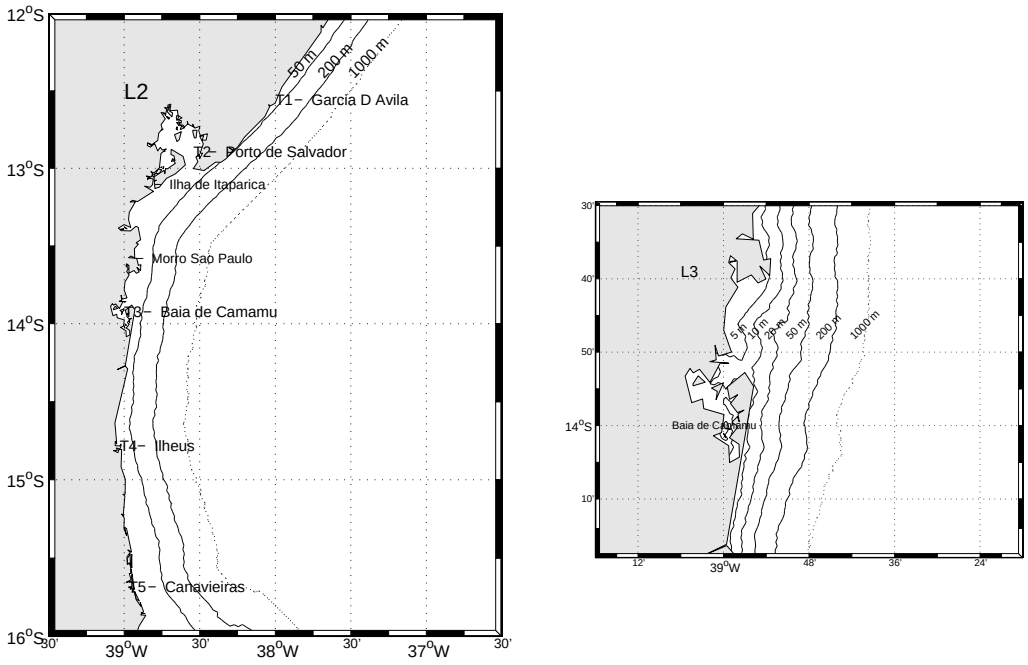

Figure 4.1: The modeling system, focusing on the off-line nesting, tidal-permitting domain (grids L2 and L3). The position for the tidal station of *Garcia d'Ávila* (T1), *Porto de Salvador* (T2), *Baía de Camamu* (T3), *Porto de Ilhéus* (T4), *Canavieiras* (T5) and the sites of *Morro de São Paulo* and *Ilha de Itaparica* are indicated on grid L2. The complete grid system with the online and offline nesting framework is depicted in Figure 1.1.

The L2 grid covers the middle EBM, from the latitudes of 12° to 15°S and the longitudes of 36.5° to 39.5°W, covering the coastal zone from North of *Salvador* to *Ilhéus*, while the finest-resolution L3 grid, focuses on the inner *Baía de Camamu* and its connection with the coastal ocean, from 13.5° to 14.3°S and from 38.3° to 39.3°W. L2 resolution is of $\sim$ 3 km consisting of 107 by 148 grid points and L3 resolution is of $\sim$ 1 km, consisting of 315 by 261 grid points. All domains have 30 vertical levels following the bottom topography, with $\theta_s = 4.0$ and $\theta_b = 0.4$, indicating increased resolution in surface and bottom [Song and Haidvogel, 1994].

Grid topography, derived from ETOPO1, a 1 arc-minute global relief model of

Earth's surface [Amante and Eakins, 2009] was merged with locally surveyed data for the near shelf and, inner *Baía de Camamu*. The bathymetric data was smoothed using a hanning filter, ensuring the bathymetric gradient fits to a maximum slope factor ($r = \nabla h/h \cong 0.2$), which is an empirical criterion to compute pressure gradient force accurately [Beckman and Haidvogel, 1993]. In this experiment, a linear bottom friction parametrization ($\tau_b = r\upsilon_b$, where υ_b stands for the velocity on the bottom level) with a typical bottom drag coefficient of r= $3.0 \times 10^{-4} m.s^{-1}$ was applied. A nonlocal, K-profile planetary (KPP) boundary layer scheme [Large et al., 1994] parameterizes the vertical mixing processes. The model setup parameters are summarized in Table 4.1.

Table 4.1: Model configuration parameters

Param.	L2	L3	
L	107	315	Pts. in longitude
M	148	261	Pts. in latitude
Δt	180 s	60 s	Baroclinic time step
Δt_f	9 s	3 s	Barotropic time step
ΔS	$1/36^\circ$ ($\sim 3km$)	$1/108^\circ$ ($\sim 1km$)	Horizontal res.
Common param.			
N	30		Number of s-levels
Θ_s	4.0		Sigma coord. surface param.
Θ_b	0.4		Sigma coord. bottom param.
h_{min}	2.0 m		Minimum model depth
T	25°C		Constant temperature
S	35 *psu*		Constant salinity
r	$3.0 \times 10^{-4} m.s^{-1}$		Linear bottom drag coeff.

The model was run for 60 days and the output time series of sea surface height and currents were analyzed with the T-TIDE package of Pawlowicz et al. [2002] to retrieve short period tidal harmonic components (M_2, S_2, K_1, O_1) on every grid points.

4.3 Tidal data

Except for *Baía de Camamu*, the tidal data used for comparison are mostly published harmonic analysis from Salles et al. [2000]. These data, mainly used for navigation purposes, were obtained from short period tidal gauge series from the tidal station of *Garcia d'Ávila*, from 12/06/62 to 13/07/62 (T1), *Porto de Salvador*, from 01/01/60 to 23/12/60 (T2), *Porto de Ilhéus*, from 10/11/76 to 11/12/76 (T4) and *Canavieiras*, from 01/01/55 to 31/12/55 (T5). Dates are indicated in the format DD/MM/YY. The Baía de Camamu (T3) data used is the one year pressure sensor series discussed on *Chapter 3*. The tidal stations geographical reference is indicated in Figure 4.1.

4.4 Results

The amplitude and co-phase charts of the modelled M_2 and 0_1 are presented in Figure 4.2. For both constituents we observe an equatorward signal propagation (clearer on the 0_1), with increased amplitudes on the coastal systems of *Baía de Camamu* and *Baía de Todos os Santos*. The S_2 and K_1 (not shown) show similar spatial pattern to the M_2 and 0_1 respectively, but smaller amplitudes.

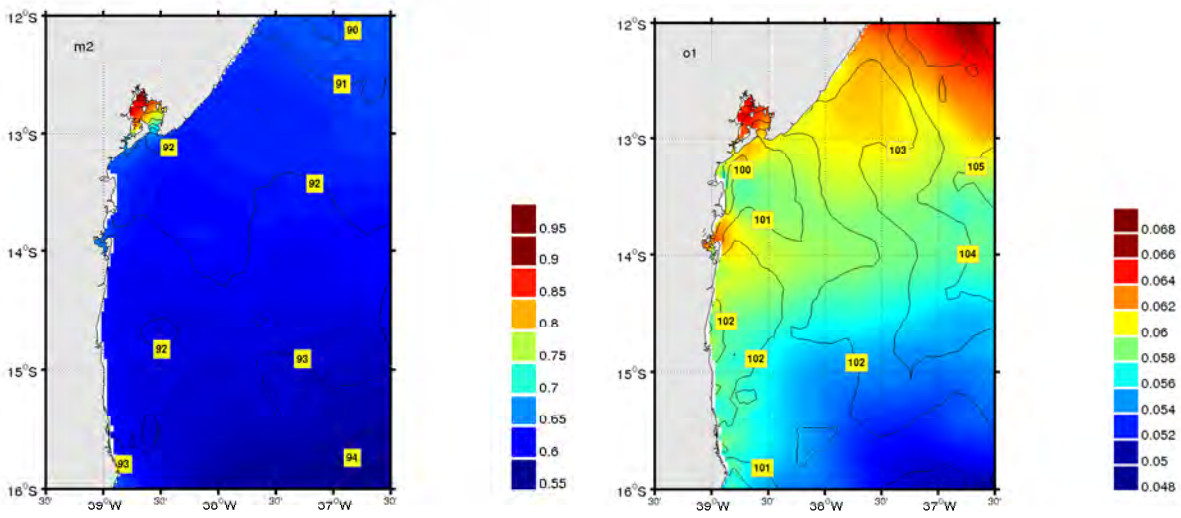

Figure 4.2: Amplitude (m) and Greenwich phases ($G°$) charts of the modeled M_2 (left) and 0_1 (right) constituents along the central zone of the Eastern Brazilian Margin (L2 grid).

The comparison of the model amplitude (cm) and Greenwich phases ($G°$) with the data from five tidal stations (see Figure 4.1 for location) are presented in Table 4.2. The computed values were obtained from the closest grid points to the tidal stations.

By quantitatively comparing the tidal amplitude for the M_2 constituent, the model discrepancy for the coastal stations of *Garcia d'Ávila*, *Porto de Ilhéus* and *Canavieiras*, varied from 8.5% at the Northernmost *Garcia d'Ávila* station to less than 6% at the Southernmost *Canavieiras* station. The largest M_2 discrepancies, of -12.5 cm and of + 13.9 cm are found on the inner bay stations of *Porto de Salvador* and *Baía de Camamu* respectively.

Table 4.2: Observed and Modeled tidal amplitude (cm) and Greenwich phases ($G°$) for *Garcia D'Avila*, *Porto de Salvador*, *Baía de Camamu*, *Porto de ilhéus* and *Canavieras* (Figure 4.1). Except for *Baía de Camamu*, whose harmonic was calculated from a one year pressure sensor series (*Chapter 3*), the remaining are from Salles et al. [2000].

Site	Freq.	**Observ.**		**Model.**		
Coord		*Amp*	$G°$	*Grid*	*Amp*	$G°$
	M_2	67.0	101	L2	61.3	091
Garcia D'Avila	S_2	26.1	114		31.5	253
(-12.56°S, -38.00°W)	O_1	6.9	118		6.0	103
	K_1	3.7	199		7.8	235
	M_2	78.0	110	L2	63.5	093
Porto de Salvador	S_2	30.5	124		32.5	256
(-12.97°S, -38.52°W)	O_1	6.6	122		6.0	101
	K_1	4.1	215		7.5	230
	M_2	74.7	117	L3	88.6	110
Baía de Camamu	S_2	27.8	136		27.9	023
(-13.92°S, -39.00°W)	O_1	6.3	131		9.4	176
	K_1	3.9	217		3.7	234
	M_2	65.6	099	L2	60.0	092
Porto de Ilhéus	S_2	26.0	114		30.5	255
(-14.78°S, -39.03°W)	O_1	5.4	127		5.9	101
	K_1	2.5	206		5.9	218
	M_2	64.0	116	L2	60.2	096
Canavieras	S_2	22.5	135		30.5	255
(-15.68°S, -38.97°W)	O_1	6.4	135		5.75	101
	K_1	3.4	207		6.7	221

For the S_2, discrepancy lower than 1% is found at the inner *Baía de Camamu* station. Among the other major constituents analyzed, the largest and lowest amplitude discrepancies are found for the K_1 and O_1 along the three coastal stations. The mean amplitude ratio between M_2 (O_1) is of 10.2, being lowest (9.4) within *Baía de Camamu*.

Comparison in terms of Greenwich phases, denotes a good response for most constituents and stations. Discrepancies lower than 20° are found for the M_2 in every station and for the K_1 along four tidal stations (*Porto de Salvador*, *Baía de Camamu*, *Porto de ilhéus* and *Canavieras*). Nevertheless, relatively high phase discrepancy are found for the S_2 constituent along the stations. By comparison, Pereira et al. [2005] modelling a region south of our domain but using some common data (*Canavieras* and *Porto de Ilhéus*), presents model results with considerable higher phase discrepancies.

Therefore, regarding the quantitative amplitude and phase response, the model reproduces the observed values reasonably well. The differences found, may be ascribed to many factors, as to the differences in position and depth between the model and the tidal station (the model results being for the closest grid point); to the usage of a linear and constant drag coefficient; to the usage of minimum model depth of 2 m within *Baía de Camamu* (by the lack of bathymetric data in some zones) or, to inaccuracies in the prescribed free surface elevations along the boundaries. Adjustment to the boundary forcing elevation are pointed by Pereira et al. [2005] as a way of improving phase discrepancies. Considering all these possible interferences, our model response is quite robust.

Regional barotropic tidal current ellipses are depicted for M_2, S_2, K_1 and O_1 constituents in Figure 4.3. Tidal ellipses over oceanic regions are weak for all four constituents, with typical values around of 1.5 cm^{-1} for M_2 and, 0.5 cm^{-1} for the O_1. The ellipses presents a predominant clockwise rotation for the M_2 constituent and counter-clockwise rotation for the remaining.

Over the shelf zones the tidal currents ellipses show a significant increase in magnitude, specially on the semidiurnal constituents. The M_2 presents a great polarization (large eccentricity) in the entrance vicinity to *Baía de Camamu* and *Baía de Todos os Santos* and, in the shelf zone comprised between *Morro de São Paulo* to *Ilha de Itaparica* (See Figure 1.1 for geographical reference), suggesting intense cross-shelf tidal currents. The tidal currents attain values around 10 to 12 cm^{-1} along the shelf zone and values higher than 30 cm^{-1} on *Baía de Todos os Santos* entrance channel and interior. The S_2 constituent presents a similar spatial distribution, but reduced values (Figure 4.3).

In the shelf zone, comprised between *Morro de São Paulo* to *Salvador*, a series of steep submarine channels, known as *Salvador Canyon* are active, transporting sediments to the deep oceanic deposits. The remarkable semidiurnal polarization and intense cross-shelf flow are possibly a major physical intervenient in this process, whose role is still to be investigated.

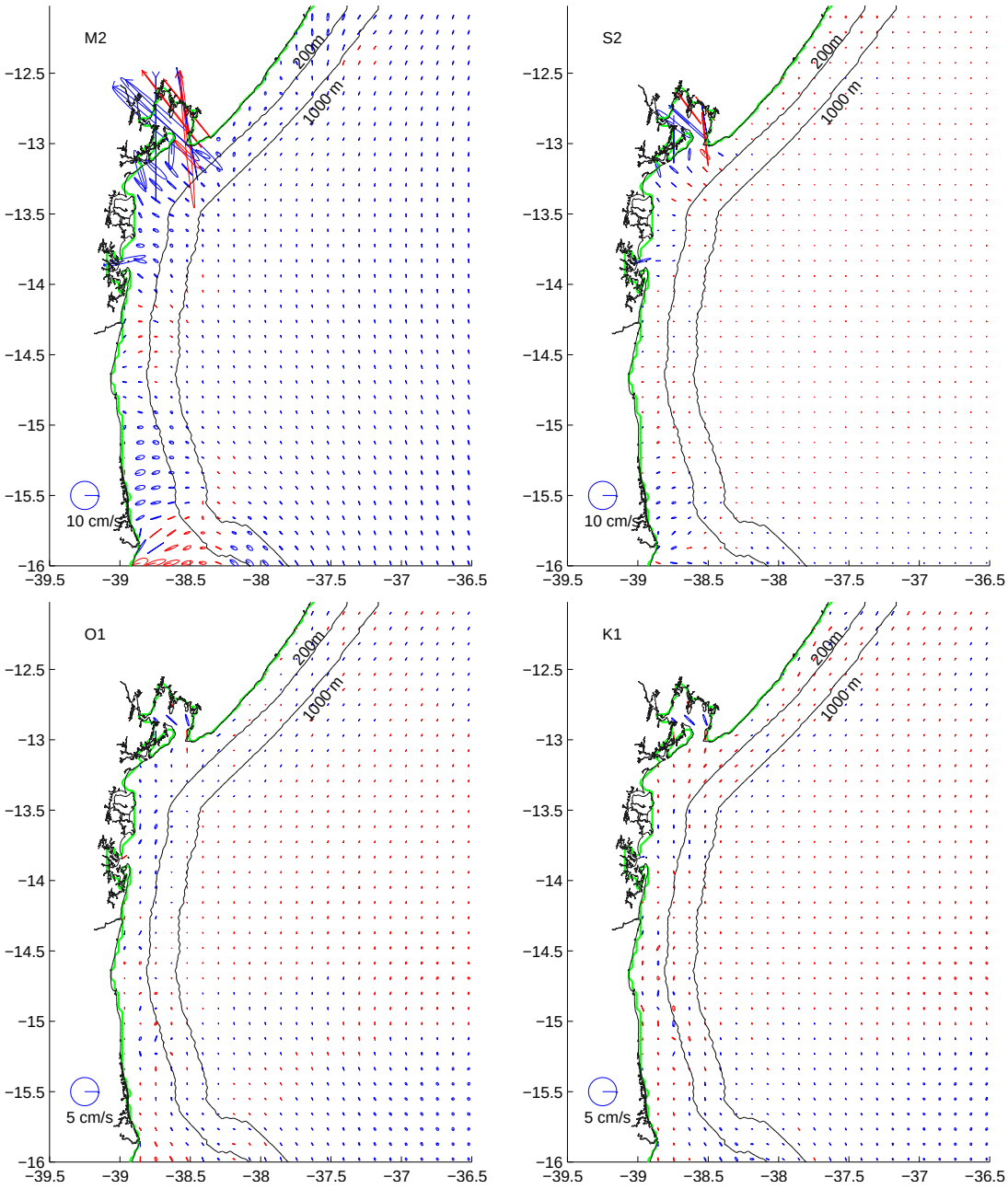

Figure 4.3: Barotropic tidal ellipses for the main semi-diurnal and diurnal tidal components (M_2, S_2, O_1, K_1) along the central zone of the Eastern Brazilian Margin (L2 grid). Tidal current ellipses expresses the major and minor axis length while the radial line inside indicates the phase relative to greenwich (G °). Red (Blue) color indicates clockwise (counterclockwise) rotation. Representation on every fourth grid point. Note the different scale on semidiurnal and diurnal components.

The tidal ellipses results for the L3 grid ($\sim 1km$), focusing on the inner *Baía de Camamu* and on the adjacent coastal ocean, are presented in Figure 4.4. From these results, its noticeable the amplification on the semidiurnal and diurnal constituents along the shelf and the great amplification and polarization on the semi-diurnal components along the system mouth and towards the inner bay system. On the diurnal components, a higher polarization occurs toward the inner bay but not an amplification. According to Prandle [1997], the diurnal currents are more sensitive to friction than the semi-diurnal ones of the same magnitude. The semi-diurnal amplification is also remarkable on the sea surface height at the inner bay stations, compared to the along-coast ones (Table 4.2).

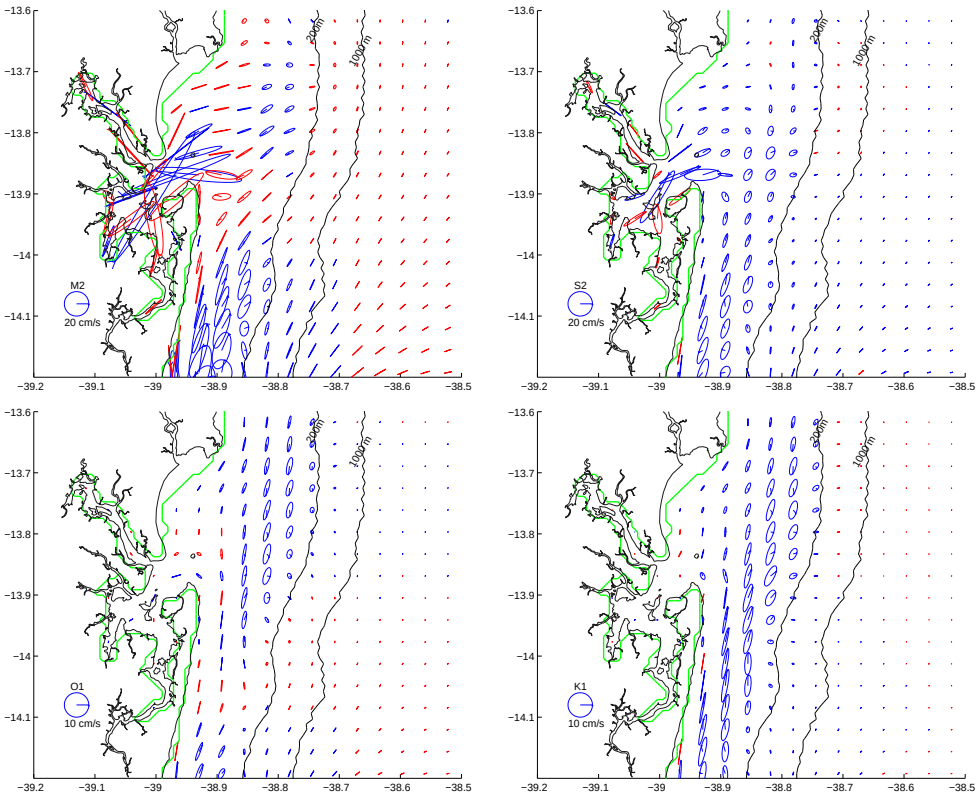

Figure 4.4: Barotropic tidal ellipses for the main semi-diurnal and diurnal tidal components (M_2, S_2, O_1, K_1,) in the shelf vicinity and inner *Baía de Camamu* (L3 grid). Red (Blue) color indicates clockwise (counterclockwise) rotation. Representation on every fourth grid point. Note the different scale on semidiurnal and diurnal components.

4.5 Conclusion

The addition of tide signal in a regional modeling system is a step forward for the establishment of a realistic coastal model, specially when one wishes to consider estuarine connections in regional study cases. In the current experiment, a third and fourth level nested grids was set over a ROMS coastal system, with the purpose of investigating the barotropic tidal propagation along different spatial scales on the Eastern Brazilian Margin and, towards the shallower domains on the shelf, near shore and inner *Baía de Camamu*.

The results indicate that the model tides compares quantitatively well with observations in terms of sea-surface height, with discrepancies in amplitude of the most energetic M2 constituent varying from 8.5% at the Northernmost station to less than 6% at the Southernmost coastal station. For the S_2 constituent, discrepancy value lower than 1% is found at the inner *Baía de Camamu* station. Comparison in terms of Greenwich phases, denotes a good response for most constituents and stations and discrepancies lower than 20° are found for the M_2 in every five tidal stations and for the K_1 along four tidal stations. Considering all possible interferences on the model results and the relatively simple configurations adopted, the model response is quite robust, showing lesser quantitative discrepancies on phase and amplitude than previews modeled results from the literature.

The model is also capable in reproducing the general field for tidal ellipses, depicting a first view of this field on the region. Because of the lack of references we could not adequately compare the model solution. We understand that there are still room for improvements, towards more realistic condition that may lead us to make stronger environmental ties. Future steps on this purpose must face with sensitivity evaluation of tidal currents to varying drag coefficients and, most importantly, to stratification.

For instance, the remarkable semidiurnal polarization and intense cross-shelf flow in the shelf vicinity of submarine canyons may be an active physical process in the sediment and debris flow dynamics, whose dynamics is still to be investigated. The stratification was not considered in this study because the interaction of barotropic tides and steep topography has the potential of generating internal tides, making the flow pattern complex with the presence of time dependent stratification. Nevertheless, internal waves has also the potential of intensifying the bottom currents and generate more polarization, as evidenced by Vitorino et al. [2002] along the *Porto* Canyon, in the northern Portuguese shelf.

Chapter 5

Final remarks and future work perspectives

Along the development of this thesis many science ideas came up. While some were incorporated into the work others although scientifically interesting were far too broad and possibly could be the theme of a dissertation itself. Some of the ideas that I believe deserves to be considered as motivations for future works or as complementary efforts on the achieved work, are discussed bellow.

In a mesoscale perspective, the implementation of a automated method for eddy identification, or even the combination of different ones, for cyclonic and anticyclonic eddies, isolating and tracking the seasonal eddies translation along the EBM (as evidenced on *Chapter 2*), on a series of consecutive years, would define the seasonal dynamics with greater precision. One objective method, the OkuboWeiss, which defines a vortex as a simple connected region with values of OkuboWeiss parameter weaker than a given threshold, was applied by Henson and Thomas [2008] for identifying and tracking anticyclonic eddies along 15 years of satellite sea level anomaly data, on the Gulf of Alaska, allowing a precise definition on the spatial and temporal variability and providing the first systematic census of anticyclonic eddies for that region. Nevertheless, Chaigneau et al. [2008], working with the same subject along the coast of Peru, shows that the rarely-used geometrical or winding-angle method, based on the curvature of the

streamline functions, was more accurate than the OkuboWeiss algorithm. This is a subject of fast growing literature, whose achievements have never been applied to the EBM.

Estuaries are transitional and complex water bodies that differ considerably from the neighboring fluvial or from the adjacent coastal marine systems on its character and management. In the present thesis, *Baía de Camamu* was investigated based on the analysis of an relatively extensive field data set covering dry (September, 2004) and rainy (July, 2005) conditions. In general, the findings of a study at one estuary can not be easily transferred to another due to its unique physical setting. In this work, a great effort was done to summarize *Baía de Camamu* physical setting (*Chapter 3*), establishing a basis for comparison.

On estuaries, water quality or sediment dynamics are complex to monitor due to both upstream (fluvial) and downstream (oceanic) sources. The tidal forcing and the fresh water discharge are key factors determining its dynamics [Miranda et al., 2002], emphasizing the estuarine transitional nature. The implementation of a numerical modelling is a necessary step forward on the science and on the monitoring *Baía de Camamu* effort. Nevertheless, due to the complex dynamical character, oversimplified models are not always suitable to investigate the hydrodynamics of an estuary while complex models are of difficult implementation due to intrinsic estuarine factors such as the variable watershed (wet and dry zones), low depth, variable river discharge or complex geomorphology, among others.

In *Baía de Camamu* pluviometry oscillates dramatically temporally (*Chapter 3*), leading to extremes in river inflow. A model effort must necessarily mimic such variabilities and in this matter. The seasonal discharge estimative presented on the appendix of (*Chapter 3*) establishes a reference for this objective. In the long term however, monitoring the discharge along the basin major tributaries should be encouraged, adding reliability to the fresh water input data.

The addition of tide signal in a regional modeling system is a necessary step on the establishment of a realistic coastal model, specially when you wish to consider estuarine connections, as on the case of Central Eastern Brazilian Margin. In Chapter 4, a third and fourth level grids was set over a ROMS configuration as step forward in the process of developing a tide-permitting model response for the zone.

Furthermore, in *Chapter 4* we have focused on barotropic tidal ellipses patterns on shelf and near coast zones. We understand that there are still room for improvements towards more realistic condition that may lead to stronger environmental ties and to fully characterization of tidal currents in the margin. Future steps on this purpose must face with sensitivity evaluation of tidal currents to varying drag coefficients and to stratification. Because the interaction of barotropic tides, stratification and steep topography has the potential of generating internal tides, intensifying the bottom currents and possibly strengthening the polarization, this is a step to be followed if the intense cross-shelf flow in the shelf vicinity of submarine canyons is to be considered. Once these steps were accomplished, the vertical structure of tidal ellipses parameters in shelf zones shall also be investigated, taking full advantage of a three dimensional simulation.

Last, because of the lack of references we could not adequately compare *Chapter 4* model solution. Time-series of shelf and estuarine currents are a must for accurate validations of tidal current ellipse components. Some efforts have been done by *Universidade Federal da Bahia* to fill this gap. The author hopes that future cooperation and personal efforts at *Universidade Estadual de Santa Cruz*, will provide the means for making novel measurements efforts on *Baía de Camamu* and adjacent shelf zone, allowing a deeper analysis of our modelling work and enhancing new objectives and studies. The present thesis however, establishes a reference for the Eastern Brazilian Margin multi-scale dynamics oceanography.

Bibliography

Alencastro, L. F., 2000. O trato dos viventes: Formação do Brasil no Atlântico Sul, séculos XVI e XVII. Companhia das Letras, São Paulo, 525 p. pages 2

Amante, C., Eakins, B. W., 2009. ETOPO1 1 Arc-Minute Global Relief Model: Procedures, Data Sources and Analysis. Technical memorandum nesdis ngdc-24, NOAA, *http* : *//www.ngdc.noaa.gov/mgg/global/global.html*. pages 101

Amorim, F. N., 2005. Caracterização oceanográfica da Baía de Camamu e adjacências e mapeamento das áreas de risco a derrames de óleo. Dissertação de mestrado. Universidade Federal da Bahia, 191 p. pages 5, 6, 53, 54, 55

ANA, 2009. Agência Nacional de águas, http://www.ana.gov.br. pages xvi, 56, 58, 59, 92

ANP, 2009. Agência Nacional de Petróleo. Ministério de Minas e Energia, http://www.brasil-rounds.gov.br. pages 5, 52, 53

Araújo, H. A., Rodrigues, R. S., 2000. Regiões Características do Estado da Bahia para Previsão de Tempo e Clima. Superintendência de Recursos Hídricos - SRH., 13p. pages 56

Backeberg, B. C., 2006. Mesoscale variability study of the Agulhas Current from satellite radar altimetry and a high resolution model. University of Bergen, Norway, 42 p. pages 18

Barroso Junior, V., 2009. Metodologia para a geração de cartas de correntes de maré em sistemas estuarinos e recintos portuários com aplicação na Baía de Todos os Santos.

Dissertação de mestrado. Universidade Federal do Rio de Janeiro, COPPE, 157 p. pages 98

Beckman, A., Haidvogel, D., 1993. Numerical simulation of flow around a tall isolated seamount. J. Phys. Oceanogr. 23, 1736–1753. pages 101

Blayo, E., Debreu, L., 1999. Adaptive mesh refinement for finite-difference ocean models: first experiments. J. Phys. Oceanogr. 29, 1239–1250. pages 99

Brachet, S., Le Traon, P. Y., Le Provost, C., 2004. Mesoscale variability from a high-resolution model and from altimeter data in the North Atlantic Ocean. J. Geophys. Res. 109 (C12025). pages 18

Calado, L., Gangopadhyay, A., Silveira, I. C. A., 2006. A parametric model for the Brazil Current meanders and eddies off Southeastern Brazil. Geophys. Res. Lett. 33 (L12602), doi:10.29/2006GL026092. pages 46

Campos, E. J. D., 2006. Equatorward translation of the Vitoria Eddy in a numerical simulation. Geophys. Res. Lett. 33 (L22607). pages 43

Carton, J. A., Chepurin, G., Cao, X., 2000a. A Simple Ocean Data Assimilation analysis of the global upper ocean 1950-95. part ii: Results. J. Phys. Oceanogr. 30, 311–326. pages 16

Carton, J. A., Chepurin, G., Cao, X., Giese, B., 2000b. A Simple Ocean Data Assimilation analysis of the global upper ocean 1950-95. part i: Methodology. J. Phys. Oceanogr. 30, 294–309. pages 16

Chaigneau, A., Gizolme, A., Grados, C., 2008. Mesoscale eddies off peru in altimeter records: Identification algorithms and eddy spatio-temporal patterns. Progress In Oceanography 79 (2-4), 106 – 119. pages 111

Cirano, M., Lessa, G. C., 2007. Oceanographic characteristics of *Baía de Todos os Santos, Brazil. Rev. Bras. Geophys. 25 (4). pages 3, 97*

Cirano, M., Mata, M. M., Campos, E. J. D., Deiró, N., 2007. A circulação oceânica de larga-escala na região oeste do Atlântico Sul: validação da climatologia anual com base no modelo de circulação global OCCAM. Rev. Bras. Geophys. 24, 209–230. pages 3, 27

CRA, 2000. Centro de Recursos Ambientais. Área de Proteção Ambiental do Pratigi. Plano de Manejo, Zoneamento- Ecológico-Econômico, Plano de Gestão e Diagnóstico Ambiental do Meio Físico, 14 p. pages 91

Da Silva, A., Young, C. C., Levitus, S., 1994. Atlas of Surface Marine Data 1994, volume 1: Algorithms and procedures. NOAA Atlas NESDIS 6, U S Department of Commerce, National Oceanic and Atmospheric Administration, Silver Spring. pages 16

Debreu, L., Vouland, C., Blayo, E., 2008. Agrif: Adaptive grid refinement in fortran. Computers and Geosciences 34 (1), 8 – 13. pages 99

Defant, A., 1960. Physical Oceanography. Vol. 1. Oxford, Pergamon Press., 729p. pages 64, 86

Dominguez, J. M. L., 2004. The Coastal Zone of Brazil - an overview. J. Coastal Res. 39, Special Issue. pages 60, 61

Ducet, N., Le Tron, P., Reverdin, G., 2000. Global high-resolution mapping of ocean circulation from TOPEX/Poseidon and ERS-1 and -2. J. Geophys. Res. 105 (C8), 19477–19498. pages 18

Egbert, G. D., Bennett, A. F., Foreman, M. G. G., 1994. Topex/poseidon tides estimated using a global inverse model. J. Geophys. Res. 99 (24), 24821–24852. pages 99

Egbert, G. D., Erofeeva, S. Y., 2002. Efficient inverse modeling of barotropic ocean tides. J. Atmospheric and Oceanic Technology. 19. pages 100

Ekau, W., 1999. Topographical and hydrographical impacts on macrozooplankton community structure in the Abrolhos Bank region, East Brazil. Arch. Fish. Mar. Res. 47 (2/3), 307–320. pages 4

Ekau, W., Knoppers, B., 2003. A review and redefinition of the large marine ecosystems of Brazil. In: Sherman, K., Hempel, G. (Eds.), Large Marine Ecosystems of the World - Trends in Exploitation, Protection and Research. Elsevier Science. pages 3, 4

Emilsson, I., 1961. The shelf and coastal waters off southern Brazil. Bolm. Inst. Oceanogr., S. Paulo 17 (2), 101–112. pages 13

Evans, D. L., Signorini, S. R., Miranda, L. B., 1983. A note on the transport of the Brazil Current. J. Phys. Oceanogr. 13 (9), 1732–1738. pages 13, 26

Gaeta, S. A., Lorenzzetti, J. A., Miranda, L. B., Susini-Ribeiro, S. M. M., Pompeu, M., Araujo, C. E. S., 1999. The Vitória eddy and its relation to the phytoplankton biomass and primary productivity during austral fall of 1995. Arch. Fish. Mar. Res. 47 (2/3), 253–270. pages 4

Gordon, A. L., 1989. Brazil Malvinas confluence - 1984. Deep-Sea Res., Part A 36 (3), 359–384. pages 13

Haidvogel, D. B., Arango, H. G., Hedstrom, K., Beckmann, A., Malanotte-Rizzoli, P., Shchepetkin, A. F., 2000. Model evaluation experiments in the North Atlantic Basin: simulations in nonlinear terrain-following coordinates. Dyn. Atmos. Oceans 32, 239–281. pages 6, 15, 17

Hansen, D. V., Rattray, M., 1966. New dimensions in estuary classification. Limnol. Oceanogr. 11, 319–326. pages 87

Hatje, V., Barros, F., Magalhães, W., Riatto, V. B., Amorim, F. N., Figueiredo, M. B., Spanó, S., Cirano, M., 2008. Trace metals and benthic macrofauna distributions in camamu bay, brazil: Sediment quality prior oil and gas exploration. Marine Pollution Bulletin 56 (2), 363 – 370. pages 51

Henson, S. A., Thomas, A. C., 2008. A census of oceanic anticyclonic eddies in the gulf of alaska. Deep Sea Research Part I: Oceanographic Research Papers 55 (2), 163 – 176. pages 111

IBGE, 2008a. Estimativas da população para 1 de julho de 2009. Tech. rep., http://www.ibge.gov.br. pages 2

IBGE, 2008b. Sintese dos indicadores sociais 2007. Tech. rep., http://www.ibge.gov.br. pages 2

Janzen, C. D., Wong, K.-C., 2002. Wind-forced Dynamics at the Estuary-Shelf Interface of a Large Coastal Plain Estuary. J. Geophys. Res. 107 (C10). pages 66

Knoppers, B., Ekau, W., Figueiredo, A. G., 1999. The coast and shelf of east and northeast Brazil and material transport. Geo-Mar. Lett. 19 (3), 171 – 178, dOI 10.1007/s003670050106. pages 3, 11, 36

Large, W. G., McWilliams, J. C., Doney, S., 1994. Oceanic vertical mixing: A review and a model with a nonlocal boundary layer parametrization. Rev. Geophys. 32, 363 – 403. pages 16, 101

Leão, Z., 2002. Abrolhos - o complexo recifal mais extenso do oceano Atlântico Sul. In: Schobbenhaus, C., Campos, D., Queiroz, E., Winge, M., Berbert-born, M. (Eds.), Sítios Geológicos e Paleontológicos do Brasil. Vol. 1. DNPM, pp. 345–359. pages 3, 4, 14

Lessa, G., Dominguez, J. M. L., Bittencourt, A. C. S. P., Brichta, A., 2001. The tides and tidal circulation of Todos os Santos Bay, Northeast Brazil: a general characterization. An. Acad. Bras. Cienc. 73 (2), 245 – 261. pages 3, 14

Marta-Almeida, M., Dubert, J., 2006. The structure of tides in the Western Iberian region. Cont. Shelf Res. 26, 385–400. pages 98

Miranda, L. B., 1985. Forma de correlação T-S de massa de água das regiões costeira e oceânica entre o Cabo de São Tomé (RJ) e a Ilha de São Sebastião (SP), Brasil. Bolm Inst. Oceanogr., S Paulo 33 (2), 105–119. pages 13

Miranda, L. B., Castro, B., Kjerfve, B., 2002. Princípios de Oceanografia Física de Estuários. Edusp, 414 p. pages 62, 64, 112

Miranda, L. B., Castro, B. M., 1982. Geostrophic flow conditions of the Brazil Current at $19°S$. *Ciência Interamericana 22, 44–48. pages 26, 27*

NCEP, 2005. National Center of Environmental Prediction Reanalysis Data. National Oceanic and Atmospheric Administration. Cooperative Institute for Research in Environmental Sciences (NOAA-CIRES). Climate Diagnostics, Center, Boulder, Colorado, USA, http://www.cdc.noaa.gov/cdc/data.ncep.reanalysis.html. pages 60, 61

Nimer, E., 1989. Climatologia do Brasil. Instituto Brasileiro de Geografia e Estatística, Rio de Janeiro, 421 p. pages 37, 60

O'Callaghan, J., Pattiaratchi, C., Hamilton, D., 2007. The response of circulation and salinity in a micro-tidal estuary to sub-tidal oscillation in coastal sea surface elevation. Cont. Shelf. Res. 27, 1947–1965. pages 61

Oliveira, O. M. C., 2000. Diagnóstico geoambiental em zonas de manguezal da Baía de Camamu - BA. Tese de Doutorado em Geoquímica Ambiental. Universidade Federal Fluminense, 249 p. pages 3, 51

Pawlowicz, R., Beardsley, B., Lentz, S., 2002. Classical tidal harmonic analysis including error estimates in MATLAB using T_TIDE. Computers and Geosciences 28, 929–937. pages 64, 102

Penven, P., 2003. Romstools users guide. technical report, Instituit de Recherche pour le Développement, 213 rue Lafayette, Paris, France, $http://www.brest.ird.fr/Roms\_tools/$. *pages 15*

Penven, P., Debreu, L., Marchesiello, P., McWilliams, J. C., 2006. Evaluation and application of the ROMS 1-way embedding procedure to the central california upwelling system. Ocean Modelling 12, 157–187. pages 14, 15, 99

Penven, P., Echevin, V., Pasapera, J., Colas, F., Tam, J., 2005. Average circulation, seasonal cycle, and mesoscale dynamics of the Peru Current System: A modeling approach. J. Geophys. Res. 110 (C10021). pages 15, 22

Pereira, A., Belem, A., Castro, B. M., Geremias, R., 2005. Tide-topography interaction along the eastern brazilian shelf. Cont. Shelf Res. 25, 1521–1539. pages 4, 36, 37, 98, 105

Prandle, D., 1997. Tidal currents in shelf seas - their nature and impacts. Progr. Oceanogr. 40, 245–261. pages 98, 108

Reid, J. L., 1989. On the total geostrophic circulation of the South Atlantic Ocean: Flow patterns, tracers and transports. Progr. Oceanogr. 23, 149–244. pages 13

Rezende, L. F., 2001. Estimativa dos padrões de circulação oceânica superficial baseado no lançamento de corpos de deriva e em derramamentos ocorridos no litoral sul do estado da Bahia. Rev. Tecnologia e Ambiente 7, 73–89. pages 4

Rodrigues, R. R., Rothstein, L. M., Wimbush, M., 2007. Seasonal variabilty of the South Equatorial Current bifurcation in the Atlantic Ocean: A numerical study. J. Phys. Oceanogr. 37, 16–30. pages 5, 12, 13, 27, 37, 48, 50

Salles, F. J. P., Bentes, F. C. M., Santos, J. A., 2000. Catálogo de Estações Maregráfica Brasileiras. Tech. rep., Fundação de Estudos do Mar, FEMAR, http : //www.femar.com.br. pages 102, 104

Saraceno, M., Provost, C., Piola, A. R., Bava, J., Gagliardini, A., 2004. Brazil Malvinas Frontal System as seen from 9 years of advanced very high resolution radiometer data. J. Geophys. Res. 109 (C5). pages 19

Schmid, C., Schaefer, G., Zenk, W., 1995. The Vitria Eddy and its relation to the Brazil Current. J. Phys. Oceanogr. (25), 2532–2546. pages 43

Schott, F. A., Dengler, M., Zantopp, R., Stramma, L., Fischer, J., Brandt, P., 2005. The shallow and deep western boundary circulation of the South Atlantic at $5° - 11°S$. *J. Phys. Oceanogr. 35, 2031–2053. pages 25, 26*

Schott, F. A., Fischer, J., Stramma, L., 1998. Transports and pathways of the upper-layer circulation in the western tropical Atlantic. J. Phys. Oceanogr. 28 (10), 1904–1928. pages 12

SEI, 2000. Superintendência de Estudos Econômicos e Sociais da Bahia. Base cartográfica Digital, www.sei.ba.gov.br. pages 55

Shchepetkin, A. F., McWilliams, J. C., 2005. The Regional Oceanic Modeling System (roms): A split-explicit, free-surface, topography-following-coordinate oceanic model. Ocean Modelling 9, 347–404. pages 6, 15, 97, 99

Silveira, I. C. A., Miranda, L. B., Brown, W. S., 1994. On the origins of the North Brazil Current. J. Geophys. Res. 99, 22501–22512. pages 13

Silveira, I. C. A., Schmidt, A. C. K., Campos, E. J. D., Godoi, S. S., Ikeda, Y., 2000. A Corrente do Brasil ao largo da costa leste brasileira. Rev. Bras. Oceanogr. 48 (2), 171–183. pages 27

Song, Y., Haidvogel, D. B., 1994. A semi-implicit ocean circulation model using a generalized topography-following coordinate system. J. Comp. Phys. 115 (1), 228–244. pages 100

Souza, T. C. M., Petrere-Jr, M., 2008. Characterization of small-scale fisheries in the camamu-almada basin, southeast state of Bahia, Brazil. Braz. J. Biol. [online]. 68, 711–719, doi: 10.1590/S1519-69842008000400005. pages 4, 51

Souza-Lima, W., Manso, C. L. C., Andrade, E. J., Grillo, J. L., 2003. Bacias Sedimentares Brasileiras. Bacia de Camamu. Phoenix 54, 1–6. pages 52

Spix, J. B., Martius, C. F. P., 1828. Reise in Brasilien. Gedrukt bei M. Lindauer, Munchen. pages 51

SRH, 2003. Secretaria de Meio Ambiente e Recursos Hídricos. Superintêndencia de Recursos Hídricos. Sistema de Informações Georeferenciadas. Série: Sistema de Informações sobre Recursos Hídricos - SIRH, www.srh.ba.gov.br. pages 55, 92

Stramma, L., England, M., 1999. On the water masses and mean circulation of the South Atlantic Ocean. J. Geophys. Res. 104 (C9), 20,863–20,883. pages 27

Stramma, L., Ikeda, Y., Peterson, R. G., 1990. Geostrophic transport in the Brazil Current region north of $20°S$. *Deep-Sea Res. 37 (12), 1875–1886. pages 5, 12, 13, 14, 25, 26, 27, 48*

Stramma, L., Schott, F., 1999. The mean flow field of the tropical Atlantic Ocean. Deep-Sea Res., Part II 46, 279–303. pages 5, 12, 60

Summerhayes, C. P., De Melo, U., Barreto, H., 1976. The influence of upwelling on suspended matter and shelf sediments off southeastern Brazil. J. Sed. Petrol. 46 (4), 819–828. pages 4

Teles-Machado, A., Peliz, A., Dubert, J., Sanchez, R. F., 2007. On the onset of the Gulf of Cadiz Coastal Countercurrent. Geophys. Res. Lett. 34 (L12601). pages 15

U. S. Department of Commerce, N., 2001. 2-minute gridded global releif data (etopo2). technical report, National Geophysical Data Center, http : //www.ngdc.noaa.gov/. pages 17

*U. S. Department of Commerce, N., 2004. Large marine ecosystems of the world. technical report, National Oceanic and Atmospheric Administration, http : //na.nefsc.noaa.gov/lme/text/lme*16*.htm. pages 3, 11*

Verger, P., 2002. Fluxo e Refluxo - Do Tráfico de Escravos entre o Golfo do Benin e a Bahia de Todos os Santos dos Séculos XVII a XIX. Currupio, Salvador, 727 p. pages 2

Vianna Filho, L., 2008. O negro na Bahia: Um ensaio clássico sobre a escravidão, 4th Edition. Edufba, São Paulo, 230 p. pages 2

Vitorino, J., Oliveira, A., Jouanneau, J., Drago, T., 2002. Winter dynamics on the northern Portuguese shelf. part 1: Physical processes. Prog. Oceanogr. 52 (129-153). pages 110

Walsh, J. J., 1988. On the nature of continental shelves. Academic Press, San Diego, 520 p. pages 50

Walters, R. A., Heston, C., 1982. Removing tidal-period variations from time-series data using low-pass digital filters 12, 112–115. pages 67

Wang, X., Chao, Y., Dong, C., Farrara, J., Li, Z., Matsumoto, K., MacWilliams, J., Paduan, J., Rosenfeld, L., Shum, C., Wang, Y., 2008. Tidal simulation using Regional Ocean Modelling System (ROMS). technical report. pages 98